Chapter 2

Biomedical Signals

2.1 THE ELECTROENCEPHALOGRAM

2.1.1 Introduction

Electrical signals produced by the brain characterize brain function and the status of the entire body. This provides the motivation to utilize digital signal-processing techniques for electroencephalogram (EEG) signals acquired from the brain of a human subject. The physiological characteristics of brain activities have numerous characteristics related to the original sources, the medium, and their actual patterns. The medium describes the path from the neurons, which are signal sources, to the electrodes, which are the sensors in which some form of source mixture is collected. An understanding of neurophysiological properties and neuronal functions of the brain, together with the working principle underlying the signal generation and acquisition, is useful when dealing with these signals for recognition, analysis, and treatment of brain disorders. EEG presents a way for diagnosing several neurological disorders and abnormalities in the human body. The recorded EEG signals from a human can be utilized for several clinical problems such as:

(a) monitoring alertness, coma, and brain death;
(b) locating areas of damage following head injury, stroke, and tumor;
(c) testing afferent pathways (by evoked potentials);
(d) monitoring cognitive engagement (alpha rhythm);
(e) producing biofeedback situations;
(f) controlling anaesthesia depth (servo anaesthesia);
(g) investigating epilepsy and locating seizure origin;
(h) testing epilepsy drug effects;
(i) assisting in experimental cortical excision of epileptic focus;
(j) monitoring the brain development;
(k) testing drugs for convulsive effects;
(l) investigating sleep disorders and physiology;
(m) investigating mental disorders;
(n) providing a hybrid data recording system together with other imaging modalities.

This list reveals that EEG has rich potential for analysis, fulfilling the need for advanced signal-processing techniques to support the clinician's interpretation (Sanei & Chambers, 2013).

2.1.2 The Nervous System

The nervous system collects and processes information from many parts of the body. It also ensures that both internal and external changes are handled correctly and quickly. The nervous system is commonly divided into the central nervous system (CNS) and the peripheral nervous system (PNS). The CNS consists of the spinal cord and the brain, whereas the PNS connects those two to the body's organs and sensory systems. Therefore, the CNS and the PNS are closely integrated. The CNS processes sensory inputs from the PNS and sends responses to the body's organs via the PNS. The nerves that carry signals to the CNS are called sensory nerves, whereas the nerves that carry signals from the CNS are called motor nerves because these signals can provoke muscle contraction (Sörnmo & Laguna, 2005).

2.1.3 The Brain

The brain, which is an extremely complex structure containing billions of interrelated neurons, represents the control center of the CNS. It controls a vast majority of our movements in conjunction with the spinal cord. Structurally, a human brain includes up to 100 functional area sections and is around 17 cm anterior to posterior. The brain's compartments have specific functions. The back region controls vision, whereas the frontal region controls movement. The number of neurons within a region determines information content and functional capability. More neurons mean more information-processing capability. The brain frequently communicates with different body systems. It also handles processing to control the body's actions. The brain transmits and receives signals through nerves in combination with the spinal cord. The cerebellum, being close to the spinal cord, controls movements by muscle activation. Thus, the cerebellum is crucial for human EEG signal analysis. The motor cortex, where action potentials are initiated, covers a large area of the brain (Deutsch & Deutsch, 1993).

2.1.4 Electroencephalography

The human brain has been the focus of extended research because it represents the most composite organic matter known to mankind. Brain functionality has been examined

Practical Guide for Biomedical Signals Analysis Using Machine Learning Techniques. https://doi.org/10.1016/B978-0-12-817444-9.00002-7

from low-level molecular and chemical properties to high-level characteristics such as learning and memory. It is well known that the brain is related to the generation of electrical activity. In 1875, Richard Caton was able to record microvolt electrical signals on the cerebral cortex of rabbits and dogs. A half century later, Hans Berger recorded electrical "brainwaves" by attaching electrodes to the human scalp for the first time in history. These experiments turned out to be the basis of EEG. EEG today represents an important noninvasive medical tool for analyzing numerous functional brain disorders and for better understanding of the human brain in general. The person interpreting the EEG must draw conclusions based on the frequency, amplitude, morphology, and spatial distribution of the brainwaves. However, the diversity of EEG patterns cannot be completely explained by any single mathematical or biological model available today. Therefore, EEG interpretation basically remains a phenomenological medical discipline (Barlow, 1993) (Fig. 2.1).

EEGs are recordings of the electrical potentials created by the brain, usually less than 300 μV. Since 1924 and Hans Berger's experiment, the study of EEG has been conducted mostly in research facilities and medical settings with the aim of detecting pathologies and epilepsies. For many years, an electroencephalographer, an individual trained to qualitatively differentiate normal and abnormal EEG activity within pretty long EEG records, was the only person qualified for EEG visual interpretation. Researchers and clinicians were left out, covered in a bunch of EEG paper records. However, the arrival of modern powerful computers and related technologies opened a whole new door of possibilities for applying various methods to quantify EEG signals (Bronzino, 1999).

The interpretation is considerably facilitated by a selection of digital signal-processing methods with different purposes such as noise reduction, extraction of information not visually obtainable, or quantification of different signal characteristics. However, this interpretation is far from completely automated. Signal-processing methods belong to one of the two general groups: analysis of spontaneous brain activity and analysis of brain potentials evoked by many cognitive and sensory stimuli. The former certainly provides a better understanding of EEG. Recently, the study of brain function has been improved with the usage of several imaging modalities; positron emission tomography (PET), single photon emission computed tomography (SPECT), and magnetic resonance imaging (MRI) are able to create good resolution for two- or three-dimensional images. These modalities provide comprehensive information on anatomy and blood flow in various brain regions. Even though EEG has lost a portion of its supremacy in the medical routine due to these modalities, it still remains a very powerful tool for the analysis of many diseases such as epilepsy, sleep disorders, and dementia. Moreover, the

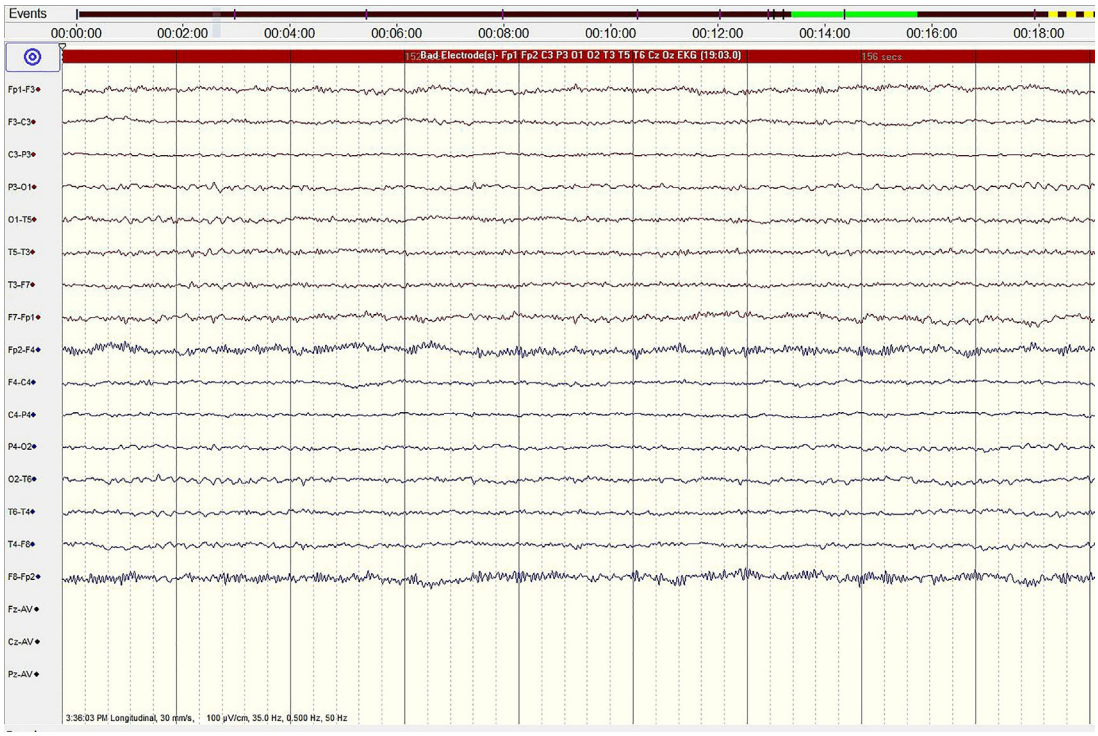

FIG. 2.1 A typical set of EEG signals of normal adult brain activity.

EEG signal is essential for real-time monitoring of progress of patients with encephalopathies or those in a coma. In these applications, the temporal resolution of the EEG is unmatched by the previously mentioned imaging modalities. Furthermore, the overall cost related to recording equipment and skilled workers required for managing the instrumentation is significantly lower than the cost related to neuroimaging. For a simple recording system, the technical demands on instrumentation are quite modest. They are limited to a set of electrodes, a signal amplifier, and a PC for data storage, signal analysis, and graphical demonstration (Sörnmo & Laguna, 2005).

The magnetoencephalogram (MEG) is another noninvasive method that measures the weak magnetic field of mass neural activity by using the SQUID, an extremely sensitive magnetic field sensor. The magnetic field is less distorted by the skull than the electrical potential, which is the main advantage of the MEG over EEG. The MEG was initially supposed to deliver information independent of the EEG (Plonsey, 1972). However, Malmivuo, Suikho, and Eskola (1997) showed that EEG and MEG signals have strong interdependence. These two recording technologies, plus three imaging techniques stated earlier, should eventually be used to complement each other due to their strengths and weaknesses (Dale & Sereno, 1993).

2.1.5 Historical Perspective

In 1875, Richard Caton employed a galvanometer and positioned two electrodes over the scalp of a human subject to record brain activity in the form of electrical signals. The concepts of EEG were then was utilized to represent the electrical neural activity of the brain. In 1920, Hans Berger discovered the existence of human EEG signals and began to work with a string galvanometer. Berger recognized the alpha rhythm as the main element of the EEG signals and the alpha blocking response. During the 1930s, he realized the first EEG recording of sleep spindles and then described the effect of hypoxia on the human brain, the nature of several diffuse and localized brain disorders, and gave an inkling of epileptic discharges. Moreover, he also dealt with cerebral localization, especially the localization of brain tumors. He also discovered a relationship between mental activities and changes in the EEG signals. The history of EEG has been a continuous process that began in the early 1930s and has brought daily improvement to experimental, clinical, and computational efforts for the analysis, recognition, detection, and treatment of a huge number of physiological and neurological anomalies of the brain and CNS. Currently, EEG signals are collected invasively and noninvasively by employing completely computerized systems. The EEG machines involve many signal-processing tools, precise and delicate measurement electrodes, and sufficient memory for long-term recordings of many hours (Sanei & Chambers, 2013).

Berger also noted that these brainwaves exhibited certain regularities rather than being completely random. For instance, he observed that these brainwaves were slower during sleep (<3 Hz) and faster during the waking period (15–25 Hz). He concluded that the brain's activity changes in a familiar fashion if the subject changes status such as from relaxation to alertness. Berger noted a noticeable increase in the amplitude of these brainwaves during sudden seizures and concluded that certain pathologic conditions may significantly affect these brainwaves. Despite all these insights, Berger's paper published in 1929 did not produce much attention. Until British investigators carried out and confirmed similar findings, the efforts of this outstanding researcher were basically overlooked (Bronzino, 1999).

In 1934, the idea of "human brainwaves" was actually accepted and the study of EEG was put on a firm foundation when Adrian and Matthews published their paper confirming Berger's findings. One of their main contributions was the identification of an "alpha rhythm" in the EEG, a regular oscillation at around 10–12 Hz recorded from the occipital lobes. They also found that, if a subject exhibited any type of attention or alertness, the alpha rhythm would disappear. An outstanding historical review of the early era of brain research can be found in an interesting text by Brazier (1968).

2.1.6 EEG Recording Techniques

Scalp recordings of the EEG allow measurement of potential variations between a signal and a reference electrode over time (Kondraske, 1986). The EEG is quite challenging for an untrained eye to interpret when compared to other biopotentials such as the electrocardiogram (ECG). This is partially due to electrode placement and the spatial mapping of functions onto different regions. The International Federation in Electroencephalography and Clinical Neurophysiology, aware that some standardization was needed, accepted the 10/20 electrode placement system (Jasper, 1958). This specific electrode montage employs 21 electrodes attached to the scalp surface at positions determined by certain anatomical reference points. Relative distances between different electrode locations on the skull perimeter are indicated by the numbers 10 and 20, which represent percentages (Fig. 2.2). Both bipolar and unipolar electrodes are used in the medical routine. The latter type needs a reference electrode located distantly or taken as the average of all electrodes (Sörnmo & Laguna, 2005).

The interelectrode distance with the 10/20 system is around 4.5 cm for a typical adult skull. If brain mapping is of importance, then better spatial resolution may be necessary. Brain mapping constitutes a technique where the EEG is represented as a topographic map projected onto

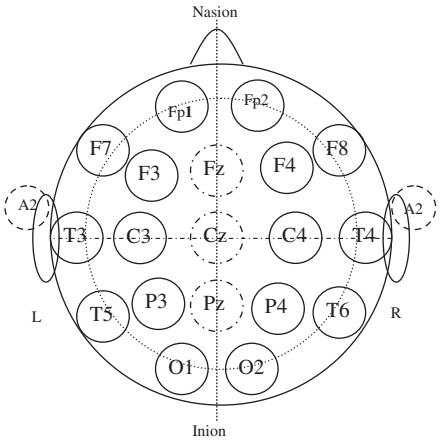

FIG. 2.2 The international 10/20 system for recording clinical EEG. The top of the nose (nasion) and the back of the skull (inion) define the anatomical reference points. The letters F, P, C, T, O, and A represent frontal, parietal, central, temporal, occipital, and auricle, respectively. Even-numbered electrodes are on the right side, whereas odd-numbered electrodes are on the left side. Z (zero) is along the midline.

the scalp. Using a small number of electrodes would incorrectly represent the brain's electrical activity due to aliasing in the spatial domain. To provide a satisfactory amount of detail, it has been specified that more than 64 electrodes should be used in brain mapping applications (Gevins & Bressler, 1988). Besides the standard 10/20 system, electrodes for eye movement monitoring, ECG, and muscle activity are crucial for discrimination of various states of vigilance or behavior. Recording equipment for EEG can be simple or elaborate. Scale electrodes consist of Ag-AgCl disks 1–3 mm in diameter, with lengthy flexible leads plugged into an amplifier. Hair and the trouble of mechanically stabilizing the electrode make it difficult to obtain low-impedance contact at the electrode-skin interface (less than 10 kΩ). Conductive electrode paste helps overcome these difficulties. For mechanical stability, contact cement is usually used to fix gauze over the electrodes. To relieve some stress and pressure, leads are typically taped to the subject. To obtain lower electrode impedance, small abrasions of the skin are sometimes performed. However, sensitive subjects complain about the irritation, which is sometimes followed by pain and infection (Bronzino, 1999).

Electrodes are the main problem for obtaining long-term recordings required for epileptic seizure monitoring. Needle electrodes are sometimes useful. They must be implanted between the skull and scalp surface, significantly increasing the risk of infection. Sometimes a more acceptable method is the use of electrodes with tiny self-contained amplifiers. Although they provide a low-impedance source to interconnecting leads, they are not a cheap option to choose. Regardless of various efforts to simplify electrode application and assure long-term stability, no single technique has been generally accepted. The procedure of measuring impedance between electrode pairs is strongly recommended as good practice, because high impedance causes distortions hardly separated from real EEG signals. Actually, some commercially available EEG devices contain built-in electrode impedance monitors. Typical DC ohmmeters should not be used because they cause a polarizing current resulting in accumulation of noise at the skin-electrode interface. Signal amplitudes of up to 10 μV can be acquired from carefully applied electrodes. With the intention of increasing signal strength to a suitable level usable as input to a recording device, significant amplification with gains approaching 106 is necessary. Because of the length of the electrodes, as well as the noisy surroundings in which recordings are usually carried out, very powerful amplifiers must be used to ensure high-quality EEG recordings. Therefore, differential amplifiers with high input impedance and high common-mode rejection ratios are crucial (Bronzino, 1999).

Special electrically isolated rooms in some facilities reduce environmental electrical noise, especially 50 or 60 Hz alternating current (AC) line noise. However, low-pass filters in the amplifier can help minimize line noise because the information of importance in the EEG lies in frequency bands below 40 Hz. If the low-pass cutoff is beyond the line noise frequency, numerous EEG amplifiers incorporate a notch filter. A notch filter is specific only for frequencies in a narrow band around line noise frequency. Using a dummy source such as a fixed 100 kΩ resistor attached to the electrodes might help remove or reduce the effect of 50 or 60 Hz sources. The output of the differential amplifier, having a dummy source as one of the input signals, represents only interfering sources' influence. If we can minimize the noise at a minimum of a factor 10 less than the EEG signals, we can probably obtain uncontaminated EEG records. Different types of recording equipment can obtain a temporary or permanent record of the EEG. Pen or multichannel chart recorders are the most common recording instruments, as they are an essential part of many commercially available EEG instruments. Recordings are taken with the moving pen on a long sheet of continuous paper that can be chosen to move at one of several constant speeds, which is carefully chosen according to the monitoring situation. Slow speeds of around 10 mm/s are reserved for spotting the spiking related with seizure activity, whereas faster speeds, which can go up to 120 mm/s, are used to detect the manifestation of individual frequency bands in the EEG (Bronzino, 1999).

Another type of recording device is a computer. One or multiple channels of analog EEG signals are constantly sampled at a fixed time interval, after which an analog-to-digital (A/D) converter translates each sample into a digital representation. Each sample is then saved in the computer's memory. The minimum amplitude that can be sampled determines the A/D converter's resolution. This amplitude

can be calculated when the range of the A/D converter is divided by 2b, where b equals the number of bits of the A/D converter. For instance, an A/D converter with a voltage range of ±10 V and 16-bit resolution can resolve sample amplitudes as small as 0.3 mV. If a proper combination of amplification and A/D converter sensitivity is selected, the smallest signal required can be resolved together with the prevention of clipping of the largest amplitudes. These samples carry all the information in the waveform if they are picked up at a sampling rate that is twice the highest frequency component of interest in the sampled signal or more. This rule is known as the Nyquist rule. We can use a low-pass filter to make sure that the signal is band-limited and choose a cutoff frequency as the highest frequency of interest. However, the sampling rate that is at least twice the filter's cutoff frequency is typically selected because physical filters do not have ideal characteristics. Moreover, we can use digital filters as soon as the signal is converted to a digital form (Bronzino, 1999).

Due to storage requirements, real-time computer recordings are useful only when the EEG is instantaneously processed or for short-term recordings. A sampling rate of 256 Hz of the 16-bit A/D converter produces 256 new data points every second. An EEG sample with a duration of 16 s contains 4096 data points, whereas a recording period of 1 h produces 921,600 points. Therefore, computer memory turns out to be an important aspect for deciding on the number of channels of EEG activity and the time length in online computer recording applications. However, additional data processing may include (Bronzino, 1999):

- compression for more effective storage;
- producing reduced features set containing only the data of interest;
- feature extraction followed by pattern recognition.

2.1.7 The EEG Measured on the Scalp

The cerebral cortex's group electrical activity is generally denoted as a rhythm due to its oscillatory, repetitive behavior. We cannot quantify the electrical activity of a particular neuron using electrodes on the scalp. The electrical signal is weakened as it propagates toward the electrodes through dense tissue layers. However, we can measure the combined activity of billions of neurons, resulting in a suitably strong electrical field at a depth of several millimeters. Currents flowing during synaptic excitation of the dendrites primarily generate this electrical field. Numerous different EEG rhythms exist. Degrees of concentration, waking, and sleeping are some of the states of a subject affecting these rhythms. The rhythms are conventionally characterized by their relative amplitude and frequency range. The degree of synchronization between the neurons influences the amplitude of the EEG signal. During synchronous excitation, the signals from individual neurons will be summed producing a large amplitude signal on the scalp. A rhythmic EEG signal, having large amplitudes at a certain rate, is produced as a result of repetitive synchronous excitation. In contrast, an arrhythmic look of the EEG with low amplitudes is a result of asynchronous excitation of the neurons and not the number of neurons. Therefore, different EEG amplitudes depend on the time distribution of the neuronal input (Sörnmo & Laguna, 2005).

The thalamus, a part of the brain with neurons possessing pacemaker properties, is partially responsible for the oscillatory rate of an EEG rhythm. These neurons possess the inherent capability to produce a rhythmic firing pattern. Organized interactions between neurons in a specific area of the cortex, such as a feedback mechanism that may happen in a neuronal network, are another reason for the rhythmic behavior. Low frequency/large amplitude rhythms are related to sleepiness and sleep states with no dreaming, whereas high frequency/low amplitude rhythms are related to awareness and dream sleep. This relationship is logical because, when the cortex is involved in information processing whether produced by sensory input or by some internal procedure, the activity level of cortical neurons is comparatively high but comparatively unsynchronized. In other words, each neuron, or very small group of neurons, is dynamically included in a slightly dissimilar feature of a complicated cognitive task; it fires rapidly but not quite at the same time as most of its neighbors. This achieves low synchrony; hence the EEG amplitude is small. On the other hand, during deep sleep, cortical neurons are not involved in information processing, and large numbers of them are phasically excited by a common, rhythmic input. In this circumstance, synchrony is higher; hence the EEG amplitude is large (Bear, Connors, & Paradiso, 1996). Despite several hypotheses, the meaning of various brain rhythms basically remains unclear. However, a really convenient clinical methodology in exploring functional states of the brain lies in the quantification of EEG rhythm characteristics (Sörnmo & Laguna, 2005).

2.1.8 EEG Rhythms and Waveforms

Signals recorded from the scalp have a frequency content not exceeding 40 Hz and amplitudes in a microvolt range up to nearly 100 μV. EEC rhythms are conventionally categorized into five frequency bands. The understanding of these bands depends on the mental state of the subject and his or her age. For instance, the EEG of an adult is significantly different from that of a newborn, containing noticeably lower frequencies. The frequency bands listed in the following section offer a clinically useful classification of different rhythms (Sörnmo & Laguna, 2005), although they are somewhat imprecise (the definitions of bands are taken from Niedermayer (1999c).

Delta rhythm (up to 4 Hz). The delta rhythm has a large amplitude, is usually perceived during deep sleep, and unobserved in the awake normal adult. However, it can be observed in an unhealthy adult, indicating brain disease (encephalopathy) or cerebral damage.

Theta rhythm (4–7 Hz). The theta rhythm arises in certain sleep stages and during sleepiness.

Alpha rhythm (8–13 Hz). The alpha rhythm is most noticeable in relaxed and awake normal subjects with closed eyes. If the eyes are open, this activity is inhibited. Therefore, the occipital regions are areas of the brain where this rhythm has the largest amplitude.

Beta rhythm (14–30 Hz). The beta rhythm, a fast rhythm with low amplitude, is mostly observed in the central and frontal regions of the scalp during some sleep stages.

Gamma rhythm (greater than 30 Hz). The gamma rhythm is associated with active information processing state of the cortex. This rhythm can be observed during finger movements with an electrode at the sensorimotor area connected to a high-sensitivity recording device.

One rhythm does not exist all the time. During long time intervals, an arrhythmic look of the EEG may prevail. Some of these rhythms (primarily gamma rhythms) last only for a few seconds, whereas most of them can last up to a number of minutes (Sörnmo & Laguna, 2005).

Spikes and sharp waves (SSWs) represent transient waveforms with an unpredictable temporal pattern (uncontrollable activity). They point to abnormal neuronal activities that can be usually found in patients with epileptic seizures (Niedermayer, 1999a). Therefore, SSWs are usually denoted as interictal (normal) because they arise between ictal (seizure) events. Both types of waveforms are normally described as having a sudden initial upstroke, with its duration as the only difference. A sharp wave has a duration in the range 70–200 ms, whereas a spike is no longer than 70 ms. Specific artifacts such as cardiac activity can affect a normal EEG so a heartbeat can sometimes be incorrectly classified as SSWs (Sörnmo & Laguna, 2005). Spikes can arise in numerous types of runs or as isolated events. Those runs are denoted as spike-wave complexes consisting of a spike accompanied with a slow wave (Niedermayer, 1999a). Spike-wave complexes take place at rates less than 6 Hz.

Sleep rhythms: The brain has three vital functional states: conscious state (awake or alert state), sleep without rapid eye movement (REM), and sleep with REM. These two sleep states occur numerous times throughout the night. Non-REM sleep represents an "idle" state during which the brain rests and relaxes. A great synchrony between neurons results in slow, large amplitude EEG rhythms during non-REM sleep (Sörnmo & Laguna, 2005). According to the sleep depth, we can divide non-REM sleep state into four different phases (Table 2.1).

TABLE 2.1 Characteristics of Four Non-REM Sleep Phases and REM Sleep

Phase	Depth	Waveforms
1	Sleepiness	Alpha dropout, vertex waves
2	Light sleep	Vertex waves, spindles, K-complexes
3	Deep sleep	Slowing, K-complexes, some spindles
4	Very deep sleep	Slowing, some K-complexes
REM	REM sleep	Desynchronization with faster frequencies

Several transient waveforms characterizing different sleep phases may occur: vertex waves, sleep spindles, and K-complexes. Vertex waves arise during the first two non-REM sleep phases (drowsiness and light sleep) and represent reactions to outside stimuli such as sounds. Sleep spindles represent eruptions of alpha-like activity shorter than a second. The K-complexes are a combination of sleep spindles and vertex waves. REM sleep represents an active state during which the brain is most likely occupied with dreaming. Thus, the EEG during REM sleep looks a lot like the EEG of the waking brain with present beta rhythms. The unbalanced rapid movement of the eyes with closed lids generates a sawtooth pattern in the EEG that can be acquired if the electrodes are located near the eyes. Ictal EEG, characterized by an irregular rhythm with a rapid increase in amplitude, represents the EEG during an epileptic seizure. Additionally, a rapid change in frequency evolving into a spiky wave rhythm indicates the onset of a seizure. The ictal EEG may show significant changeability from seizure to seizure. Therefore, the manual or automatic detection of epileptic seizures is quite a challenging task (Sörnmo & Laguna, 2005).

The EEG has demonstrated its power in monitoring and diagnosing several diseases or disorders such as:

- Epilepsy
- Alzheimer disease
- Huntington's disease
- Sleep disorders
- Brain-computer interface (BCI)

2.1.9 Uses of EEG Signals in Epileptic Seizure Detection and Prediction

EEG analysis has improved considerably with the extensive use of mathematical modeling and machine learning tools. Machine learning tools have also enabled

the classification of patterns within the EEG to enhance recognition, making EEG signals valuable for recognition of brain disorders and primary pathologies. Therefore, several studies on the characteristics of EEG signals related to neurological diseases have been carried out (Begg, Lai, & Palaniswami, 2007).

Epilepsy is a neurological disorder that affects more than 50 million people worldwide. It is the second most common neurological disorder (D'Alessandro et al., 2003) after stroke. Epilepsy is a severe disease characterized by temporary changes in the bioelectrical functioning of the brain. These fluctuations cause irregular neuronal synchronization and seizures that affect awareness, sensation, or movement. Epileptic seizures are triggered by extremely synchronized activity of large groups of neurons. Among the wide spectrum of mechanisms that result in such a pathologic activation are brain injuries of various types, physical abnormalities of the cerebral cortex, and physiological conditions resulting in network excitability changes. Depending on the localization and extent of ictal epileptic activity, epileptic seizures can cause a variety of temporary changes in perception and behavior (Meier, Dittrich, Schulze-Bonhage, & Aertsen, 2008). Epileptic seizures represent unexpected bursts of wild electrical activity in a group of cerebral cortex neurons. Due to the location of the focus (origin) of the electrical activity and sequential enrollment of various brain regions, epileptic seizures may manifest in numerous ways. For instance, some sort of auditive or visual sensation follows seizures that has its focus located in the sensory regions of the cortex. A group of neurons with reduced functionality is referred to as the epileptic focus (Sörnmo & Laguna, 2005).

Seizure EEG signals contain characteristic patterns that health professionals use to distinguish them from normal (nonseizure) EEG signals. Therefore, their detection may be used to respond to a forthcoming or ongoing seizure. Also, automated recognition techniques have been tested to decrease the amount of data and enable quicker and more accurate detection of the pathological EEG waveforms that characterize epileptic seizures. In addition, a few techniques have been suggested to identify spikes in the EEG to predict epileptic events (Begg et al., 2007).

During normal conditions, we have a stable relationship between inhibitory and excitatory signals. The former signals prevent neurons from firing and thus decrease the brain's electrical activity, whereas the latter signals force neurons to fire. Nonetheless, an important cause of epilepsy lies in an impaired balance between these two actions. The reason for producing this imbalance or unstable condition hides inside the neurotransmitters responsible for chemical transfer of the signals in the synapse. Consequently, bursts of wild electrical activity will arise when the inhibitory neurotransmitters are inactive, or the excitatory ones are excessively active. This neurotransmitter imbalance can be improved by increasing inhibitory activity or decreasing excitatory activity, which is the main challenge of antiepileptic drugs (Sörnmo & Laguna, 2005).

Epileptic seizures, although rarely causing long-lasting injuries or death, may result in loss of consciousness or cause slight mental confusion. Seizures possess an extremely variable time duration and rate of occurrence. Their duration may range from several seconds to several minutes. There are epileptic patients who experience just a few seizures during their entire life, whereas some of them have several seizures during a single day. Therefore, Niedermayer (1999b) created a scheme to classify seizures into groups based on EEG characteristics. Groups are formed based on the epileptic seizure focus (origin): primary generalized seizures include the whole brain, yet partial seizures start in a limited brain area. The latter group is associated with a single epileptic focus, which cannot be said for the former group. Therefore, we can treat some partial seizures by eliminating a small part of the cortex during surgery. To make sure we correctly bordered the location of the epileptic focus, a series of very systematic and in-depth studies and examinations must be carried out before surgery. A partial seizure may sometimes progress to other brain areas. Such seizure is denoted as a partial seizure with secondary generalization (Sörnmo & Laguna, 2005).

Pathological conditions such as brain injury and tumors, stroke, infections, and genetic factors may all cause epilepsy. But the exact cause of epilepsy cannot be determined for most epileptic patients. Although imaging techniques such as MRI can identify physical defects of the brain, EEG grew into the routine procedure for epilepsy diagnosis. In a fairly silent and dark room, a subject's EEG is recorded for 30 minutes in clinical investigation. To examine the changes in the EEG associated with light, the subject is requested to open and close the eyes. Finally, two activation methods are used to provoke waveforms related to epilepsy. The subject is faced with a flashing strobe light (photic stimulation) or told to breathe quickly and deeply (hyperventilation). Sleep deficiency may also be taken into account. The EEG acquired in clinical investigation may point toward seizures, even though that EEG is often recorded between seizures (the interictal EEG). The manifestation of SSWs in one of the brain's lobes may indicate that partial seizures started in that specific lobe. Likewise, the existence of primary generalized seizures may be spotted if spike-wave complexes are present in both brain hemispheres (Sörnmo & Laguna, 2005).

It is usually required to record the EEG during long periods to catch an ictal EEG. In this situation, the subject is often captured on film in the hospital for a few days. The neurologist can therefore draw a parallel between EEG and visual recordings to improve judgment. This form of recording is denoted as a video EEG. Another form of recording can be carried out at home during at least one day and is denoted as an ambulatory EEG. The EEG is

recorded during daily situations using a small digital recording device positioned on a belt around the subject's stomach (Waterhouse, 2003). This is a cheaper method than video EEG and contains both sleeping and waking phases. Itching is occasionally caused because several electrodes need to be attached to the scalp for a long time. If the subject scratches the head, a noise is introduced into the EEG recording. Noise can also be caused by blinking or grimacing, which may sometimes look like waveforms of a physiological origin making the analysis of an ambulatory EEG quite difficult (Sörnmo & Laguna, 2005).

Health specialists use distinctive patterns within ictal (seizure) EEG waveforms to differentiate them from interictal (nonseizure) EEG waveforms. Any form of long-term EEG monitoring creates huge amounts of data as a result. This data requires a lot of time to be properly analyzed. To reduce the amount of data and allow quicker and better detection of abnormal EEG signals related to epileptic seizures, automatic detection systems have been tested. Moreover, a few methods have been suggested to predict epileptic seizures by discovering spikes in the EEG. Several signal-processing techniques that consider the mathematical representation of interictal and ictal data are essential for the design of these detection algorithms (Khan & Gotman, 2003). Noise and artifact elimination is an additional factor that should be taken into consideration. An effective seizure prediction algorithm may warn a patient wearing an ambulatory recording device to consider proper security actions before the seizure occurs (Sörnmo & Laguna, 2005).

A medical application designed to control seizures is comprised of two systems (Winterhalder, Maiwald, Voss, & Aschenbrenner-Scheibe, 2003):

- A seizure prediction algorithm that raises an alarm when it senses an upcoming seizure
- A system that acts to control a seizure

Systems that control seizures include an effective anticonvulsive agent in the epileptic focus or electrical stimulation of the vagus nerve (Elger, 2001). Moreover, one simple alert of an upcoming seizure may be enough for a patient to leave dangerous situations or actions, such as climbing stairs or playing sports. For further development of seizure prediction approaches, three limitations must be addressed (Maiwald et al., 2004).

Valuation measures of seizure prediction approaches differ; also the term "seizure prediction" is not explicitly defined. Researchers haven't paid too much attention to the dependency between sensitivity and the false prediction rate or specificity because the performance of many prediction approaches is characterized only by the sensitivity. High sensitivity is one of the goals when developing seizure prediction methods. A missed alarm for a seizure may cause dangerous situations. However, a lot of false predictions may cause side effects as a result, for example, delivering too much medication or electrical stimulation. A patient may also be unaccepting of a seizure-warning device and stop using it. Therefore, satisfactory sensitivity and specificity must be achieved by seizure-prediction methods. A valuation of several algorithms has shown that high prediction sensitivity cannot be achieved without accepting low specificity (Aschenbrenner-Scheibe et al., 2003; Maiwald et al., 2004; Winterhalder et al., 2003). Comparing the performance of prediction methods is quite difficult because they have been developed and tested on different EEG databases.

Seizure prediction is still qualified as a "long and winding road" regardless of the decades of research (Mormann, Andrzejak, Elger, & Lehnertz, 2007). Generally, seizure prediction methods are based on the extraction of EEG features calculated over a short time window of a few seconds to a few minutes. There exist univariate measures, calculated separately for each EEG channel, and bivariate (or multivariate) measures, which quantify some relationship between two or more EEG channels. Many univariate features have been investigated for seizure prediction (Esteller et al., 2005; Harrison, Frei, & Osorio, 2005; Jerger, Weinstein, Sauer, & Schiff, 2005; Jouny, Franaszczuk, & Bergey, 2005). However, none have succeeded in that task, proving the superiority of bivariate measurements for seizure prediction (Mormann, Kreuz, Rieke, Andrzejak, & Kraskov, 2005).

EXAMPLE 2.1 The following MATLAB code was used to plot normal and epileptic EEG signals. For this example, Bonn EEG dataset will be used. You can download the data from the following website: http://epileptologie-bonn.de/cms/front_content.php?idcat=193&lang=3&changelang=3

Dataset Information: This epilepsy dataset is the widely used EEG dataset that has five sets denoted A–E, each containing 100 single-channel EEG segments of 23.6-s duration. Sets A and B are composed of segments taken from EEG recordings of five healthy volunteers employing a standardized electrode placement scheme (cf. Fig. 2.2). Subjects were relaxed in an awakened state with eyes open (A-Z.zip) and eyes closed (B-O.zip), respectively. Sets C-N.zip, D-F.zip, and E-S.zip were created from an EEG archive of presurgical diagnosis. EEG data collected from subjects who had attained complete seizure control after resection of one of the hippocampal formations were properly identified to be the epileptogenic zone. Set D was taken from the epileptogenic zone and those in set C from the hippocampal formation of the opposite hemisphere of the brain. Although sets C and D include only activity recorded during seizure-free intervals, set E only includes seizure activity. Here, segments were chosen from all recording

revealing ictal activity. After 12-bit analog-to-digital conversion, the data were sampled at 173.61 Hz. Band-pass filter settings were 0.53–40 Hz (12 dB/oct.). Exemplary EEGs are depicted in Fig. 2.3. The following MATLAB code is used to plot each signal:

```
%% Ch2_EX_1.m
clc
clear
%Load Sample EEG Data downloaded from the web site
%http://epileptologie-bonn.de/cms/front_content.php?idcat=193&lang=3&changelang=3
load AS_BONN_ALL_EEG_DATA_4096.mat

%Plot Normal EEG Signal
subplot(2,1,1);
plot(A(:,1));
title('Normal EEG Signal')
ylabel('Amplitude')
axis ([0 4096 -inf inf])

%Plot Epileptic Seizure
subplot(2,1,2);
plot(E(:,1))
title('Epileptic Seizure')
xlabel('Samples')
ylabel('Amplitude')
axis ([0 4096 -inf inf])
```

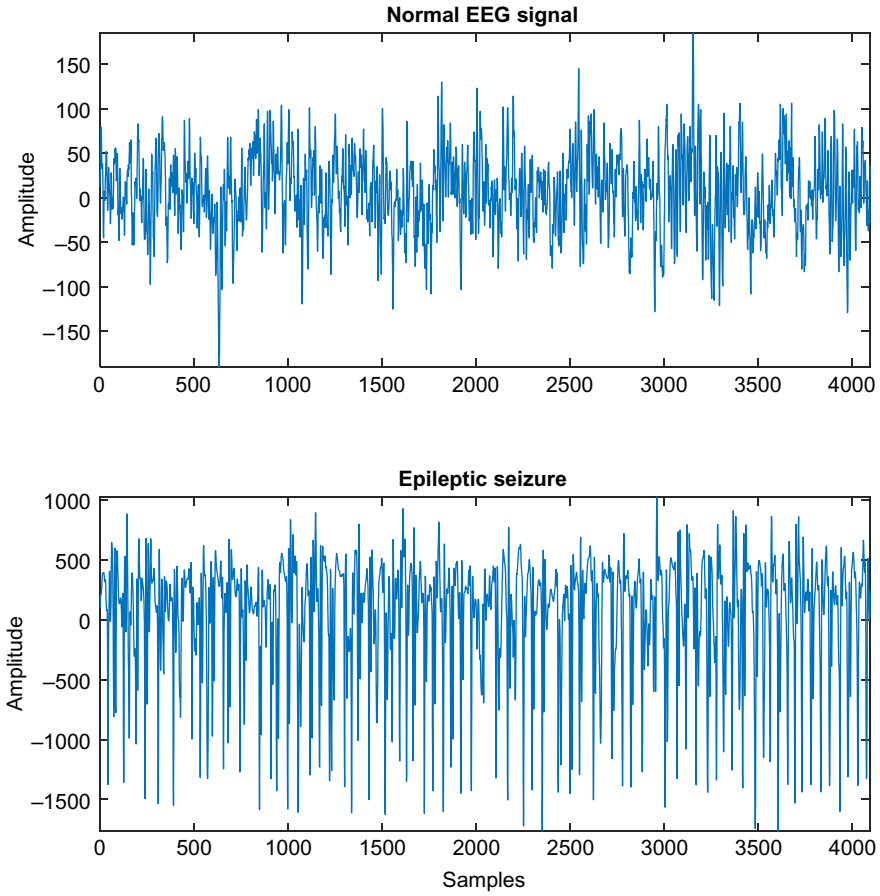

FIG. 2.3 Drawing of normal EEG signal and seizure activity.

EXAMPLE 2.2 The following MATLAB code was used to plot the interictal, preictal, and ictal EEG signals. For this example, EEG dataset collected at the Children's Hospital Boston was used. You can download the data from the following website: https://www.physionet.org/pn6/chbmit/

Dataset Information: This database, collected at the Children's Hospital Boston, consists of EEG recordings taken from pediatric subjects with intractable seizures. Recordings, grouped into 23 cases, were recorded from 22 subjects (5 males, ages 3–22; and 17 females, ages 1.5–19). All signals were sampled at 256 Hz with 16-bit resolution. The international 10–20 system of EEG electrode positions and nomenclature was employed for these recordings. In a few records, other signals are also recorded, such as an ECG signal and a vagal nerve stimulus (VNS) signal. The file RECORDS includes a list of all 664 .edf files involved in this collection, and the file RECORDS-WITH-SEIZURES lists the 129 of those files that contain one or more seizures. Exemplary EEGs are depicted in Fig. 2.4. The following MATLAB code is used to plot each signal:

```
%% Ch2_EX_2.m
clc
clear
%Load Sample EEG Data downloaded from the web site
%https://www.physionet.org/pn6/chbmit/
load AS_PHYSIONET_EEG_DATA.mat

%Plot INTERICTAL EEG Signal
subplot(3,1,1);
plot(EEGINTERICTAL(:,2));
title('Interictal EEG Signal')
ylabel('Amplitude')
axis ([0 2048 -inf inf])
```

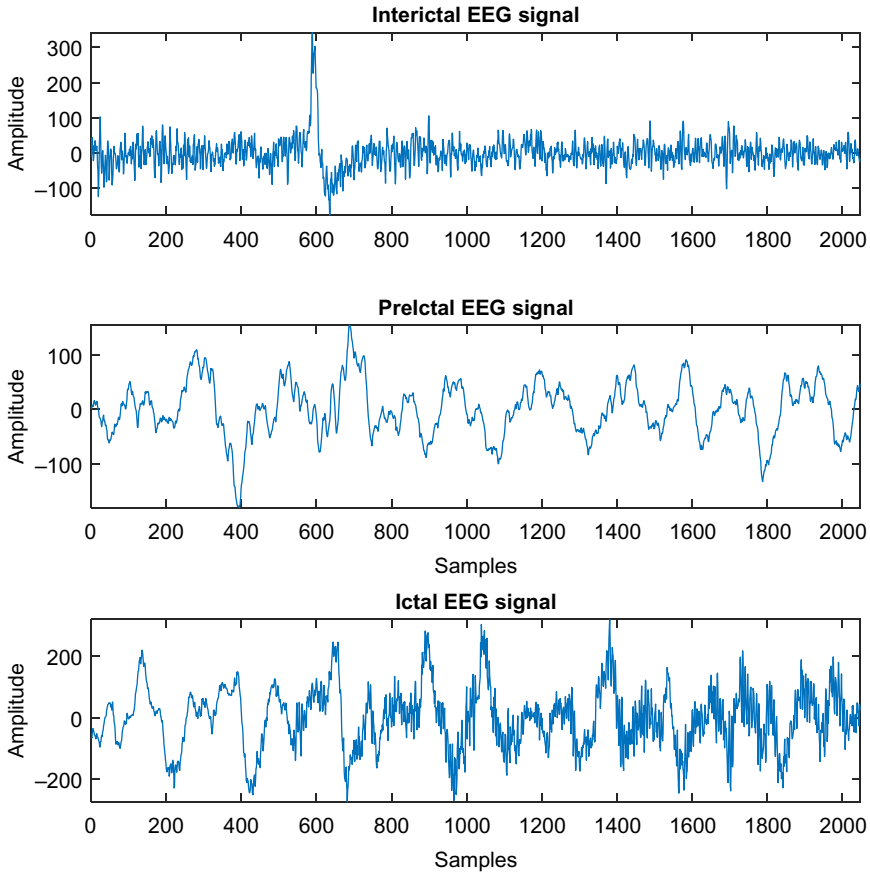

FIG. 2.4 Drawing of interictal, preictal, and ictal EEG signals.

```
%Plot PreIctal EEG Signal
subplot(3,1,2);plot(EEGPREICTAL(:,2))
title('PreIctal EEG Signal')
xlabel('Samples')
ylabel('Amplitude')
axis ([0 2048 -inf inf])

%Plot Ictal EEG Signal
subplot(3,1,3);plot(EEGICTAL(:,2))
title('Ictal EEG Signal')
xlabel('Samples')
ylabel('Amplitude')
axis ([0 2048 -inf inf])
```

2.1.10 Uses of EEG Signals in Brain-Computer Interfacing

A motor function injury can be one of the most disturbing results to the nervous system. Growth of the BCI during the last decades has enabled interactions or control of external devices such as computers and artificial prostheses with EEG. In a straightforward BCI framework, the user is trained to imagine movement of different body parts, and the computer recognizes different patterns of the simultaneously recorded EEG activity. BCI provides a link between the brain and the physical world without any physical contact. The main goal of BCI is to employ the electrical signals produced by the neurons of the brain and generate the signals necessary to control some external devices. The most imperative application is to energize paralyzed organs or bypass the disabled parts of the human body. BCI systems may appear as a unique interaction mode for people with different neuromuscular disorders, such as stroke, amyotrophic lateral sclerosis (ALS), spinal cord injury, and cerebral palsy (Sanei, 2013).

EEG signals are employed in BCI to interpret them into commands for external device control, such as computers, tablets, mobile phones, wheelchairs, and prostheses. BCI framework offers a new connection between the brain and the world that circumvents the human body. Hence, this framework can be employed to improve the life-quality of people with disabilities (Gao, Guan, Gao, & Zhou, 2015). BCI systems are conventionally implemented to support people who have different anomalies such as a locked-in state. Because locked-in patients are reliant on others, BCI can offer them better quality of life with greater autonomy. Recently, researchers were interested in different applications of BCI technology to enhance neurorehabilitation for people with strokes and other chronic disorders (McFarland & Wolpaw, 2017).

The main goal of EEG signal processing in BCI is to implement a framework to create an interaction between a person and an external device such as a robotic arm, a wheelchair, or a speller without physical contact. Such a framework can help handicapped people and enable them to perform their regular activities. Actually, the disease does not affect cognitive functions such as seeing, hearing, and understanding what is occurring, but it affects the control of muscles. Any normal way of interaction with the environment is lost when the motor pathway is lost. BCI offers an option for communication in such situations. Hence, a BCI is a direct interaction between the brain and a machine/computer receiving instructions directly from the brain without physical involvement (Graimann, Allison, & Pfurtscheller, 2009). Fig. 2.5 represents EEG-controlled assistive devices.

BCI systems are categorized as invasive (intracranial) and noninvasive in terms of signal acquisition. Noninvasive BCI systems employ EEG signals to interpret a subject's thoughts or intentions into a device-control signal that enables a disabled person to interact with a computer, wheelchair, or prosthesis. The mental practice of hand or foot movement can be achieved by motor imagery (MI) without executing it (Zarei, He, Siuly, & Zhang, 2017). P300 event-related potential (ERP) (da Silva-Sauer, Valero-Aguayo, de la Torre-Luque, Ron-Angevin, & Varona-Moya, 2016; Gao et al., 2015; Lafuente, Gorriz, Ramirez, & Gonzalez, 2017; Lee & Kim, 2018; Sellers, Krusienski, McFarland, Vaughan, & Wolpaw, 2006; Shahriari & Erfanian, 2013), slow cortical potentials, oscillations in alpha and beta range (Guger et al., 2001; Pfurtscheller et al., 2006), and steady-state visual evoked potentials (SSVEP) (Zhang, Guan, & Wang, 2008) have been employed in BCI systems. The common BCI technique is the P300-based ERP, which happens about 300 ms after an occasional or substantial stimulus is received (da Silva-Sauer et al., 2016; Wolpaw, Birbaumer, McFarland, Pfurtscheller, & Vaughan, 2002). Most of the time, MI approaches are used for BCI systems based on oscillations to produce event-related synchronization (ERS) and event-related desynchronization (ERD) in the α and β frequency bands of the EEG. These kinds of BCI

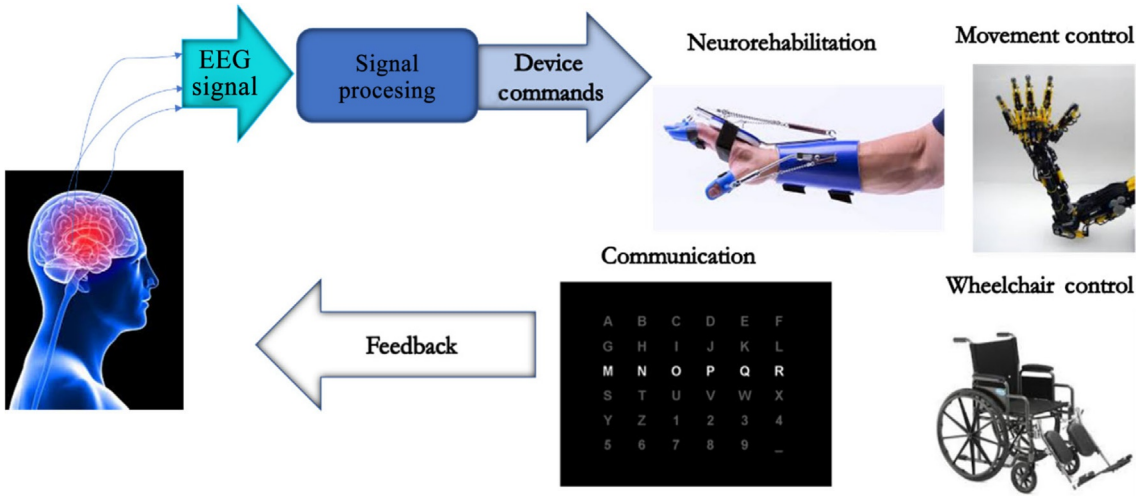

FIG. 2.5 Representation of EEG-controlled assistive devices.

systems are employed for navigation of wheelchairs or cursor control on computer screens. Consequently, many MI-based BCI methods such as foot movement, left/right hand movement, tongue movement, and/or mental counting are implemented. Flickering lights, which carry EEG oscillations with the same frequency as the stimulation source, are employed in SSVEP-based BCI systems. SSVEP schemes employ different stimulation frequencies to control robots or mobile phones. On the other hand, P300-based BCI systems employ the P300 component in the EEG to generally enhance the communication speed of spelling devices (Guger et al., 2009). The computer's actions can be controlled by the subject's thoughts after the training phase. Hence, BCI systems mainly employ EEG signals to control a wheelchair, a robotic arm, or a computer cursor (Sanei, 2013). Farwell and Donchin (1986) initially implemented a BCI system that employed the oddball paradigm to allow the subject to spell words on a computer by successively selecting alphabet letters. In this model, all the alphabet letters and other useful symbols are displayed on the computer screen allowing the subject to select a required character by visually concentrating on the relevant cell for a short time; in the meantime, the column or row representing the focused cell flashes producing a P300 component in the EEG (Shahriari & Erfanian, 2013).

BCI constructed on selective attention needs peripheral stimuli, which can be diverse tangible stimulations, different tones, or flashing lights with different frequencies. In an archetypal BCI system, each stimulus is used to control the BCI system. The subject should pay attention to the related stimulus to choose a command. Visual attention can be realized with P300 potentials or SSVEPs. A P300-based BCI system employs stimuli of flash sequence, which are generally letters or symbols used to control a robot arm, mobile robot, or cursor. Discriminatory attention to a definite flashing letter or symbol produces a brain pattern termed P300 seen about 300 ms after the stimulus. This P300 is detected by the BCI system to define the letter or symbol the user selected (Graimann et al., 2009).

Limb movement or a single muscle contraction alters brain activity, and imagining the movement also alters the so-called sensorimotor rhythms. The decrease of oscillatory activity is ERD and the increase of oscillatory activity is ERS. MI is the movement imagination without performing the actual movement, forming ERD/ERS patterns. Hence, BCI can control by imagining right hand, left hand, feet, and tongue movements. MI BCI is an ability that must be learned contrary to the BCI based on selective attention, and it does not depend on external stimuli (Graimann et al., 2009). Hence, it is crucial to correctly recognize distinct MI classes associated with a realized task using classification methods, because an MI-based BCI system converts the subject's motor intention into a command signal by means of MI states (Siuly, Li, & Zhang, 2016).

EXAMPLE 2.3 The following MATLAB code is used to plot right hand and foot imagery EEG signals. For this example, BCI Motor Imagery Dataset IVa from the BCI competition will be used. You can download the data from the following website: http://www.bbci.de/competition/iii/

Dataset Information: This dataset was taken from five healthy subjects. Subjects were seated in a relaxed chair with arms resting on armrests. This dataset includes only data from the four initial sessions without feedback. Visual cues indicated which of the following three motor imageries the subject should perform for 3.5 s: (L) left hand, (R) right hand, (F) right foot. The presentation

of target cues was intermitted by periods of random length, 1.75–2.25 s, where the subject could relax. There were two types of visual stimulation: (1) targets were designated by letters seeming behind a fixation cross and (2) a randomly moving object designated targets. From subjects al and aw, two sessions of both types were acquired, whereas from the other subjects, three sessions of type (2) and one session of type (1) were acquired. Continuous EEG signals are collected from 118 channels, and markers designated the time points of 280 cues for each of the five subjects (aa, al, av, aw, ay). Only cues for the classes "right" and "foot" are provided for the competition. The EEG signals were recorded by employing BrainAmp amplifiers and a 128-channel Ag/AgCl electrode cap from ECI. 118 EEG channels were measured at positions of the extended international 10/20 system. Signals were band-pass filtered between 0.05 and 200 Hz and then digitized at 1000 Hz with 16-bit (0.1 μV) accuracy. The downsampled EEG signals at 100 Hz also exist. The data was collected and prepared by Dornhege, Blankertz, Curio, and Muller (2004). Exemplary EEGs are depicted in Fig. 2.6. The following MATLAB code was used to plot each signal:

```
%% Ch2_EX_3.m
clc
clear
%BCI Competition III Data Set IVa
%Load Sample EEG Data downloaded from the web site
%http://www.bbci.de/competition/iii/
load BCI_III_IVa_aa_train.mat

%Plot Right Hand Imagery Movement EEG Signal
subplot(2,1,1);
plot(w(111,:));
title('Right Hand Imagery Movement EEG Signal')
ylabel('Amplitude')
axis ([0 350 -inf inf])

%Plot Foot Imagery Movement EEG Signal
subplot(2,1,2);
plot(w(112,:))
title('Foot Imagery Movement EEG Signal')
xlabel('Samples')
ylabel('Amplitude')
axis ([0 350 -inf inf])
```

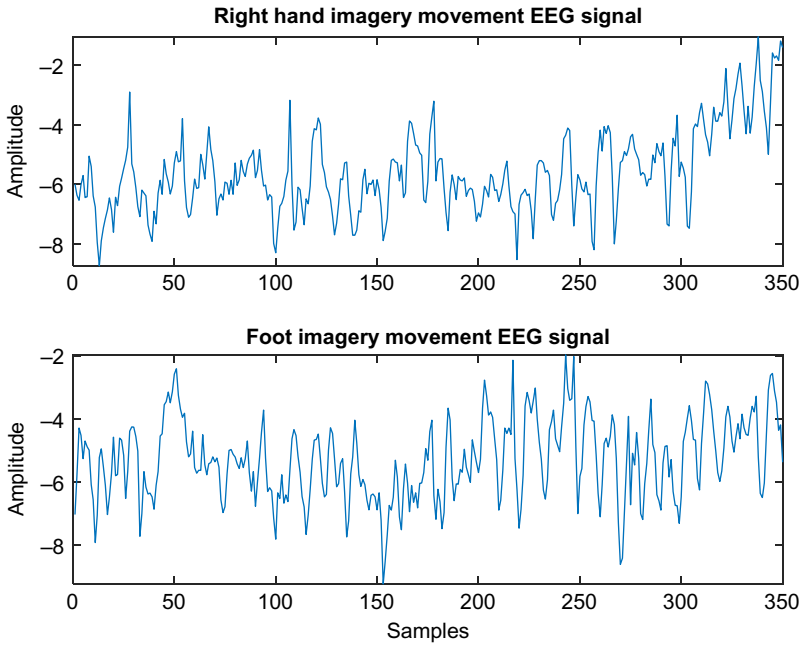

FIG. 2.6 Drawing of right hand and foot imagery EEG signals.

2.1.11 Uses of EEG Signals in Migraine Detection

Migraine is a persistent neurological disorder with highly severe symptoms such as throbbing pain in one or both sides of the brain and sensitivity to the light. Importantly, it is the third most prevalent disease, affecting one in every seven persons. It is worth mentioning that the migraine is globally ranked as the seventh most disabling disease and the first among the neurological disorders (Trust, 2014). However, migraine would often be misdiagnosed due to its overlapping symptoms with other diseases such as tension headache, epilepsy, and strokes. In the past decades, a plethora of studies have been conducted aimed at highly accurate migraine identification. One particular method from these studies has already shown promising results, which is flash stimulation. The basis for this approach is the analysis of the subject's neural responses, recorded with multichannel EEG under flash stimulation at different frequencies for variable amounts of time in seconds (Akben, Subasi, & Tuncel, 2010).

EXAMPLE 2.4 The following MATLAB code is used to plot each EEG signal. For this example, Healthy and Migraineur EEG data collected from Neurology Department at Kahramanmaras Sutcu Imam University was used.

Dataset Information: An 18-channel (10–20 system) Nicolet One Machine was used to record the data. EEG data was collected from Neurology Department at Kahramanmaras Sutcu Imam University from migraineurs and healthy subjects. Fifteen migraineurs (two males, thirteen females) with ages ranging from 20 to 34 years (mean age ± standard deviation: 27 ± 4.4 years), diagnosed according to the diagnostic criteria proposed by the International Headache Society (IHS), and fifteen control subjects (five males, ten females) with ages ranging from 19 to 35 years (mean age ± standard deviation: 26 ± 5.3 years) participated in the experiment. The experiment was conducted in a dimly lit room. None of the participants had taken any drugs before the recordings. All participants were in the interictal (pain-free) state while in a couchant position. 10–20 EEG system used to collect the EEG data. EEG signals were collected at 256 Hz sampling frequency. Each stimulation was 30 s long at a frequency of 4 Hz. This dataset was used in (Akben et al., 2010; Akben, Subasi, & Tuncel, 2011), where a different analysis strategy was considered. Exemplary EEGs are depicted in Fig. 2.7. The following MATLAB code was used to plot each signal:

```
%% Ch2_EX_4.m
clc
clear
%Migraineur EEG Data Set
%Load Sample EEG Data
load Migraine.mat
```

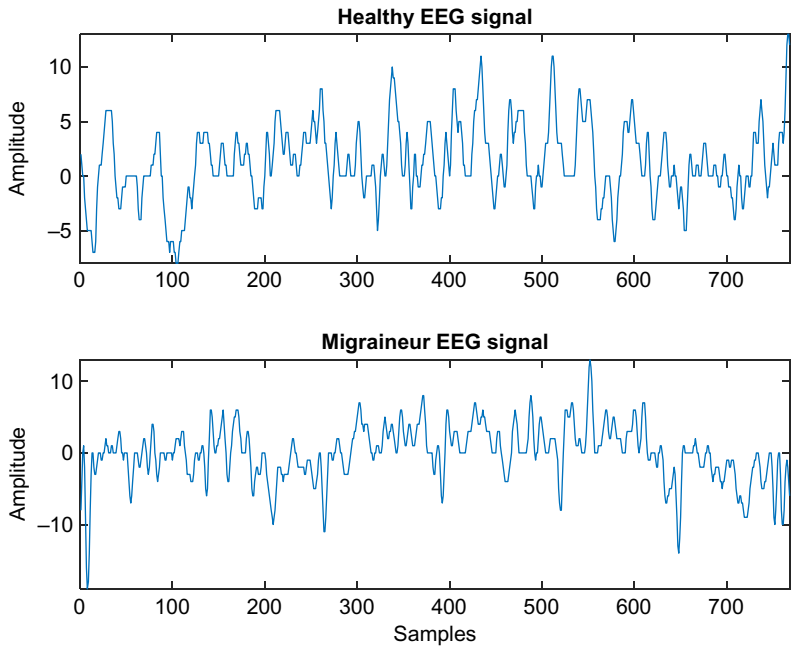

FIG. 2.7 Drawing of healthy and migraineur EEG signals.

```
%Plot Healthy EEG Signal
subplot(2,1,1);
plot(Healthy(:,1));
title('Healthy EEG Signal')
ylabel('Amplitude')
axis ([0 768 -inf inf])

%Plot Migraineur EEG Signal
subplot(2,1,2);
plot(Migraineur(:,1))
title('Migraineur EEG Signal')
xlabel('Samples')
ylabel('Amplitude')
axis ([0 768 -inf inf])
```

2.1.12 Uses of EEG Signals in Source Localization

The brain is separated into a large number of regions that produce a synaptic electric current or local magnetic field. Brain activities can be thought to create signal sources that are either spontaneous or related to the normal rhythms of the brain as a result of brain stimulation or corresponding to physical movements. Localization of brain signal sources using only EEGs has been an active area of research during the last few years. Such source localization is needed to study the brain's functional, mental, physiological, and pathological abnormalities, and even problems corresponding to various body disabilities, and finally to determine the sources of abnormalities such as tumors and epilepsy. Although general localization of brain sources is a problematic task, there are some simple circumstances in which the localization problem can be simplified and accomplished (Sanei & Chambers, 2013).

Based on the corresponding channel position that created the abnormal signals, the focus of epilepsy is defined by clinical diagnosis and surgical results. Hence, EEG is a decisive method for epilepsy evaluation (Xiaoying et al., 2012). The main issue for neurosurgery is the noninvasive initial seizure discharge localization, defining the region of the brain that is the abnormal activity source. Even though epilepsy diagnosis depends on an individual's medical history, EEG is crucial for detection and diagnosis (Xiaoying et al., 2012).

EEG signals recorded from the brain help us understand brain functions and malfunctions (Pereda, Quian Quiroga, & Bhattacharya, 2005; Stam, 2005). The goal of these records is to localize the areas of the brain in which seizures begin and to evaluate if the patient may benefit from neurosurgical resection of these brain areas. Hence, these kinds of intracranial epilepsy patient recordings are a challenging area of applications for the analysis of the signal (Lehnertz, 2008). There is an increasing indication that this interdisciplinary analysis may give helpful information about epileptic focus localization even from the seizure-free interval (Andrzejak, Chicharro, Lehnertz, & Mormann, 2011; Andrzejak, Widman, Lehnertz, David, & Elger, 2006; Varotto, Tassi, Franceschetti, Spreafico, & Panzica, 2012). This is very important, because every seizure can be a health-threatening event, and neurologists are trying to decrease the occurrence of seizures. There is increasing indication of surrogates that may be crucial for an effective evaluation of epileptic seizures from EEG recordings.

Seizure detection in EEG recordings can be helpful in epileptogenic foci localization (Robyn, Mingui, Mark, & Robert, 2000). Different methods are used to analyze the ictal EEG (Corsini, Shoker, Sanei, & Alarcon, 2006; Feldt, Osterhage, Mormann, Lehnertz, & Zochowski, 2007; Swiderski, Osowski, Cichocki, & Rysz, 2007) for seizure detection and prediction. Invasive seizures observed with depth electrode arrays may help localization of seizures. However, even with these techniques, the sources of the seizure cannot be fully defined every time by visual analysis of EEG recordings (Schlkopf & Smola, 2002). For the epileptic focus localization, analysis of EEG signals is very important (Rutkowski, Zdunek, & Cichocki, 2006; Swiderski, Osowski, Cichocki, & Rysz, 2008).

The intracranial EEG recordings taken from subjects suffering from pharmacoresistant focal-onset epilepsy were used. The aim of these signals was to determine the part of the brain to be surgically removed in an epilepsy patient. This results in two different types of signals: the first type recorded from areas of the brain where the changes of ictal EEG signal were noticed ("focal signals") and the second type recorded from areas of the brain that were not included at the seizure's onset ("nonfocal signals") (Ralph, Kaspar, & Rummel, 2012). The ictal areas might create an interictal spike at the time of its onset and, therefore, the clusters covering most spikes start at the most active zone. Localization of this zone and focus of activity in the brain determined by these spike clusters could provide evidence for exact locations of epileptogenic tissue in the surgical evaluation (Pedro et al., 2012).

EXAMPLE 2.5 The following MATLAB code is used to plot focal and nonfocal EEG signals. For this example, epileptic source localization data was used. You can download the data from the following website: http://ntsa.upf.edu/downloads/andrzejak-rg-schindler-k-rummel-c-2012-nonrandomness-nonlinear-dependence-and

Dataset Information: There are two types of files with F and N involving focal and nonfocal signal pairs, respectively. Each Zip file involves 750 separate text files. The number in the file name is related to the index of the signal pair included in this file. Every text file includes one distinct signal pair. The *x*-signal is included in the first column, and the *y*-signal is involved in the second column. Commas divide the two columns. All files have 10,240 rows. Succeeding rows are related to the subsequent samples. The files have no headers (Andrzejak, Schindler, & Rummel, 2012). Exemplary EEGs are depicted in Fig. 2.8. The following MATLAB code was used to plot each signal:

```
%% Ch2_EX_5.m
clc
clear
%Load Sample EEG Data downloaded from the web site
%http://ntsa.upf.edu/downloads/andrzejak-rg-schindler-k-rummel-c-2012-
nonrandomness-nonlinear-dependence-and
load FOCAL_NFOCAL.mat

%Plot Focal EEG Signal
subplot(2,1,1);
plot(focal(1:4096,1));
title('Focal EEG Signal')
ylabel('Amplitude')
axis ([0 4096 -inf inf])

%Plot Non-Focal EEG Signal
subplot(2,1,2);
plot(nfocal(1:4096,1))
title('Non Focal EEG Signal')
xlabel('Samples')
ylabel('Amplitude')
axis ([0 4096 -inf inf])
```

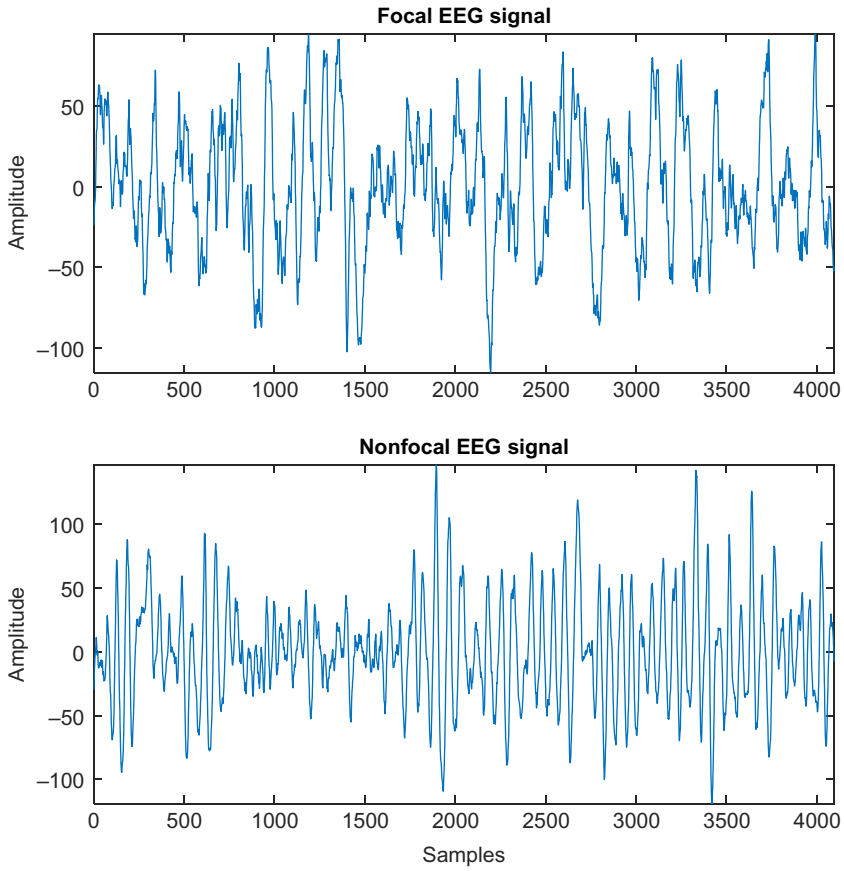

FIG. 2.8 Drawing of focal and nonfocal EEG signals.

2.1.13 Uses of EEG Signals in Sleep

Sleep is a passive condition in which the brain is separated from the rest of the body. EEG allows a researcher to collect electrical activity of the brain during sleep. Lack of sleep affects the function of the brain. With continuous lack of adequate sleep, the part of the brain that controls memory, language, planning, and sense of time can be affected, and judgment weakens. The sleep state is an imperative indication of diagnosing psychological abnormality and mental disease. Although sleep was thought to be a passive state, it is a dynamic procedure, and our brains are active during the sleep. Our mental and physical health, and immune system are affected by sleep. Brain activity during sleep and wakefulness achieves several stimulating and preventative forces produced by the brain. Sleep is essential for the brain to remain healthy. Sleep deprivation results in a drowsy individual unable to concentrate. Moreover, it causes weakening of memory and physical performance, and a reduced ability to implement mathematical calculations and other mental tasks. If sleep deprivation continues, hallucinations and mood swings might occur. Sleep deprivation has a main effect on cognitive functioning as well as on emotional and physical health. Disorders such as sleep apnea that creates extreme daytime sleepiness have been linked to high blood pressure and stress. Sleep helps individuals keep optimal emotional and social functioning while awake; during sleep, rest is given to the parts of the brain that control emotions and social interactions (Sanei, 2013).

There are two different sleep states that alternate in cycles, and each state is considered a different type of EEG activity. Sleep is composed of nonrapid eye movement (NREM) and REM sleep. NREM is further subdivided into four stages: I (drowsiness), II (light sleep), III (deep sleep), and IV (very deep sleep). During the night, the NREM and REM stages of sleep alternate. Stages I, II, III, and IV are followed by REM sleep. A complete sleep cycle from the beginning of stage I to the end of REM sleep generally takes about 1½ h. The resultant sleep is comparatively short and, for most cases, a duration of 10–30 min is enough (Sanei & Chambers, 2013).

NREM Sleep: Stage I (drowsiness) is a very light sleep and is thought as a transition between wakefulness and sleep. Drowsiness demonstrates age-dependent changes. The theta activity of late infancy and early childhood is a noteworthy representative of such ages. Later in childhood and in the decreasing years of life, the drowsiness contains a large amount of slowed activity mixed with the posterior alpha rhythm. However, gradual or abrupt alpha dropout in adults represents the onset of drowsiness. Deep drowsiness contains the appearance of vertex waves. Before the appearance of the first spindle trains, vertex waves occur in the transition from stage I to II. A vertex wave is a compound potential, a small spike discharge of positive polarity followed by a large negative wave that is a typical discharge wave. It might happen as an isolated event with larger amplitude than a normal EEG. In old persons, they become small, inconspicuous, and hardly visible. Another indication of deep drowsiness is the positive occipital sharp transients (POST) of sleep. Spindles (sigma activity) happen mainly in the frontal lobe of the brain. They are recognized as a group of rhythmic waves represented by gradually increasing, then progressively decreasing amplitude. Stage II of sleep arises throughout the sleep period and signifies 40%–50% of the total sleep time. During stage II, brainwaves slow down with infrequent bursts of rapid waves. There is no eye movement during this stage. Slow frequencies ranging from 0.7 to 4 Hz are generally predominant; their voltage is high, with a very prominent occipital peak in small children that gradually falls as age increases. K-complexes occur in stage II and create a substantial response to arousing stimuli. For wave morphology, the K-complex contains an initial sharp component, followed by a slow component that fuses with a superimposed fast component. In stage III, delta waves begin to appear. They are combined with smaller and faster waves. Sleep spindles still exist around 12–14 Hz but progressively vanish as the sleep becomes deeper. In stage IV, delta waves are the main waves seen in the brain. Delta or slow wave sleep (SWS) cannot be recognized easily during routine EEG. Stages III and IV are generally differentiated from each other by the percentage of delta activity. Both of them denote up to 20% of total sleep time. During stages III and IV, all eye and muscle movement stops. It is not easy to wake up somebody during these two stages. If somebody is awakened during deep sleep, s/he does not regulate instantly and frequently feels sleepy and confused for several minutes after waking up (Sanei & Chambers, 2013).

REM Sleep: REM sleep contains 20%–25% of the total sleep, follows NREM sleep, and occurs four or five times during a normal 8- to 9-h sleep interval. The first REM sleep interval of the night might be less than 10 min in duration, whereas the last interval can exceed 60 min. REM sleep is generally related to dreaming. During REM sleep, the eyeballs move quickly, the breathing and heart rates are quick and irregular, blood pressure increases, and there is a loss of muscle tone (paralysis). The brain is very active during REM sleep, and the whole brain metabolism might be increased by as much as 20%. EEG activity acquired in the brain during REM sleep is similar to wakefulness. As the first phase of REM cannot be seen before 60–90 min after the start of sleep, the assessment of REM sleep takes a longer waiting period. The EEG in the REM stage presents low voltage activity with a slower rate of alpha rhythms (Sanei & Chambers, 2013).

Even though physical activities of body are covert to a great extent, internal brain activities during sleep have an influence that cannot be easily understood or explained. A set of highly complex patterns occurs in the human brain during sleep. Recently, a large amount of effort has been

devoted to sleep analysis studies and their relationship with other psychological states. So far, very little is known about sleep. Unfortunately, the number of subjects suffering from sleep disorders is not insignificant, and it affects subjects' everyday activities and health conditions in different ways. Objective sleep monitoring and analysis is usually done by an expert examining several sleep stages for an entire night. Currently, polysomnography (PSG) is the "paragon of excellence" in sleep analysis. PSG can be thought as a multivariate system that records several biomedical signals, such as electrooculogram (EOG), EEG, ECG, and electromyogram (EMG), simultaneously. As soon as the biomedical signals are recorded, the next common step could be to agree on how the recorded signal should be scored. Rechtschaffen and Kales (R & K) (Rechtschaffen & Kales, 1968) proposed a guide for classification of sleep that later became a gold standard and is now employed as a tool for classification of sleep stages despite its weaknesses (Himanena & Hasan, 2004; Hirshkowitz, 2000). The R & K standard was further developed by the American Academy of Sleep Medicine (AASM) (Iber, Ancoli-Israel, Chesson, & Quan, 2007). Consequently, sleep scoring differentiates wakefulness (W) and one of two sleep stages: REM and NREM. NREM can be further separated into four different stages enumerated as 1, 2, 3, and 4. Often NREM 3 and NREM 4 are combined into one sleep stage called slow-wave sleep (SWS). However, there might still be certain disagreement in manual scoring of sleep stages as a result of experts' biased decisions and training education. Thus, there is a requirement to create an objective, nonbiased, automated sleep scoring system (Alickovic & Subasi, 2018).

EXAMPLE 2.6 The following MATLAB code was used to plot different sleep stages of EEG signals. For this example, the Sleep-EDF Database (Expanded) was used. You can download the data from the following website: https://physionet.org/pn4/sleep-edfx/

Dataset Information: The PSG dataset includes hypnograms (expert annotations of sleep stages), which come from two studies. The *PSG.edf files are whole-night polysomnographic sleep recordings including EEG (Fpz-Cz and Pz-Oz channels), EOG, submental chin EMG, and an event marker; the SC*PSG.edf files involve rectal body temperature and oronasal respiration. The *Hypnogram.edf files involve annotations of the sleep patterns relevant to the PSGs. These hypnograms includes different sleep stages: W, R, 1, 2, 3, 4, M (Movement time), and ? (not scored). All hypnograms were manually scored by well-trained technicians according to the Rechtschaffen and Kales manual (Rechtschaffen & Kales, 1968). The SC* files (SC = Sleep Cassette) were taken from 79 healthy Caucasians aged 25–101 without any sleep-related medication. Two PSGs of about 20 h each were recorded during two subsequent day-night periods at the subjects' homes. The EOG and EEG sampling frequency was 100 Hz. The submental-EMG signal, oronasal airflow, rectal body temperature, and event marker were sampled at 1 Hz. The ST* files (ST = Sleep Telemetry) were obtained from 22 Caucasian males and females without other medication. Subjects had mild difficulty falling asleep but were otherwise healthy. The PSGs of about 9 h were collected in the hospital for two nights, one of which was after temazepam intake. EOG, EMG, and EEG signals were sampled at 100 Hz, and the event marker at 1 Hz. Exemplary EEGs are depicted in Fig. 2.9. The following MATLAB code was used to plot each signal:

```
%% Ch2_EX_6.m
clc
clear
%Load Sample EEG Data downloaded from the web site
%https://physionet.org/pn4/sleep-edfx/
load SC4001E0-PSG.mat

%Plot AWAKE EEG Signal
subplot(3,2,1);
plot(sleepW(:));
title('AWAKE EEG Signal')
ylabel('Amplitude')
axis ([0 256 -inf inf])

%Plot SLEEP STAGE I EEG Signal
subplot(3,2,2);
plot(sleepI(:))
title('SLEEP STAGE I EEG Signal')
xlabel('Samples')
ylabel('Amplitude')
axis ([0 256 -inf inf])
```

```
%Plot SLEEP STAGE II EEG Signal
subplot(3,2,3);
plot(sleepII(:))
title('SLEEP STAGE II EEG Signal')
xlabel('Samples')
ylabel('Amplitude')
axis ([0 256 -inf inf])

%Plot SLEEP STAGE III EEG Signal
subplot(3,2,4);
plot(sleepIII(:))
title('SLEEP STAGE III EEG Signal')
xlabel('Samples')
ylabel('Amplitude')
axis ([0 256 -inf inf])

%Plot SLEEP STAGE IV EEG Signal
subplot(3,2,5);
plot(sleepIV(:))
title('SLEEP STAGE IV EEG Signal')
xlabel('Samples')
ylabel('Amplitude')
axis ([0 256 -inf inf])

%Plot REM SLEEP EEG Signal
subplot(3,2,6);
plot(sleepR(:))
title('REM SLEEP EEG Signal')
xlabel('Samples')
ylabel('Amplitude')
axis ([0 256 -inf inf])
```

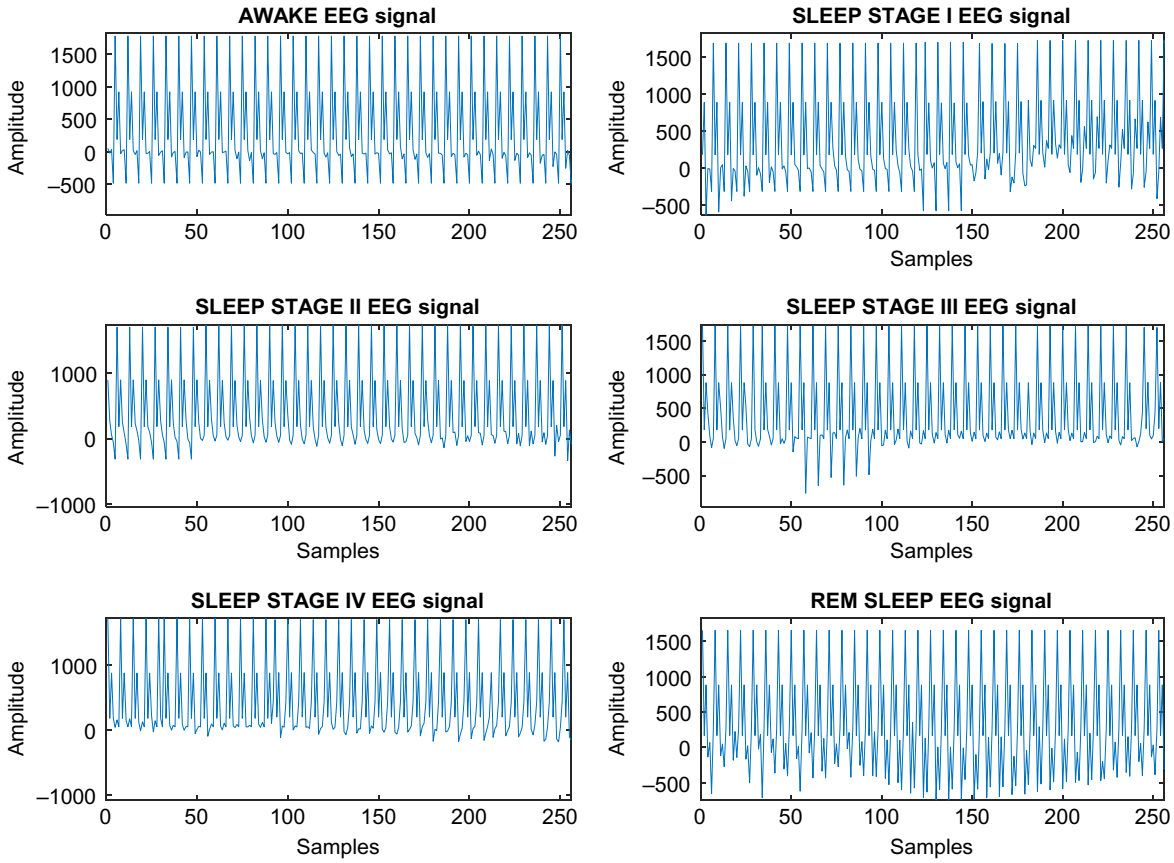

FIG. 2.9 Drawing of EEG signals of different sleep stages.

2.1.14 Uses of EEG Signal for Emotion Recognition

Emotion is a psychophysiological process activated by conscious and/or unconscious perception of a human being and is frequently related to disposition, mood, personality, temperament, and motivation. Emotions play an important role in human communication and can be expressed either verbally through emotional vocabulary or by expressing nonverbal cues such as intonation of voice, facial expressions, and gestures (Koelstra et al., 2012).

More common emotions, such as anger, happiness, surprise, fear, shame, disgust, sadness, interest, contempt, suffering, love, tension, and mirth, have been investigated by researchers in emotion understanding, control, and regulation mainly by analyzing the brain's signals and images. EEG signal processing and analysis techniques have been used for detection and recognition of emotions. Studies in engineering, computer science, neuroscience, and psychology aim to develop devices that identify human affect, and monitor and model emotions. In computer science, affective assessment is a division of the study developing machine learning that deals with the design of systems and devices for processing, interpretation, and recognition of human emotions. Therefore, new techniques can be produced to indirectly assess stress, frustration, and mood through natural interaction and conversation, or by making the computers more emotionally intelligent, especially when responding to a person's frustration in a way that reduces negative feelings, which can be a required research direction in emotion recognition and regulation. EEG helps connectivity, localization, and synchronization of the brain for different emotions to extract and process highly valuable emotion-related information. Recognition and classification of emotional EEG signals are generally complex, and advanced signal-processing methods are required (Sanei, 2013). The goal of affective computing is to fill this gap by detecting emotional cues occurring during human-computer interaction and synthesizing emotional responses. Characterizing multimedia content with relevant, reliable, and discriminating tags is vital for multimedia information retrieval (Koelstra et al., 2012)

Emotion research is an interdisciplinary field that incorporates research in computer science, psychology, neuroscience, and cognitive science. For neuroscience, researchers aim to find out the neural circuits and brain mechanisms of emotion processing. For psychology, there are numerous basic theories of emotion from different scientists, and it is imperative to create computational models of emotion. The modeling and detection of human emotions are the main studies of sentimental computing employing machine learning and pattern recognition techniques. Among numerous methods for emotion recognition, the technique based on EEG signals is more consistent because of its objective evaluation and high accuracy in comparison with other external appearance clues such as facial expression. Understanding the brain's response under dissimilar emotional states can primarily improve the computational models for emotion recognition. Several psychophysiology researches have confirmed the correlations between human emotions and EEG signals (Sammler, Grigutsch, Fritz, & Koelsch, 2007). Furthermore, with the rapid progress of wearable devices and dry electrode techniques (Chi et al., 2012; Grozea, Voinescu, & Fazli, 2011; Huang, Wu, Wong, & Lin, 2015), it is now possible to realize EEG-based emotion recognition from laboratories to real-world applications, such as driving fatigue detection and mental state monitoring (Liu, Chiang, & Hsu, 2013; van Erp, Lotte, & Tangermann, 2012; Zheng & Lu, 2015).

EXAMPLE 2.7 The following MATLAB code was used to plot EEG signals with negative, positive, and neutral emotions. For this example, SEED Emotion Recognition data was used. You can download the data from the following website: http://bcmi.sjtu.edu.cn/~seed/index.html

Dataset Information: The SEED database contains EEG signals of 15 subjects who were recorded while they were watching emotional film clips. Every subject was asked to carry out the experiments in three sessions. There were 45 total experiments in this dataset. These used emotional film clips as stimuli in the experiments. The choice of criteria for film clips were: (a) the length of the whole experiment must not be too long in case it would make subjects fatigue; (b) the videos must be understood without explanation; and (c) the videos must elicit a single desired target emotion. Different film clips (positive, neutral, and negative emotions) were selected to receive the highest match across participates. The length of each film clip was about 4 min. Each film clip was well designed to achieve coherent emotion and maximize emotional meanings. There were 15 total trials for each experiment. There was a 15 s hint before every clip and 10 s feedback after every clip. The order of demonstration was organized in a way that two film clips targeting the same emotion were not presented successively. For the feedback, participants are asked to describe their emotional reactions to every film clip by carrying out the questionnaire instantly after watching every clip. The EEG signals of each subject were saved as separate files with the name of the subjects and the date. Fifteen subjects (7 males and 8 females; Mean: 23.27, SD: 2.37) participated in the experiments. These files included a preprocessed, downsampled, and segmented version of the EEG data in MATLAB (.mat file). The data was downsampled to 200 Hz. A band-pass frequency filter from 0 to 75 Hz was applied. The EEG segments were extracted related to every movie. There are totally 45 .mat files, one for per experiment. Every person carried out the experiment three times within a week. Every subject file includes 16 arrays; 15 arrays included preprocessed and segmented EEG data of 15 trials in one experiment. An array name, LABELS, contains the label of the corresponding emotional labels (−1 for negative, 0 for neutral, and +1 for positive). The EEG was acquired according to the international 10-20 system for 62 channels. Exemplary EEGs are depicted in Fig. 2.10. The following MATLAB code was used to plot each signal:

```
%% Ch2_EX_7.m
clc
clear
%Load Sample EEG Data downloaded from the web site
%http://bcmi.sjtu.edu.cn/~seed/index.html
load EMOTIONSDAT.mat

%Plot NEGATIVE EEG Signal
subplot(3,1,1);
plot(NEGATIVE(1,:));
title('NEGATIVE EMOTION EEG Signal')
ylabel('Amplitude')
axis ([0 4096 -inf inf])

%Plot POSITIVE EEG Signal
subplot(3,1,2);
plot(POSITIVE(1,:))
title('POSITIVE EMOTION EEG Signal')
xlabel('Samples')
ylabel('Amplitude')
axis ([0 4096 -inf inf])

%Plot NEUTRAL EEG Signal
subplot(3,1,3);
plot(NEUTRAL(1,:))
title('NEUTRAL EMOTION EEG Signal')
xlabel('Samples')
ylabel('Amplitude')
axis ([0 4096 -inf inf])
```

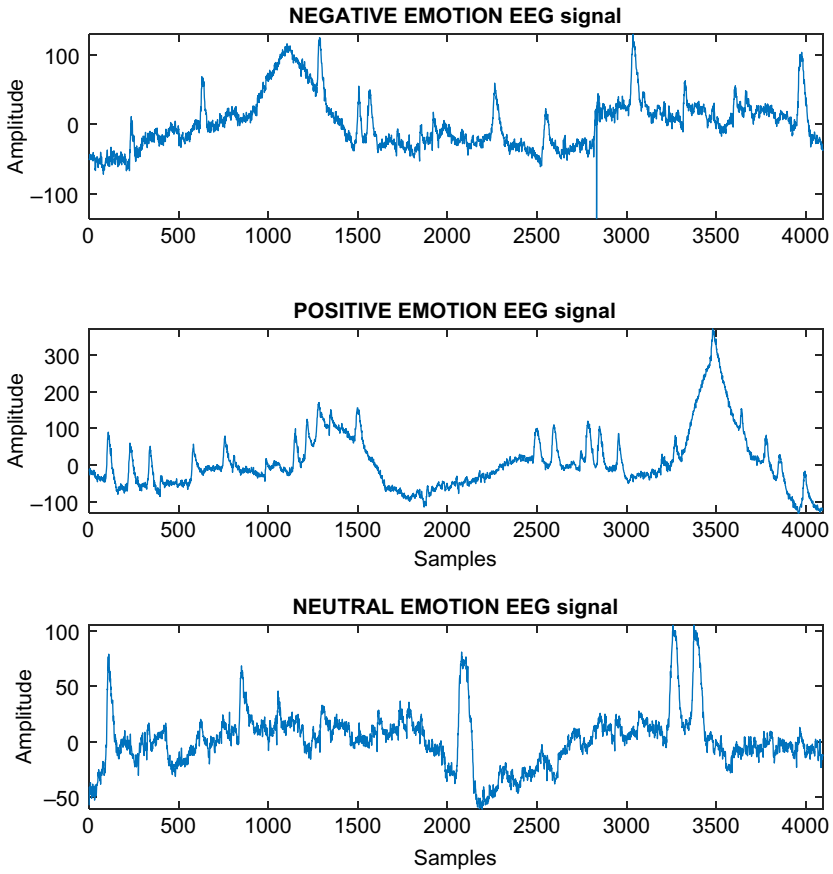

FIG. 2.10 Drawing of EEG signals with positive, negative, and neutral emotions.

2.1.15 Freiburg EEG Database for Epileptic Seizure Prediction and Detection

The Freiburg EEG database was recorded at the Epilepsy Center of the University Hospital of Freiburg, and it consists of invasive EEG recordings of 21 patients suffering from pharmacorefractory (or medically intractable) focal epilepsy. Every subject had between two and five seizures, with an average value of approximately 4.2 seizures per patient. For 21 patients, around 17 Gigabytes of EEG data is available. Totally, 88 seizures including preictal data and at least 24 h of seizure-free (interictal) data are available. More precisely, 509 h of interictal and 73 h of preictal or ictal EEG data is available. Epilepsy doctors visually inspected the EEG data to find the epileptic focus required for surgery. Recordings over several days were sampled using 60 channels with at least 256 Hz (Uni-Freiburg, 2011).

The epileptic focus was located in the hippocampus in eight patients. Eleven patients had the epileptic focus located in neocortical brain structures, whereas two patients had the epileptic focus in both. Intracranial grid, strip-, and depth-electrodes were used to record directly from focal areas. These electrodes were also responsible for obtaining fewer artifacts and high signal-to-noise ratio. Subdural electrodes were implanted via burr holes or open craniotomy, and depth electrodes were implanted stereotactically. Neurofile NT digital video EEG system with 128 channels, 256 Hz sampling rate, and a 16 bit analogue-to-digital converter was used to sample the EEG data. A notch filter removed the line noise (50 Hz). There were gaps of 1–3 s between recording blocks because recording had to be momentarily stopped for technical reasons. Every patient contains "interictal" and "ictal" datasets. The former dataset covers approximately 1 day of seizure-free EEG recordings, whereas the latter is comprised of files with epileptic activity and at least 50 min preictal data. Only 13 patients contained at least 1 day of continuous interictal recordings. Remaining patients did not have a seizure-free day during monitoring. In those cases, interictal EEG data segments with duration of less than 24 h were linked together, producing at least 1 day of seizure-free EEG recordings per patient. The recordings of six electrode contacts were available for each patient: three focal and three extrafocal (Uni-Freiburg, 2011).

All times of day were included when recording EEG data. There were 243 h of total interictal recording that was recorded between 9 a.m. and 9 p.m., whereas the remaining 265 h belonged to the time period between 9 p.m. and 9 a.m. The average time between the end of the interictal period and the following seizure was 9 h 36 min, whereas the minimum time was 1 h 18 min for patient 14. This time interval was greater than 3 h for all the remaining patients. Similarly, the average time between the last seizure and the beginning of the following interictal period was 5 h 18 min (Schelter et al., 2006). For every subject, a qualified epileptologist chose six contacts of all implanted electrodes after visual inspection of the raw data. Three contacts were chosen from the areas included early in ictal/seizure activity, and the remaining three were selected from areas not included or included later during seizure. Moreover, certified epileptologists determined the onset and end of all 88 seizures after visual examination based on detection of distinctive seizure patterns in intracranial EEG prior to clinically manifest seizures (Uni-Freiburg, 2011).

2.2 THE ELECTROMYOGRAM

2.2.1 Introduction

The human skeletal-muscular system first and foremost provides the forces needed to perform a variety of activities. Such a system consists of two subsystems, that is, the nervous system and the muscular system, together creating the neuromuscular system (Begg et al., 2007). Motion and arrangement of limbs are administered by electrical signals propagating back and forth among the muscles and the PNS and CNS (Bronzino, 1999). The CNS administers via nerve signals and muscle excitation. Nerves might be understood as wires conducting electrical currents; the nerve heads (nuclei) begin in the spinal column, and their long axonal bodies enlarge distant and deep, exciting single motor entities in different muscles. The skeletal-muscular system is composed of muscle sets connected to bones via tendons, and a motion is performed once nerve signals produce muscle contractions or relaxations that either attract or repel the bone (Begg et al., 2007).

After pathologic circumstances occur in the motor system, either in the spinal cord, the motor neurons, the muscle, or the neuromuscular junctions, the properties of the electrical signals in the muscle are altered. Cautious recording and analysis of electrical signals in the muscle (via EMGs) may therefore offer important help in finding and diagnosing irregularities not just in the muscles but moreover in the entire motor system. EMG is the recording and understanding of these muscle activity's potentialities. Initially, EMGs were recorded mainly for investigative or diagnostic aims, but with the progression of bioelectric technology, EMGs also turned out to be a basic instrument in accomplishing artificial control of limb motion, such as functional electrical stimulation (FES) and rehabilitation (Bronzino, 1999).

Neuromuscular illnesses consist of abnormalities initially appearing in the nervous system, in the neuromuscular junctions, and in the muscle fibers. These abnormalities have distinct degrees of harshness, from negligible damage to muscle, to amputation caused by neuron or muscle death. In more harsh illnesses such as ALS, death is generally

assured. Early and correct diagnosis is essential for enhanced patient prediction and increased chance for rehabilitation. In a majority of cases, clinical testing is insufficient to detect and prevent disorders from spreading (Preston & Shapiro, 2012) because many dissimilar abnormalities could be the result of a specific symptom. The correct diagnosis of a disorder is, for that reason, of supreme significance so more purposeful healing can be achieved. At present, electrodiagnostic (EDX) studies composed of nerve conduction studies (NCS) and EMG are employed for assessment and identification of patients with neuromuscular diseases. EMG was first used as a method of analyzing neuromuscular states established on cell action capabilities throughout muscle activity. Characteristics of the EMG waveform (0.01–10 mV and 10–2000 Hz on average) can indicate the position, etiology, and kind of anatomy. As an example, an EMG pulse interval shows the position and network of the metabolic status of the muscle fiber (Emly, Gilmore, & Roy, 1992), yet irregular spikes can show myopathy. Notice, on the other hand, that EDX methods help doctors in illness discovery, however they are hardly ever helpful for confirming the diagnosis and in difficult situations, more invasive tools like muscle biopsies or more enhanced imaging methods like ultrasound or MRI are necessary. The understanding of EMG is, as a rule, performed by trained expert neurologists who, besides examining EMG waveforms, employ other methods such as needle conduction researches and muscle acoustics. Trouble appears once there are hardly any specialists to meet the demand of patients and, consequently, it is imperative to build up automated diagnostic systems established on EMG readings. This imperative offers a range for the usage of machine learning methods for the discovery and classification of neuromuscular irregularities based on EMG processing. These smart systems will help doctors in the discovery of abnormalities of the neuromuscular system. Other usages of EMG signal processing such as motion control of prostheses, ergonomics, and intention detection will also make use of enhancements in machine learning methods. The goal of smart diagnostic and artificially administered neuromuscular systems is to primarily preprocess the raw EMG signal and, after that, extract the characteristic data or features. Features that may be extracted include time and frequency domain data, Fourier coefficients, autoregressive coefficients, wavelet coefficients, and a wide range of quantities derived from other signal-processing methods. These data may then be employed as input data for classifiers such as decision trees and support vector machines (SVMs), which may classify neuromuscular diseases or find the intention to propagate. The challenge in this case is to invent signal-processing methods that protect or confine significant discriminatory data so as to give a good quality set of features for classification (Begg et al., 2007).

The EMG signal points out the electrical state of skeletal muscles and holds the data related to the construction and purpose of the muscles that initiate various body parts to activate. The EMG signal carries data related to the controller effect of the CNS and PNS on the muscles. Intrinsically, the EMG signal gives an extremely helpful description of the neuromuscular system because numerous pathological procedures, regardless of how they appear in the nervous system or the muscle, are apparent by the changes in the signal's features. In the last few decades, the quality of EMG signal understanding has been significantly enhanced, and with the improvement of new signal-processing methods, we now better understand the muscles' electrophysiology (Sörnmo & Laguna, 2005). EMG analysis is more precise than clinical tests in determining the kinds of muscle fibers included in an abnormality. EMG analysis can show irregular physical sensory nerve phenomenon even though the patient still has normal motor-nerve conduction. Moreover, EMG analysis may help a medical worker in diagnosing without a need for a muscle biopsy (Begg et al., 2007). Progress in engineering and technology have taken EMG beyond the conventional diagnostics to consider its use in various areas such as ergonomics, exercise physiology, rehabilitation, movement analysis, biofeedback, and myoelectric control of prostheses as well (Sörnmo & Laguna, 2005).

2.2.2 The Electromyograph and Instrumentation

The basic recorder of motor unit action potential (MUAP) is the EMG, a tool employed for recording the action potential of the motor unit. There exist two fundamental kinds of EMGs: needle or fine wire EMG and surface EMG (sEMG). EMG tools are comprised of electrodes, a signal acquisition system with audio and visual screens, biosignal amplifiers, and low-pass and band-pass filters. A satisfactory EMG system also results in minimal noise and artifacts. Almost all EMG tools have standardized settings for signal features, for example, gain, common mode rejection ratio, input impedance, and filter bandwidth (Begg et al., 2007; Preedy & Peters, 2002).

2.2.3 EMG Electrodes

Needle electrodes or intramuscular wire electrodes are favored over surface electrodes because they can enter the individual motor units straightaway and evaluate the coming action potentials more precisely. The most widely employed needle electrode is the concentric ring needle with a monopolar single electrode. Other needle electrodes are used by single-fiber EMG (sFEMG) and macro-EMG (Togawa, Tamura, & Oberg, 1997). Different from needle

electrodes, wire electrodes are more simply bent and used for kinesiology works. The wires are physically removed after the recording. The deepness and position of injection is significant to acquire correct interpretations. Usually, a ground electrode is employed, and evaluations are made concerning ground voltage. The ground electrode is usually positioned in an area having no muscle motion. The disadvantage of employing these electrodes is the discomfort to patients or test subjects. sEMG electrodes are a more efficient option than needle and wire techniques because they are confined. These electrodes are composed of Ag/AgCl and found in the shapes of bars or discs. It is recommended to apply gel or paste to acquire a desirable interface for signal acquiring contrary to use of dry or separated electrodes that have built-in higher noise extortion (Begg et al., 2007).

2.2.4 Signal Acquisition

EMG data are recorded in the hospital EMG lab by an electromyographer employing either noninvasive sEMG or needle EMG relying on the sensitiveness of the equipment used. The doubted area of irregularities is determined for EMG recording. After that, the EMG is recorded for a planned amount of time, and then the acquired signal is differentially amplified, band-pass filtered, and digitized. All EMG recordings either from sEMG or needle EMG display alterations in voltage potentials because of intracellular activity, either in the nerve or muscle (Preston & Shapiro, 2012). The procedure where an intracellular electric potential is sent via the extracellular fluid and tissue is called volume conduction. Volume conduction can be presented as near-field or far-field potentials via layers of skin or fat. EMG investigation of skeletal muscle contains four elements:

a. *Insertional activity*: The injection and motion of the needle electrode in the muscle appears as explosions of short potentials called insertional activity.
b. *Spontaneous activity*: Spontaneous activity recorded with the unmoving muscle, in other words, with the needle not moving in a relaxed muscle.
c. *MUAP morphology and stability*: When the beginning action has been determined, the MUAP waveform and shape may be processed. The shape of the individual MUAPs may offer ideas as to the etiology of the abnormality, if their physiological generation is correctly interpreted.
d. *MUAP recruitment*: The amount of motor units recruited by the CNS may also be deducted from the recorded EMG waveforms. These can evaluate physical strength and are helpful for the discovery of neuromuscular diseases (Begg et al., 2007).

Routine oscilloscope settings consist of a sweep speed going from 2 to 20 ms/cm and an optimum gain to maximize the recorded potentials without shortening the extremum. The sensitivity varies from 50 to 500 μV/cm for insertional and spontaneous activities and from 100 μV to 1 mV/cm for motor unit potentials. Apparently, a smaller amplification is sufficient for the examination of larger potentials. Most researchers apply the low-frequency filter of 10–20 Hz and high-frequency filter of 10 kHz, and also some choose to decrease the lower limit to 2 Hz or less while finding the waveform of motor unit potentials (Bronzino, 1999).

2.2.5 Signal Amplification and Filtering

Subsequent to amplification, the signal is primary band-pass filtered, sampled, and then low-pass filtered again. Butterworth or Chebyshev filters are commonly used in the equipment, and there is rarely the requirement to define the cutoff or band-pass frequencies. This is principally due to a larger allocation of the EMG signal power known to be part of the 5- to 500-Hz frequency scope of the power density spectra. sEMG recordings are usually in the range of the 10- to 350-Hz band in as much as filtering within 10–150 Hz or 50–350 Hz, for example, it is not desired because the parts of the signal's power higher than 150 Hz and lower than 50 Hz are removed. Intramuscular recording ought to be formed with the suitable rising of the high-frequency cut-off to a low point of 450 Hz or by using a band-pass filter of 10–450 Hz. The previously described levels are perfect filter settings that can be attuned if full condition is provided for working so (Begg et al., 2007).

2.2.6 Signal Digitization

After the analog signal is gathered, amplified, and band-pass filtered, it is ready to be digitized and stored on a computer for further processing. During digitization, sampling is accomplished at the Nyquist rate that is at least double the highest frequency cut-off of the band-pass filter. For instance, if a band-pass filter of 10–350 Hz is employed, the lowest sampling rate ought to be 700 Hz (350×2) or possibly higher to enhance accuracy and resolution. In certain cases, a low-pass filter is employed to primary smooth the EMG signal so that a lower sampling rate (50–100 Hz) may be applied for digitization. The raw unfiltered EMG signal may be stored in the computer applying a sampling rate larger than 2.5 kHz as well. It should be noticed that the signal should be influenced by high-frequency noise and band-pass filtered as explained earlier. The changeover of the analog EMG signal to digital signal may be achieved by using an A/D converter having 8- to 12-bits resolution. Digitized signals may be additionally normalized, for example in force/torque experiments where normalization is performed with respect to the maximum voluntary contraction (MVC). This process asks the subjects

to be in good order, and trained to bypass variability and experimental incompatibilities. Normalization can also be accomplished comparative to joint angle or muscle length, velocity of reduction or extension, or applied load (Begg et al., 2007).

2.2.7 The Motor Unit Action Potential

The contraction of muscle tissue activates various body organs such as the eyes and limbs, and propagates liquids inside the body. Being dependent on its aims, the muscle can be classified as skeletal, smooth, or cardiac. Skeletal muscle is linked to the skeleton and creates motion and location of the body, although smooth muscle is located inside the intestines and blood vessels. In skeletal muscle, contraction is regulated by electrical impulses, such as action potentials that travel along the CNS and PNS, and the muscles. The action potentials are sent down the axons of the motor neurons, develop in the brain or the spinal cord, and sent to the muscle fibers. Every motor neuron is linked to muscle fibers via a specialized synapse called the neuromuscular junction, which permits action potentials to excite muscle contraction. Considered jointly, a motor neuron and the fibers to which it is linked (excites) consist of a motor unit and stands for a functional contraction unit. Regarding the aims of the muscle, a single motor unit consists of several muscle fibers or more than a thousand muscle fibers [1, 2]. Muscles controlling precise motions, for instance, those of an eye or a finger, have a fewer number of muscle fibers per motor unit than muscles regulating gross motions, for instance, those while running and exercising. The contraction of a muscle fiber is started at the moment when neuronal action potentials arrive at the neuromuscular junction and fire action potentials that disperse on the volatile membranes of the muscle fiber. MUAP outcomes from spatial and temporal accomplishments are the sum of the single action potentials as they disperse via the various muscle fibers of an individual motor unit. The EMG signal outcomes, on the other hand, are from the addition of the various MUAPs close enough to the recording electrode. The amount of MUAPs inside the pick-up (discovery) area of the electrode is dependent on the chosen type of electrode and is generally larger than one because fibers of various motor units are positioned in the whole muscle. Motor unit achievement is a basic muscular procedure where the force applied by muscle contraction is regulated by the CNS using spatial and temporal accomplishment of motor units. Spatial accomplishment represents the force being increased by using more motor units, whereas temporal accomplishment means that force is raised by the firing of action potentials at quicker rates. Even though both kinds of accomplishment can happen at the same moment, spatial accomplishment prevails from lower levels of muscle contraction until a majority of motor units have been achieved. At high levels of muscle contraction, temporal accomplishment prevails and causes the motor units to have firing rates around 50 Hz or quicker. A high firing rate means that each MUAP waveform cannot be distinguished any further because temporal superimposition, and the outcoming EMG signal, displays a noise-like, random occurrence, thought as an interference pattern. Motor units are commonly achieved considering their magnitude, beginning with the most diminutive motor units, with bigger units increasingly achieved for raising the capability of muscle contraction. As a consequence, primary activation is not strong and is preceded by a smooth incline in strength via the consecutive summation of larger, more powerful motor units. Investigation of motor unit accomplishment at low levels of muscular contraction is significant for identification of abnormalities connected to the nervous system (neuropathy) and muscular tissue (myopathy). The accomplishment pattern is generally determined in terms of the firing rate of the initial motor unit when the second motor unit is reached. Without any problems, the accomplishment rate is distinguished because of the occupancy of a fewer number of active motor units. A neuropathic accomplishment pattern is defined by a firing rate of the first motor unit that passes 20 Hz prior to the second motor unit appearance. However, a myopathic muscle is defined by an accomplishment pattern where fewer motor units are already activated at minimum self-imposed contraction to generate the required force; therefore, a myopathic accomplishment pattern is linked to various MUAPs of various shapes (Sörnmo & Laguna, 2005).

The activities to determine a motor unit potential consist of amplitude, rise time, duration, phases, stability, and territory. A broad range of neuromuscular abnormalities changes the waveform in various but distinguishing combinations. Therefore, these kinds of abnormalities assist to differentiate primary muscle disorders from disorders of neuromuscular junction and lower motor neurons. A lessening in spike duration and amplitude describes motor unit potentials in myopathies connected to a random loss of single fibers (Kimura, 1989).

The data in an intramuscular EMG signal can be divided into two simple types, that is to say, morphology and firing pattern, a most helpful method to distinguish the two when models are developed and processing algorithms for the EMG signal. Some essential characteristics of each type can be summarized as follows:

Morphology: A morphologic characterization of the MUAP waveform is necessary to perform typical clinical investigation and consists of the next parameters taken from the intramuscular EMG. Amplitude is the peak-to-peak amplitude of the MUAP and is in the range of 0.25–5 mV for a healthy case. The amplitude is evaluated by the amount of active muscle fibers inside the nearest direct electrode. Generally, large amplitudes are connected to neuropathies

and small amplitudes to myopathies (Sörnmo & Laguna, 2005). Clinical education and computer simulation show that surface measuring can assist in distinguishing neuropathy from myopathy. Considering the amplitude, a larger amount of muscle fibers inside a 2-mm radius of the electrode tip provides this evaluation. The value, on the other hand, alters noticeably, with a tenuous activity of the recording electrode chiefly representing an amplitude alteration. The ratio between the surface and amplitude evaluates the "thickness" of the potential, which changes much less with alterations in electrode location. The mix of amplitude and surface/amplitude ratio significantly enhances discrimination, finding around 70% of neurogenic alterations, compared to just 15%–30% by duration criteria alone (Kimura, 1989).

The number of phases of a MUAP waveform shows the degree of disarrangement of action potentials traveling in various individual fibers. Although the action potential of a single fiber consists of just one or two phases, the recording electrode discovers the addition of action potentials of numerous fibers that, because of changing degrees of disarrangement, may produce an MUAP with many phases. Polyphasic MUAPs consist of more than four phases and are largely seen in neuropathic and myopathic circumstances (Sörnmo & Laguna, 2005). In neurogenic disorders, polyphasic MUAPs appear because of the slow conduction velocity in infantile nerve sprouts or slow conduction velocity in reinnervated but still atrophied muscle fibers. Alterations in muscle fiber size may also result in polyphasic MUAPs in myopathic disorders (Bronzino, 1999).

The number of phases, evaluated by determining and counting positive and negative peaks to and from the baseline, is equal to the amount of baseline crossings plus one. Usually, motor unit potentials consist of four or less phases. Polyphasic motor unit potentials, having more than four phases, outcomes from desynchronized discharges of individual muscle fibers, likely showing fiber size changeability more than random fibers loss. These potentials do not pass 5%–15% of the overall population in a healthy muscle, if they are recorded using a concentric needle electrode. Polyphasic activities usually occur when a monopolar needle is used, although no research has found the precise occurrence. Some action potentials demonstrate a couple of "turns" or directional alterations with no baseline crossing. These rough action potentials or, less suitably, complex or pseudopolyphasic potentials, show desynchronization between discharging muscle fibers as well (Kimura, 1989).

Duration is termed as the onset and end of the MUAP waveform, that is, the time interval among the initial and last appearance of the waveform already passing the defined amplitude threshold, for example, 5 μV. The duration is dependent on the amount of muscle fibers inside the motor unit and rises as the amount of fibers rises. The average MUAP duration is 2–10 ms. Yet because the motor unit region might be larger than the pick-up range of the electrode, MUAP duration does not give data related to the overall magnitude of a large motor unit. MUAP duration will rise if a motor unit has a increased amount of fibers because of the reinnervation (Bronzino, 1999).

Duration is measured between the first take-off and arrival to the baseline. Different from the spike amplitude, and completely determined by a very minor amount of muscle fibers close to the electrode, the duration of a motor unit potential reveals the movement from a larger amount of muscle fibers inside the interest zone of the recording are in a concentric needle, spreading 2.0–2.5 mm from the core. For that reason, a minor needle change or rotation does not affect the duration as much as the amplitude. The duration usually is the range between 5 and 15 ms, with regard to the subject age. In one study, the values obtained at the ages of 3 and 75 years were 7.3 and 12.8 ms in biceps brachii, 9.2 and 15.9 ms in tibialis anterior, and 4.3 and 7.5 ms in the facial muscles, respectively. Another study working with four proximal and distal muscles of the upper and lower limbs in 111 healthy subjects between 20 and 80 years of age discovered no noticeable rise of the average duration before the age of 55. Cases aged more than 55 revealed a minor affinity to larger duration. The usage of a wide-open amplifier band-pass, joined with improved signal-to-noise ratio (SNR), outcomes in a much lengthier duration, up to 30 ms recorded either with a single-fiber electrode or a macroelectrode. Considering this condition, the net time of single action potential from end-plate zone to musculotendinous junction can show complete duration of MUAP (Kimura, 1989).

Rise time is a rising function of the space between the electrode and the nearest active muscle fiber. A petite rise time combined with minor MUAP amplitude can, for that reason, show that the amplitude is decreased because of fiber atrophy more than because of a huge space between the electrode and the nearest fiber. The rise time is measured as a time lag from the first positive peak to the following negative peak, and assists to find an approximate length among the recording tip of the electrode and the discharging motor unit. A far-away unit takes a higher rise time due to the resistance and capacitance of the overriding tissue performing as a high-frequency filter. This type of discharge is accompanied by a dull sound, showing the requirement to relocate the electrode nearer to the source. Overall, a rise time smaller than 500 μs confirms recording from inside the motor unit region, however there are some arguments for reduced border criteria. This kind of a motor unit results in a sharp, crisp sound at the loudspeaker that gives a significant idea to the nearness of the unit to electrode. The evaluation of the rise time approves the appropriateness of the recorded potential for numerical amplitude evaluation (Kimura, 1989).

Area indicates the amount of fibers neighboring the electrode; on the other hand, different from MUAP amplitude, MUAP area is determined by MUAP duration and is, for that reason, affected by fibers in a larger area matched to that of MUAP amplitude (Bronzino, 1999).

Turns stands for the complication of the MUAP, such as the number of phases; on the other hand, because a usable turn does not need a baseline crossing such as valid phase, the number of turns is more elusive to alterations in the MUAP waveshape. To differentiate accurate turns from signal noise, consecutive turns have to be offset by a minimal amplitude difference (Bronzino, 1999).

In a healthy subject, MUAP morphology generally stays stabilized from discharge to discharge. Destabilized morphology can still appear when the neuromuscular junction is broken, outcoming in known nerve action potentials obstructed from transmitting. Therefore, some of muscle fibers of the motor unit might not be actuated. In these kinds of cases, MUAP may in reality increase twice from one discharge to following one and, from time to time, can be followed by alteration in the number of phases. Gradual alterations in MUAP morphology can be seen when the biochemical characteristics of a motor unit alter, for instance, happening during muscle tiredness, or when the relative position of the electrode versus the motor unit alters (Sörnmo & Laguna, 2005).

Firing pattern: A muscle contraction is maintained via continual stimulation of the motor units, with every motor unit connected to a specific train of MUAPs. As the number of active motor units rises, the recording electrode finds a rising amount of concurrent MUAP trains, and single MUAP trains turn to be harder to distinguish from each other. The MUAP's repeating timing determines the firing pattern and carries data on how the CNS regulates the motor unit. The firing pattern is generally regular (rhythmic) having quite little changeability of consecutive interfering intervals, for example, the times among consecutive MUAPs have the same source while contracting. In the case of regular firing patterns, it is frequently satisfactory to describe the pattern by mean firing rate, characterized as the inverse of the average duration of the interfering intervals. Under voluntary muscle control, a motor unit ordinarily starts firing at a rate of 4–5 Hz, even though lower rates can be seen because of the induced activity behind intentional control, and its rate raises as the force increases. The biceps brachii might illustrate the average firing rate for normal muscle where the frequency of the motor units is between 7 and 12 Hz at the lowest level of muscle contraction. This level is defined as a percentage of MVC that stands for a subject-specific contraction measure. While rising isometric I force, the average firing rate of the biceps brachii rises to obtain an upper limit of around 20 Hz at 100% MVC. When evaluating motor unit irregularities, it is generally essential to consider that various muscles have their own particular firing rates, and also the rates when additional motor units are to be recruited. Although the average firing rate is a basic parameter for investigation of intramuscular EMGs, it is not desirable when describing abnormal firing patterns seen while there are dynamic contractions with fast alterations in the force level. The identical restriction also refers to the description of firing patterns related to impaired neuromuscular transmitting, where the interfering intervals expose augmented changeability. Therefore, alternative rhythm parameters are guaranteed that more suitably show the transient characteristics of a firing pattern (Sörnmo & Laguna, 2005).

2.2.8 Myoelectric Signal Recording

Myoelectric activity is evaluated invasively by employing a needle electrode or noninvasively by positioning an area electrode on the skin covering the muscle. The needle EMG is a regular clinical way applied for diagnostic goals, whereas the sEMG is studied and computerized in many applications such as prosthesis control, ergonomics, movement and gait analysis, and sports medicine. The needle EMG is evaluated by placing a needle electrode through the skin straight into the muscle. This method gives a high-resolution, localized characterization of the muscle's electrical activity, although it is relatively unpleasant for the patient. The needle electrode's pick-up area depends on its particular system and can comprise of only one or two muscle fibers. The monopolar needle electrode asks for a reference electrode positioned further away from the needle insertion point at an electrically neutral site such as over a bone. The concentric needle electrode bypasses the reference electrode by citing the electrode active surface to the needle cannula. Both types of needle electrodes are employed in clinical EMG signal recordings. By inserting several needle electrodes at various positions, a more careful description of a large muscle's electrical activity may be received. The sEMG shows the gross activity generated by a huge number of motor units. Its spatial resolution is more controlled than that of the needle EMG, and the MUAP high-frequency content becomes smoothed. The positioning of surface electrodes is dependent on the muscle under consideration and includes factors such as muscle fiber placement, anatomical landmarks, and minimization of electrical cross-talk from other muscles. The sEMG is principally employed when the activation time and the signal amplitude consist of the desirable data, for instance, regarding researches of motor behavior or myoelectric prosthesis regulation. The sEMG does not, in general, permit the discovery of single MUAPs, even though MUAP trains can be found at low levels of muscle contraction. An additional improvement of the surface electrode method is the linear electrode array, created to give spatial characterization of myoelectric activity. It is possible to record the sEMG at lower sampling rates than the needle EMG because the middle tissue among the motor units and the surface electrode works as a low-pass filter of the electrical signal. Most of the spectral power of the sEMG is less than 400–500 Hz, meaning that a sampling rate of 1 kHz or higher is needed. In the case of the needle EMG, the sampling rate should be selected so that various MUAP waveforms that contain

frequencies ranging up to 10 kHz are correctly regenerated; thus, a frequently used sampling rate is 50 kHz. The recording of an EMG is connected to various forms of noise and artifacts that, to different degrees, restrain the quality of the signal. In the sEMG, electrode motion artifact outcomes from relative propagation among the skin and the electrode and by distortion of the skin under the electrode. Because this form of artifact is low frequency in nature, having majority of its spectral components less than 20 Hz, it can be decreased by using high-pass filtering with no important changes in the EMG signal's spectral content. Like in the conditions when an EEG signal is recorded, inadequate protection of the EMG electrode cable makes it sensitive to electromagnetic fields resulting from currents propagating in close electrical devices or power lines. As a consequence, the recorded EMG signal will be comprised of power line interference at a frequency of 50–60 Hz. Filtering methods are used for removal of a narrowband noise component. Nevertheless, these filtering methods can be applied for the processing of EMG signals as well (Sörnmo & Laguna, 2005).

2.2.9 Neuromuscular Disorders

Neuromuscular disorders are commonly anomalies found around the PNS. They can be categorized depending on the location and reason of the disorders. Two main disorders are neuropathy and myopathy, which are described in this section (Begg et al., 2007).

Neuropathy is a term to define a disease of nerves that cause pain and some disability. The cause of neuropathic disorders differs, which includes injury, infection, diabetes, alcohol abuse, and cancer chemotherapy. It can be categorized as mononeuropathy and polyneuropathy. When the neuropathic disorder is caused by the malfunction of a single nerve, it is called mononeuropathy. Some types of neuropathies are median nerve entrapment, ulnar neuropathy, radial neuropathy, peroneal neuropathy, femoral neuropathy, facial mononeuropathy, and trigeminal neuropathy. Median nerve entrapment is the most common mononeuropathy found in the arms and hand. The nerve is compressed or placed in an unusual position, which disturbs the function and causes pain. EMG is generally used to distinguish median nerve entrapment from lesions of the proximal median nerve, brachial plexus, and cervical nerve roots. Ulnar neuropathy is caused by compression of the ulnar nerve at the elbow, which is difficult to find a real location using either EMG or the other EDX methods. Radial neuropathy disorders are at the radial nerve, which extends from the brachial plexus to the wrist. Radial neuropathy is less studied than ulnar neuropathy. The three general lesions that cause radial neuropathy are the spinal grove, axilla lesion, and lesions of the posterior interosseous and superficial radial sensory nerves. Peroneal neuropathy is the most common neuropathy in the lower extremities of the body. Peroneal neuropathy is a problem with the peroneal nerve where it occurs at the fibular neck of the calf. It causes sensory disturbances of the calf and foot region, usually causing a lack of feeling and weakness. Femoral neuropathy is disorders at the femoral nerve, which runs parallel to the femoral artery and innervates the quadriceps muscle. Generally, it is not observed by EMG diagnosis, because it has similar signs as the lumbar plexus lesion in peroneal neuropathy. Usually, it causes buckling knees, difficulty with lifting objects, drifting of feet, and some deadness and weakness at the thigh and calf region. Facial mononeuropathy is facial palsy, which generally known as the idiopathic Bell's palsy. This problem is related to some other disorders such as diabetes, leprosy, stroke, and herpes zoster. Weakness in the lower facial region and facial spasm are some symptoms of facial neuropathy. Trigeminal neuropathy is disorder at the trigeminal nerve, which carries the nerve impulse to the face and motor fibers. The patient with trigeminal neuropathy has difficulty in chewing and numbness over the ipsilateral face.

When a group of nerves or all nerves of a peripheral nerve are affected, it is termed polyneuropathy. Polyneuropathies are similar because of the insufficient manner where sensory nerves react to failure. EMG diagnosis is not beneficial for polyneuropathy, because patients with polyneuropathy have normal electrophysiological characteristics. Myopathy is a disorder generally related to the skeletal muscle caused by injury of a muscle group or some genetic mutation. Myopathy avoids the normal task of affected muscles. Therefore, the patient suffering with myopathic diseases has weak muscles and, depending on severity of disorder, has a problem with performing regular tasks or finds it impossible to make any movement by using the affected muscles. Some common types of myopathies are muscular dystrophy (MD), Becker muscular dystrophy (BMD), Duchenne muscular dystrophy (DMD), congenital muscular dystrophy, Emery-Dreifuss muscular dystrophy (EDMD), myotonic muscular dystrophy (MMD), distal muscular dystrophy (DD), limb-girdle muscular dystrophy (LGMD), facioscapulohumeral muscular dystrophy, and oculopharyngeal muscular dystrophy (OPMD). MD is the most common form of myopathy, which causes muscle weakness and degeneration. It can be hereditary or acquired. While reviewing EMG readings, it is characterized by short MUAP duration and reduced amplitude. Congenital muscular dystrophy (CMD) occurs before birth because of genetic mutation. The necessary proteins for muscles are not produced. It can cause mental slowness and disability for life. DMD influences involuntary muscle such as the heart muscle. It occurs in children of all ages and is genetic in origin. This disorder causes muscles to waste away because of a lack of dystrophin protein. It is severe, and survival after the age 30 is grim. BMD is similar to DMD, but it starts in adolescence and may cause heart failure. EDMD occurs in children of all ages and is caused by gene

mutation. It causes weakness and wasting upper body. MMD arises at adulthood and is caused by gene defect. It grows slowly with starting weakness at the facial muscles and moves to other parts of the body. DD affects young to middle-aged adults and is caused by gene mutation. It occurs in the leg but is not a fatal disease. LGMD occurs at the waist and lower limbs. It grows slowly and causes some cardiopulmonary problems and wasting of the limbs. OPMD is caused by gene defection or mutation and affects the face and eyes (Begg et al., 2007).

2.2.10 Uses of EMG Signals in Diagnosis of Neuromuscular Disorders

The needle EMG is the usual clinical recording method employed for diagnosis of neuromuscular pathology. When, for example, a patient goes to a doctor for muscle weakness, recording of the needle EMG during contraction of specific muscles will be performed. The morphology of single MUAP waveforms gives the necessary clinical data regarding the muscle's skill in response to the CNS. This data may assist to identify irregular activity in situations such as muscle irritation, injury to nerves in the arms and legs, pinched nerves, and MD. The needle EMG is also used for nerve wounds and can be employed to find out if the wound heals and goes back to normal with complete muscle reactivity, for instance, by analyzing alterations in motor unit accomplishment over a definite time period. The diagnostic EMG is comprised of the investigation of unplanned motor action ocurring throughout muscle relaxation. In ordinary situations, the muscle is electrically quiet during a relaxation period; on the other hand, irregular unplanned waveforms and waveform patterns can be produced that are connected with spontaneous muscular activities and seizures (Sörnmo & Laguna, 2005).

EXAMPLE 2.8 The following MATLAB code was used to plot healthy, ALS, and myopathic EMG signals. For this example, EMGLAB data was used. You can download the data from the following website: http://www.emglab.net/emglab/Signals/signals.php

Dataset Information: EMG signals were taken from EMGLAB website (http://www.emglab.net/). The clinical EMG signals were acquired under normal conditions for MUAP analysis. The EMG signals were recorded at low voluntary and constant level of con traction with a standard concentric needle electrode. The EMG signals were filtered between 2 Hz and 10 kHz, and consist of a control group, a group of patients with ALS, and a group with myopathy. There were 10 normal subjects (four females and six males) aged 21–37 years in the control group. There were eight patients (four females and four males) between 35 and 67 years old in the ALS group. There were seven patients (two females and five males) between 19 and 63 years old in the myopathy group (Nikolic, 2001). Exemplary EMGs are depicted in Fig. 2.11. The following MATLAB code was used to plot each signal:

```
%% Ch2_EX_8.m
clc
clear
%Load Sample EMG Data downloaded from the web site
%http://www.emglab.net/emglab/Signals/signals.php
load EMGDAT.mat

%Plot HEALTHY EMG Signal
subplot(3,1,1);
plot(CON(:,2));
title('HEALTHY EMG Signal')
ylabel('Amplitude')
axis ([0 8192 -inf inf])

%Plot ALS EMG Signal
subplot(3,1,2);
plot(ALS(:,2))
title('ALS EMG Signal')
xlabel('Samples')
ylabel('Amplitude')
axis ([0 8192 -inf inf])

%Plot MYOPATHY EMG Signal
subplot(3,1,3);
plot(MYO(:,2))
```

```
title('MYOPATHY EMG Signal')
xlabel('Samples')
ylabel('Amplitude')
axis ([0 8192 -inf inf])
```

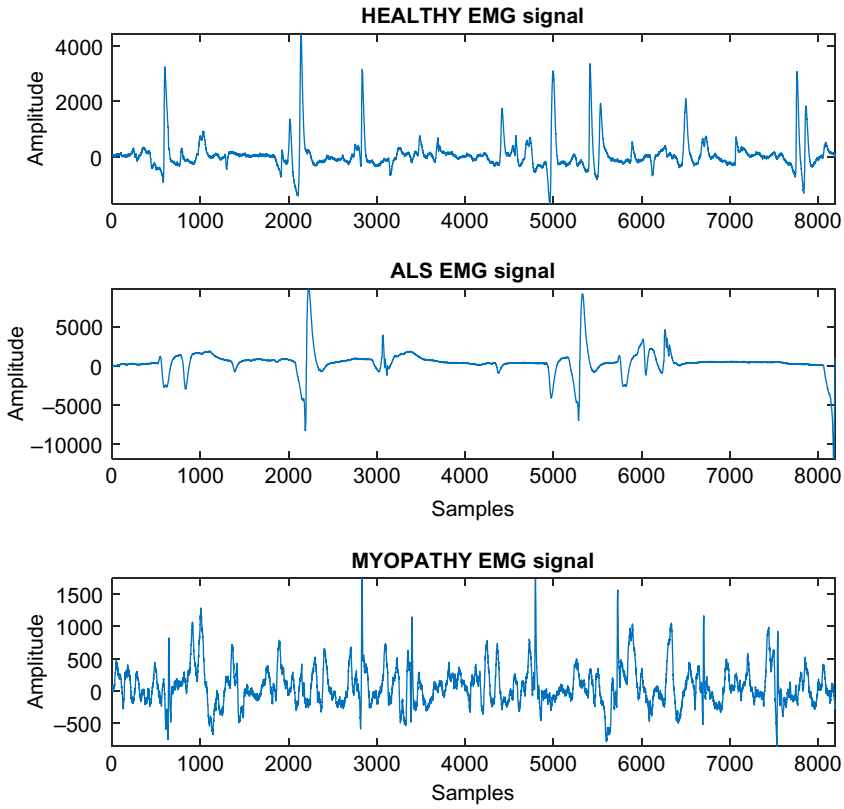

FIG. 2.11 Drawing of three different EMG signals (healthy, ALS, and myopathy).

2.2.11 Uses of EMG Signals in Prosthesis Control

Myoelectric-controlled prostheses are employed by persons lacking upper limbs or with amputations. The EMG signal is received from surface electrodes placed on muscles, which are brought to the prosthesis; the signal's properties are analyzed and interpreted to activate the required function. Considering the category of prosthesis, the regulation data goes from simple on/off commands produced by only one muscle to complex multifunction commands produced by an assembly of muscles. The single-muscle regulator is commonly found on the EMG amplitude in such a way that muscle contractions of various strengths, as shown by various amplitudes, may distinguish among hand closing and opening, or elbow flexion and extension. A multifunction prosthesis mixes the usage of several electrodes over diverse muscle assemblies using improved signal-processing algorithms to increase the amount of data capable of being extracted with regard to the active muscle state. The multifunction prosthesis accomplishes finer accuracy of the user's intention by studying transient signal patterns based on contractions, applying time, frequency, or time-frequency methods. It is essential to understand that the improvement of algorithms for prosthetic control is connected to a real-time restraint (Sörnmo & Laguna, 2005). Human hands are very important because they play an important role for grasping and manipulating different objects. Even the loss of a single hand affects human activity, and a prosthetic hand is a solution for equipping the armless subject. Currently, muscle signals control hand prostheses. Control is possible after hand amputation because a substantial amount of the muscles exist in the arm stump to control a prosthesis (Kurzynski, Krysmann, Trajdos, & Wolczowski, 2016).

Biomedical signals are the set of body signals that characterize a physical variable of interest. A biomedical signal such as EMG is used to control the prostheses' movement. Upper limb prosthesis structures are primarily based on myoelectric control, identifying EMG signals that arise during muscle contraction on the skin surface. Because most of the muscles that produce finger motion is left in the stump

after a hand amputation, these muscles are employed for control of prosthesis motion (Wojtczak, Amaral, Dias, Wolczowski, & Kurzynski, 2009). Because the analysis of EMG signals is used widely in medical diagnostics, sports, rehabilitation, and prosthesis control, the recognition of EMG signals offers substantial support for the automation of human tasks. A novel application of EMG signal classification is the individual skeletal muscle contraction in which the relevant EMG signals are employed to control a machine action after classification. But the challenge is the prosthetic hand control where the hand is multitalented to accomplish different movements, such as gesticulation or the playing of musical instruments by grasping and manipulating several objects. The loss of a hand intensely decreases opportunities to work, and the loss of both hands essentially eliminates independent work. The goal of a prosthetic hand is to moderately re-establish the function of the lost limb, particularly its working functions and ability to perform different movements and to achieve different finger configurations. The muscle signals, which usually control contemporary prostheses, are related to healthy hand and finger movements and should be acquired noninvasively by appropriate sensors positioned above the muscles on the skin. Hence, EMG-controlled prosthetics use surface signals taken from the hand stump muscles and then distinguishing the category of intended prosthesis action by classifying them (Wołczowski & Zdunek, 2017).

People with disability conditions might experience different modern life technologies than people without disabilities. Doorknobs, kitchen tools, or shirt buttons that do not have any effect on a large portion of individuals might end up as an obstacle for somebody who has a disability. Replacing a doorknob with a lever door handle might make a huge difference to that individual, and would be welcomed and valued toward others. A straightforward buttonhook device, although it is not handy for most people, might help somebody who faces difficulties in manipulating buttons. Certain innovations have overcome independence obstacles for disabled persons, whereas other technologies provide the ability to overcome environmental barriers (Kim, Choi, Moon, & Mun, 2011). These supportive technologies might work by enhancing a person's abilities. The hand is one of the most important elements of a human being, used as a basic element in the sense of feeling. The hand is used in real-life experience to feel appearances and textures, and perform basic lifting functions. With a controlled muscle movement, for example, the basic function of the arm is to grip, lift, wave, and perform other rotational motions of the arm. For amputees, a prosthesis hand is an artificial device used to replace a missing part. The hand prosthesis is an improved though functional hand which can be equipped and manipulated to perform different functions. For instance, the myoelectric arm uses a controlled muscle contraction generated from an electrical charge to transfer and strengthen the control center. In this manner, with a controlled movement, an amputee can perform normal functions of the arm such as gripping, feeling, and waving among other hand-related movements.

EXAMPLE 2.9 The following MATLAB code was used to plot the sEMG signals related to basic hand movements. For this example, sEMG for Basic Hand Movements Dataset was used. You can download the data from the following website: https://archive.ics.uci.edu/ml/datasets/sEMG+for+Basic+Hand+movements#

Dataset Information: The data were sampled at 500 Hz, band-pass filtered using a Butterworth Band-Pass filter with low and high cut-off at 15 and 500 Hz, respectively, and a notch filter at 50 Hz to eliminate line interference artifacts. The signal was recorded from two differential EMG sensors, and the signals were conducted to a 2-channel EMG system by Delsys Bagnoli Handheld EMG Systems. The experiments include freely and repeatedly grasping of different items that were crucial to conduct the hand movements. The force and speed were purposely left to the subject's will. There were two forearm sEMG electrodes, Flexor Capri Ulnaris and Extensor Capri Radialis, Longus and Brevis, detained in place by elastic bands with the reference electrode in the middle to collect information about muscle activation. Five healthy subjects (two males and three females) of the same age approximately (20- to 22-year-old) conducted six grasps for 30 times each. The measured time was 6 sec. There exists a mat file for each subject. The subjects were required to repeatedly carry out the following six movements that can be thought as daily hand grasps:

(a) Spherical: for holding spherical tools
(b) Tip: for holding small tools
(c) Palmar: for grasping with palm facing the object
(d) Lateral: for holding thin, flat objects
(e) Cylindrical: for holding cylindrical tools
(f) Hook: for supporting a heavy load

More information can be found in Sapsanis, Georgoulas, and Tzes (2013). Exemplary EMGs are depicted in Fig. 2.12. The following MATLAB code was used to plot each signal:

```
%% Ch2_EX_9.m
clc
clear
%sEMG for Basic Hand movements Data Set
%Load Sample sEMG Data downloaded from the web site
%https://archive.ics.uci.edu/ml/datasets/sEMG+for+Basic+Hand+movements#
load sEMG_UCI_BHM.mat

%Plot Spherical sEMG Signal
subplot(3,2,1);
plot(F1_spher_ch1(1,:));
title('Spherical sEMG Signal')
ylabel('Amplitude')
axis ([0 3000 -inf inf])

%Plot Tip sEMG Signal
subplot(3,2,2);
plot(F1_tip_ch1(1,:))
title('Tip sEMG Signal')
xlabel('Samples')
ylabel('Amplitude')
axis ([0 3000 -inf inf])

%Plot Palmar sEMG Signal
subplot(3,2,3);
plot(F1_palm_ch1(1,:))
title('Palmar sEMG Signal')
xlabel('Samples')
ylabel('Amplitude')
axis ([0 3000 -inf inf])

%Plot Lateral sEMG Signal
subplot(3,2,4);
plot(F1_lat_ch1(1,:))
title('Lateral sEMG Signal')
xlabel('Samples')
ylabel('Amplitude')
axis ([0 3000 -inf inf])

%Plot Cylindrical sEMG Signal
subplot(3,2,5);
plot(F1_cyl_ch1(1,:))
title('Cylindrical sEMG Signal')
xlabel('Samples')
ylabel('Amplitude')
axis ([0 3000 -inf inf])

%Plot Hook sEMG Signal
subplot(3,2,6);
plot(F1_hook_ch1(1,:))
title('Hook sEMG Signal')
xlabel('Samples')
ylabel('Amplitude')
axis ([0 3000 -inf inf])
```

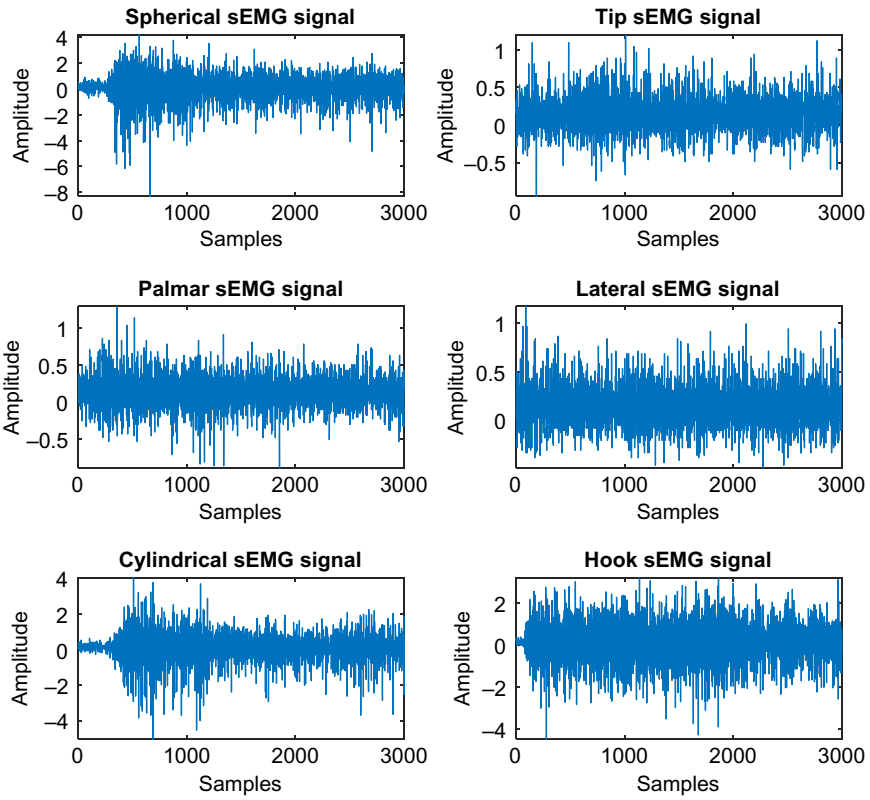

FIG. 2.12 Drawing of sEMG signals taken from six different hand movements.

2.2.12 Uses of EMG Signals in Rehabilitation Robotics

EMG-controlled assistive devices are also used for stroke treatment in intensive therapy to help with rehabilitation. In such cases, intentions of a patient's activity can be achieved using the sEMG (Lum, Burgar, Shor, Majmundar, & Van der Loos, 2002; Riener, Nef, & Colombo, 2005). With recent technological improvements, active exoskeleton robots assist with rehabilitation applications, human power augmentation, assistive robotics, impairment evaluation, and haptic communication in virtual and teleoperated environments. The human body commands must be understood by these robots to help humans. Therefore, EMG signals should be acquired and analyzed for control of the exoskeleton robot (Sasaki, Noritsugu, & Takaiwa, 2005). Exoskeleton robots have two controllers working together simultaneously: the robot controller and the human muscle. Upper-limb exoskeleton robots need to be controlled differently than conventional industrial and field robots, because humans operate both commands, and the control system employs these commands as part of its decision-making components. The exoskeleton maturely implements the real decisions of the human operator. However, there are still challenges in making decisions based on the motion intention identifications of the robot user (Abdullah, Subasi, & Qaisar, 2017).

The best approach to design an upper limb exoskeleton robot controller is to focus on the controller input information. In modern techniques, the input consists of human biomedical signals and platform-independent control signals. Various strategies are applied in different fields of applications. The EMG signals have been successfully used as human biomedical signal inputs to some exoskeleton developments such as upper-limb exoskeleton robots (Lo & Xie, 2012). For example, in Gopura, Kiguchi, and Li (2009), a muscle model based on EMG control was proposed to control a 7DOF (Degrees of Freedom) upper-limb exoskeleton robot. The user can adapt the method. Most upper-limb disabled people can use it. Control methods for upper-limb exoskeleton robots using EMG are mostly of a binary (on/off) nature (Lenzi et al., 2009). A good design would allow a high accuracy of motion intention classification for even a physically weak person who cannot properly generate daily motions (Abdullah et al., 2017).

EXAMPLE 2.10 The following MATLAB code was used to plot the sEMG signals related to different physical actions. For this example, sEMG Physical Action Dataset was used. You can download the data from the following website: https://archive.ics.uci.edu/ml/datasets/EMG+Physical+Action+Data+Set

Dataset Information: One female and three male subjects (aged 25–30 years) who have experienced aggression in circumstances such as physical fighting were employed in the experiment. Every subject had to implement 10 normal and 10 aggressive activities through 20 distinct experiments. The Essex robotic arena was the main experimental hall in which the data collection took place. The subjects' performance was collected by the Delsys EMG apparatus, interfacing human activity with myoelectrical contractions. Based on this context, the data recording procedure included eight skin-surface electrodes located on the upper arms (biceps and triceps) and upper legs (thighs and hamstrings). The overall number of electrodes was eight that corresponded to eight input time series, one for a muscle channel. Each time series contains ∼10,000 samples (∼15 actions per experimental session for each subject). Exemplary EMGs are depicted in Fig. 2.13. The following MATLAB code was used to plot each signal:

```
%% Ch2_EX_10.m
clc
clear
%EMG Physical Action Data Set
%Load Sample sEMG Data downloaded from the web site
%https://archive.ics.uci.edu/ml/datasets/EMG+Physical+Action+Data+Set
load sEMG_UCI_PA_NOR.mat

%Plot Bowing sEMG Signal
subplot(5,2,1);
plot(Bowing(1:4096,1));
title('Bowing sEMG Signal')
ylabel('Amplitude')
axis ([0 4096 -inf inf])

%Plot Clapping sEMG Signal
subplot(5,2,2);
plot(Clapping(1:4096,1))
title('Clapping sEMG Signal')
xlabel('Samples')
ylabel('Amplitude')
axis ([0 4096 -inf inf])

%Plot Handshaking sEMG Signal
subplot(5,2,3);
plot(Handshaking(1:4096,1))
title('Handshaking sEMG Signal')
xlabel('Samples')
ylabel('Amplitude')
axis ([0 4096 -inf inf])

%Plot Hugging sEMG Signal
subplot(5,2,4);
plot(Hugging(1:4096,1))
title('Hugging sEMG Signal')
xlabel('Samples')
ylabel('Amplitude')
axis ([0 4096 -inf inf])

%Plot Jumping sEMG Signal
subplot(5,2,5);
plot(Jumping(1:4096,1))
title('Jumping sEMG Signal')
xlabel('Samples')
ylabel('Amplitude')
axis ([0 4096 -inf inf])

%Plot Running sEMG Signal
subplot(5,2,6);
plot(Running(1:4096,1))
title('Running sEMG Signal')
```

```
xlabel('Samples')
ylabel('Amplitude')
axis ([0 4096 -inf inf])

%Plot Seating sEMG Signal
subplot(5,2,7);
plot(Seating(1:4096,1))
title('Seating sEMG Signal')
xlabel('Samples')
ylabel('Amplitude')
axis ([0 4096 -inf inf])

%Plot Standing sEMG Signal
subplot(5,2,8);
plot(Standing(1:4096,1))
title('Standing sEMG Signal')
xlabel('Samples')
ylabel('Amplitude')
axis ([0 4096 -inf inf])

%Plot Walking sEMG Signal
subplot(5,2,9);
plot(Walking(1:4096,1))
title('Walking sEMG Signal')
xlabel('Samples')
ylabel('Amplitude')
axis ([0 4096 -inf inf])

%Plot Waving sEMG Signal
subplot(5,2,10);
plot(Waving(1:4096,1))
title('Waving sEMG Signal')
xlabel('Samples')
ylabel('Amplitude')
axis ([0 4096 -inf inf])
```

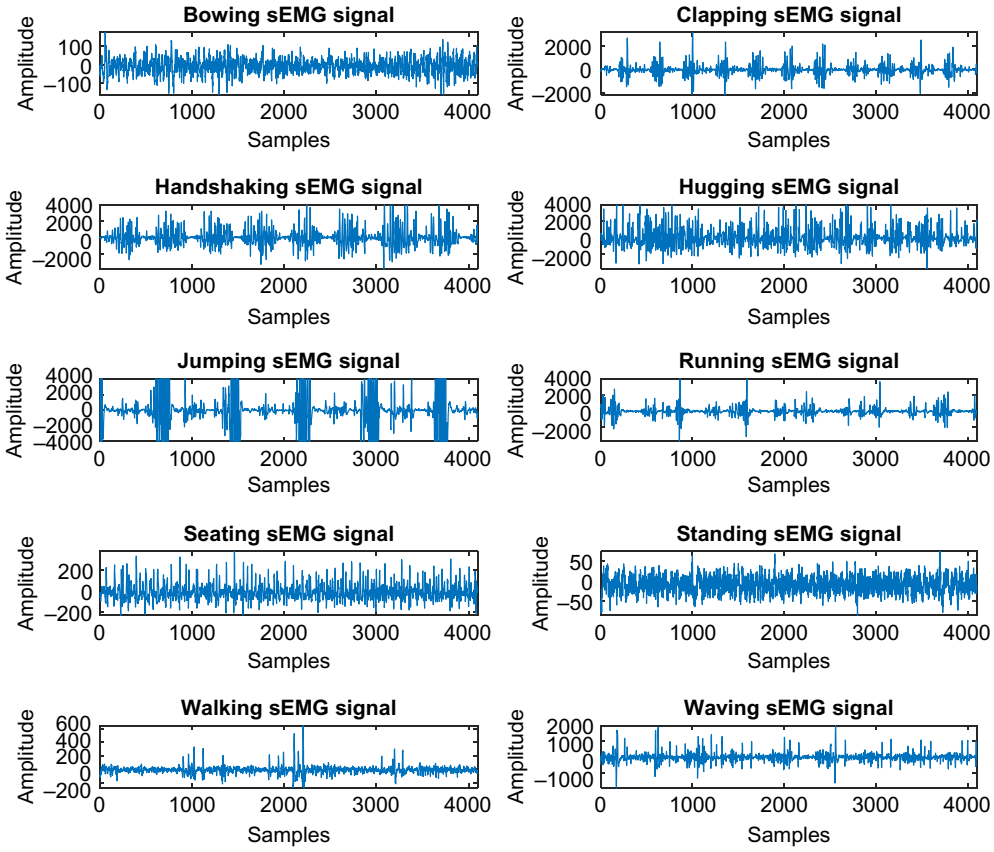

FIG. 2.13 Drawing of sEMG signals for 10 different physical actions.

2.2.13 Other EMG Applications

Kinesiology: Kinesiology refers to the investigation of body movement and has the goal of understanding the processes regulating movement. The sEMG is vital for a number of characteristics of kinesiology, comprising the learning of motor regulation approaches, mechanics of muscle contraction, and gait. To illustrate, the EMG pattern recorded during gait is described by consecutive spurts reflecting periods of muscle activation. Definition of the times for each spurt's beginning and termination, followed by an investigation of the outcoming beginning/termination timing pattern, is a vital duty for clinical evaluation of numerous movement abnormalities. The EMG pattern analysis is eased by signal-processing methods that automate the definition of spurts and describe the beginning/termination timing pattern (Sörnmo & Laguna, 2005).

Ergonomics: The amplitude of the sEMG signal offers an appreciated, numerical evaluation of muscle load, frequently employed to evaluate a physical load while working. In ergonomic study, the EMG signal is frequently recorded for the duration of light, repetitious effort with special interest to evaluate the movement of explicit muscles at known work locations. After being mixed with other ergonomic data, the consequence of the myoelectric signal study can eventually assist to bypass work-related irregularities, construct enhanced workplaces, and enhance efficiency. The investigation of muscle weakness is fundamental in ergonomics because of the natural desire to bypass weakness in work conditions. A valuable explanation of muscle weakness is the situation when a subject no longer can hold a requisite force. Regarding signal-processing methods, a weakened muscle contraction is demonstrated by a gradual rise in sEMG signal amplitude and noteworthy fluctuations in its power spectrum (Sörnmo & Laguna, 2005).

2.3 THE ELECTROCARDIOGRAM

2.3.1 Introduction

The ECG is the recording of electrical activities originating from the heart on the body surface. Waller first noticed it in 1889 (Waller, 1889). He used his pet bulldog as the signal source and a capillary electrometer as the recording device. Later, in 1903, Einthoven improved this technology by using the string galvanometer as the recording device and using human subjects with a variety of cardiac irregularities. He is primarily meritorious for introducing a number of concepts still in use today: counting the classification of a variety of waves, defining a number of standard recording sites using the arms and legs, and creating the initial theoretical assembly through which the heart is modeled as a single-time varying dipole (Einthoven, 1903). The acronym "EKG" came from Einthoven's native Dutch language, because the root word "cardio" is spelled with a k. With the aim of tracing an ECG waveform, a differential recording between two points on the body surface is performed. Conventionally, every differential recording is called a lead. Einthoven specified three leads named with the Roman numerals I, II, and III. Because the body is understood to be merely resistive at ECG frequencies, the four limbs can be considered as wires connected to the torso. For this reason, lead I may possibly be recorded from the person's shoulders without ruining any of the cardiac data (Berbari, 2000).

The progress of the ECG continued for 30 years when F. N. Wilson appended concepts of a "unipolar" recording (WIlson, Johnson, & Hill, 1934). He designed a reference point by connecting three limbs together and finding the average of their potentials, discovering that personal recording site on the limbs or chest surface can be differentially recorded having an identical reference point. He broadened the biophysical models to design the concept of the cardiac origin placed inside the volume conductor of the body. He incorrectly considered that the central terminal was a true ground potential. On the other hand, from the mid-1930s until today, the 12 leads are made up of 3 limb leads; 3 leads in which the limb potentials are referenced to a modified Wilson terminal (the amplified leads (Goldberger, 1942)); and 6 leads located across the chest and referenced to the Wilson terminal, which form the basis of the standard 12-lead ECG. These sites are historically based, have a built-in redundancy, and are not best suited for every kind of cardiac event. An ECG will record the voltage difference from any two sites. The ECG signals are usually in the range of ± 2 mV and need a recording bandwidth of 0.05–150 Hz. Complete technical specification for ECG equipment is suggested by both the American Heart Association (EC11a, 1984) and the Association for the Advancement of Medical Instrumentation (Bailey, Berson, & Garson, 1990).

Body surface mapping indicates the usage of numerous recording sites (>64) set on the body so that isopotential surfaces could be calculated and analyzed over time. This concept still has a role in many researches. Other subgroups of the 12-lead ECG are used in limited-mode recording events such as tape-recorded ambulatory ECG (typically 2 leads), in intensive care monitoring at the bedside (typically 1 or 2 leads), or telemetered within regions of the hospital from patients who are not restrained to bed (1 lead). The recording electronics of these ECG systems have come from the typical progress of contemporary instrumentation, for example, vacuum tubes, transistors, integrated chips, and microprocessors. Usage of computers with the ECG for machine reading was one of the first usages of computers in medicine (Jenkins, 1981). Of importance in computer-based systems was substitution of a human reader and explanation of the standard waves and intervals. Initially this was

performed by connecting the ECG machine to a centralized computer using phone lines. The contemporary ECG machine is entirely integrated with an analog front end, a 12- to 16-bit analog-to-digital (A/D) converter, a computational microprocessor, and dedicated input-output (I/O) processors. These systems find a dimensional matrix derived from the 12 lead signals and examine this matrix using a set of rules to attain the final set of interpretive statements (Pryor, Drazen, & Laks, 1980). The better hospital-based system will record these changes and keep a large database of all ECGs accessible by all permutations of parameters, for example, all females, older than age 30, or with an inferior congenital heart disease (Berbari, 2000).

There are hundreds of demonstrative approaches where a particular diagnosis is made for every ECG, but there are only about five or six major classification sets for which ECG is used. The initial step in ECG analysis requires computation of the rate and rhythm for the atria and ventricles, including any conduction instability, either in the connection among the different chambers or within the chambers themselves. Then feature identification connected to the presence or absence of scarring due to a myocardial infarction would be performed. The ECG has been a principal method for evaluating chamber size or growth, but one might argue that more precise data in this area would be received by noninvasive imaging technologies (Berbari, 2000).

In recent times, the high-resolution ECG has been expanded, by which the digitized ECG is signal-averaged to lessen random noise (Berbari, Lazzara, Samet, & Scherlag, 1973; Berbari, Lazzara, & Scherlag). This concept, tied with postaveraging high-pass filtering, is used to identify and compute low-level signals ($\sim$1.0 μV) not visible with standard procedures. This computer-based concept has allowed the recording of actions prognostic of prospective life-threatening cardiac actions (Berbari, 2000; Simson, 1981).

2.3.2 Electrocardiogram Signals

Every ECG instrument has horizontal and vertical calibration lines. Horizontal lines are used for voltage calculation and are scaled such that 1 mV is equal to a deflection of 10 tiny segments in either the upward (positive) or downward (negative) direction. Vertical lines on the ECG refer to time calibration for the period of the signal and are usually calibrated so that 2.5 cm in the horizontal direction represents 1 s. Each horizontal section is divided into five segments representing 0.2 s with smaller units further subdivided into 0.04 s segments. ECG traces are generally recorded on specialized ECG paper printed with thin (Julian, Campbell-Cowan, & McLenachan, 2005) vertical lines 1 mm distant interspaced with thick vertical lines at 5 mm distance. This separation is comparable to that of the instrumentation itself and can be employed to compute the heart rate. Assuming a regular heartbeat, the heart rate can be calculated by counting the number of little squares between two consecutive R waves and dividing by 1500; on the other hand, one can add up the large squares and divide by 300 (Begg et al., 2007).

2.3.3 Physiology

The heart consists of four chambers; the upper two chambers are called atria, and the lower two chambers are called ventricles. The atria are thin-walled, low-pressure pumps that collect blood from the venous circulation. Positioned in the upper right atrium are a group of cells that operate as the main pacemaker of the heart. Throughout a composite alteration of ionic concentration crossways, that is, the cell membranes (the present supply), an extracellular potential field is created, which excites bordering cells, and a cell-to-cell transmission of electrical actions occurs. Because the body operates as a purely resistive medium, these potential fields expand to the body surface (Geselowitz, 1989). The nature of the body surface waves is dependent on the total of tissue activating at one time and the relative speed and direction of the activation wave front. Thus the pacemaker potentials produced by a tiny tissue mass are not visible on the ECG. As the activation wave front faces the amplified mass of atrial muscle, the beginning of electrical activity is noticed on the body surface, and the initial ECG wave of the cardiac cycle is visible. This is the P wave, and it symbolizes the start of the atria. Transmission of the cardiac impulse continues from the atria through a sequence of dedicated cardiac cells (the A-V node and the His-Purkinje system), which once more are too undersized in total mass to produce a signal large enough to be visible on the typical ECG. There is a small, fairly isoelectric section following the P wave. Once the large muscle mass of the ventricles is wound up, a fast and big deflection is visible on the body surface. The excitement of the ventricles initiates their contraction and gives the most important force for circulating blood to the organs of the body. This great wave seems to include several components. The original downward deflection is the Q wave, the original upward deflection is the R wave, and the terminal downward deflection is the S wave. The polarity and real existence of these three components rely on the site of the leads on the body as well as a large number of irregularities that might exist. Generally, the big ventricular waveform is commonly called the QRS complex despite its structure. Following the QRS complex is one smaller fairly isoelectric section. Following this smaller section, the ventricles go back to their electrical resting condition, and a wave of repolarization is visible as a low-frequency signal identified as the T wave. In a few persons, a little peak happens at the end or after the T wave, which is

the U wave. Its source has never been fully recognized, but it is thought to be a repolarization potential (Berbari, 2000). The heart is one of the main organs of the human body, crucial to our existence. It is basically a huge pump, its only function is to keep blood circulating and keep the organs alive (Begg et al., 2007).

2.3.4 The ECG Waveform

The QRS complex is an electrical ventricular system and is the most well-known waveform showing electrical activity inside the heart. It is the basis for automatic recognition of heart rate and also as an access point for classification schemes and ECG data-compression algorithms (Kohler, Hennig, & Orglmeister, 2002). The QRS complex morphology describes the mechanical action of the heart, offering a view into how each chamber functions. The waves of depolarization extending all the way through the heart via each cardiac cycle produce electrical impulses. These impulses travel via a variety of body fluids, that is, blood, up to the body's surface where they can be recorded using surface electrodes. These signals are then sent to an ECG. The main characteristics of the QRS wave that describe significant data related to cardiac health are as follows (Begg et al., 2007):

(a) P wave
(b) QRS complex
(c) T wave
(d) QRS intervals

P Wave: The original P wave is due to electrical action coming from atrial contraction (systole). In cardiovascular diseases (CVDs), the P wave can turn out to be unclear and shown as irregular. An inverted P wave resulting from positive to negative altered voltage symbolizes that polarization of the atria is irregular (Julian et al., 2005). This indicates that the source of the pacemaker signal is not in the SA node but could arrive from somewhere else, for example, the atrium or the AV node. If the P wave has a seemingly broadened or notched characteristic, this shows a stoppage in the depolarization of the left atrium, which could indicate trouble in the conduction system. Right atrial growth (P pulmonale) can direct high P waves, usually growing more than 3 mm on the ECG trace (Begg et al., 2007).

QRS Complex: The QRS complex is the ventricular contraction (systole) consisting of the Q wave, which is the first negative deviation, followed by the R wave, a positive (upward) deviation. Any negative deflection following immediately after the R portion is termed the S wave. Models of abnormal QRS complexes could reveal a couple of R waves present or cases where the R part is not present. This wave's analysis is dependent on the ECG electrode/lead recording. Unusually large Q waves could indicate MI, opposite to a healthy Q wave, which is not normally higher than 2 mm in amplitude or 0.03 s in width. The QRS complex is generally not larger than 0.1 s and on average is of 0.06 to 0.08 s duration (Begg et al., 2007).

T Wave: Subsequent to ventricular contraction, the ventricles relax (diastole) producing the T wave. Contrasted with the earlier two wave segments, the T wave is a repolarization wave, usually lasting for 0.25–0.35 s subsequent to ventricular depolarization. In this phase, the lower heart chambers are relaxing electrically and getting ready for their subsequent muscle contraction. Atria repolarization is also present, but the signal amplitude is generally covered by the larger QRS complex because of ventricular contraction and is consequently hard to notice. The T wave goes in the same direction as the QRS component because repolarization happens from epicardium to endocardium, in a direction reverse to depolarization, which continues from endocardium to epicardium. T waves are generally not higher than 5 mm in the typical leads. Unusually high T waves may indicate MI, whereas smoothened T waves can be sign of myxedema or hypokalemia (Begg et al., 2007).

QRS Segment Intervals: Besides the wave shapes, the time intervals are essential in the assessment of cardiac health. Among the start of the P wave and the start of the QRS complex is the PQ interval; because the Q wave is frequently not present, this interval is also called the PR interval and stays for the time among the start of atrial contraction and the start of ventricular contraction (normally about 0.16 s). In cases where heart disease is present, particularly with scarred or reddened heart tissue, a longer PR interval may be noticed as more time is necessary for the depolarization wave to extend through the atrial myocardium and the AV node. Reduced PR intervals could represent that the impulse is coming in the junction tissue or could be because the Wolff-Parkinson-White syndrome (Begg et al., 2007; Julian et al., 2005).

The ST segment is an additional interval significant for recognition of many CVDs. As a rule, it comes as a leveled straight line among the QRS complex and the T wave. An eminent or dejected ST segment (relying on the ECG lead being noticed) is an indication of MI because the heart muscle is injured or does not collect enough blood, resulting in a disorder in ventricular repolarization. Pericarditis can be discovered by noticing ST segments concaving upward over a many cardiac cycles. In digitalis therapy, it has been found that ST segments are depressed with a tender drooping, whereas the T wave stays unchanged or flattened (Begg et al., 2007).

The QT interval lasts roughly 0.35 s and gives relevant data concerning the state of ventricular contractions. Its duration decreases as the heart rate goes up, and typically the QT interval does not last more than half the time between the earlier RR interval for rates among 60 and 90 beats per min. From time to time, this is hard to compute

because it cannot be instantly noticed. But extended QT intervals can point to the danger of ventricular tachycardia (VT) or the occurrence of certain drugs, for example, antidepressants (Begg et al., 2007).

2.3.5 Heart Diseases

There are different heart arrhythmias. In this chapter, four major heart arrhythmias are selected because these are the most frequent arrhythmias. These are premature ventricular contraction (PVC), atrial premature contraction (APC), right bundle branch block (RBBB), and left bundle branch block (LBBB). In the following text, a short description of these four arrhythmias will be given.

Premature Ventricular Contraction: PVCs are the result of an irritable ventricular focus. They may be uniform (identical form) or multiform (different forms). Typically, PVC is followed by a full compensating break because the sinus node timing is not interrupted. In general, the sinus rate gives the subsequent sinus impulse on time. Quite the opposite, PVC may be followed by a noncompensatory pause if the PVC comes into the sinus node and restarts its timing; this causes the subsequent sinus P wave to show up earlier than expected. Its rate is dependent on the rate of the original rhythm. Rhythm is irregular whenever PVC occurs. PVC is not related to P wave and PR interval. QRS lasts longer than 0.1 s.

Atrial Premature Contraction: APC, also called PAC in the literature, is another important heart arrhythmia. A single contraction happens before the subsequent estimated sinus contraction. After the APC, sinus rhythm typically resumes. Its rate is dependent on the rate of underlying rhythm, and rhythm is abnormal whenever APC occurs. P wave is present and may have various shapes. PR interval is also present and varies in PAC. Duration of QRS is normal, ranging from 0.06 to 0.1 s.

Right Bundle Branch Block: Third most frequent heart arrhythmia is RBBB. QRS complex lasts more than 0.10 s. QRS axis may be normal but may also deviate to the right. It broads S wave in leads I, aVL, V5, and V6. Its RSR pattern in lead V1 with R is higher than R QRS pattern in V5 and V6. ST-T is fuzzy and in reverse direction to terminal segment of QRS (this is not ST elevation or ST depression).

Left Bundle Branch Block: Fourth arrhythmia that will be discussed is LBBB. It is similar to RBBB. QRS complex lasts more than 0.1 s. It is mainly negative in leads V1 and V2 and positive in V5 and V6. Absence of small, normal Q waves is noticed in I, aVL, V5, and V6. Its wide monophasic R waves are found in I, aVL, V1, V5, and V6 (Jones, 2008).

2.3.6 Uses of ECG Signals in Diagnosis of Heart Arrhythmia

CVDs are one of the main causes of mortality worldwide. The creation of accurate and fast techniques for automated ECG heartbeat signal classification is vital for clinical diagnosis of different CVDs (Thaler, 1999), for example, an arrhythmia. Notion arrhythmia is employed to represent a group of circumstances in which irregular electrical activities coming from heart are characterized by ECG beats or patterns (Chazal, O'Dwyer, & Reilly, 2004; Pan & Tompkins, 1985). ECG is an effective, simple, noninvasive tool for heart disease recognition. Medical doctors investigate several waveforms based on their characteristics (amplitude, polarity, etc.) and diagnose and treat based on this investigation.

EXAMPLE 2.11 The following MATLAB code was used to plot the normal, APC, PCV, LBBB, and RBBB ECG signals. For this example, MIT-BIH Arrhythmia Database was used. You can download the data from the following website: https://www.physionet.org/physiobank/database/mitdb/

Dataset Information: Boston's Beth Israel Hospital and MIT have maintained a study on arrhythmia analysis and related subjects. One of the first chief achievements of this effort was the MIT-BIH Arrhythmia Databas, which started distributing in 1980. The database was the first publicly accessible dataset of standard test material for the assessment of arrhythmia detectors and has been employed for this aim as well as for basic research into cardiac dynamics at more than 500 sites worldwide. The MIT-BIH Arrhythmia Database includes 48 half-hour extracts of 2-channel ambulatory ECG recordings, taken from 47 subjects studied by the BIH Arrhythmia Laboratory between 1975 and 1979. Twenty-three signals were selected randomly from a set of 4000 24-h ambulatory ECG signals recorded from a mixed population of inpatients (about 60%) and outpatients (about 40%) at Boston's Beth Israel Hospital; the remaining 25 recordings were chosen from the same set to contain less common but clinically important arrhythmias that would not be well represented in a small random sample. The ECG signals were sampled at 360 Hz per channel with 11-bit resolution over a 10-mV range. Two or more cardiologists individually interpreted each record; disagreements were resolved to get the computer-readable reference annotations for each beat (approximately 110,000 annotations in all) included with the database. The entire MIT-BIH Arrhythmia Database has been freely accessible since PhysioNet's inception in September 1999. Exemplary ECGs are depicted in Fig. 2.14. The following MATLAB code was used to plot each signal:

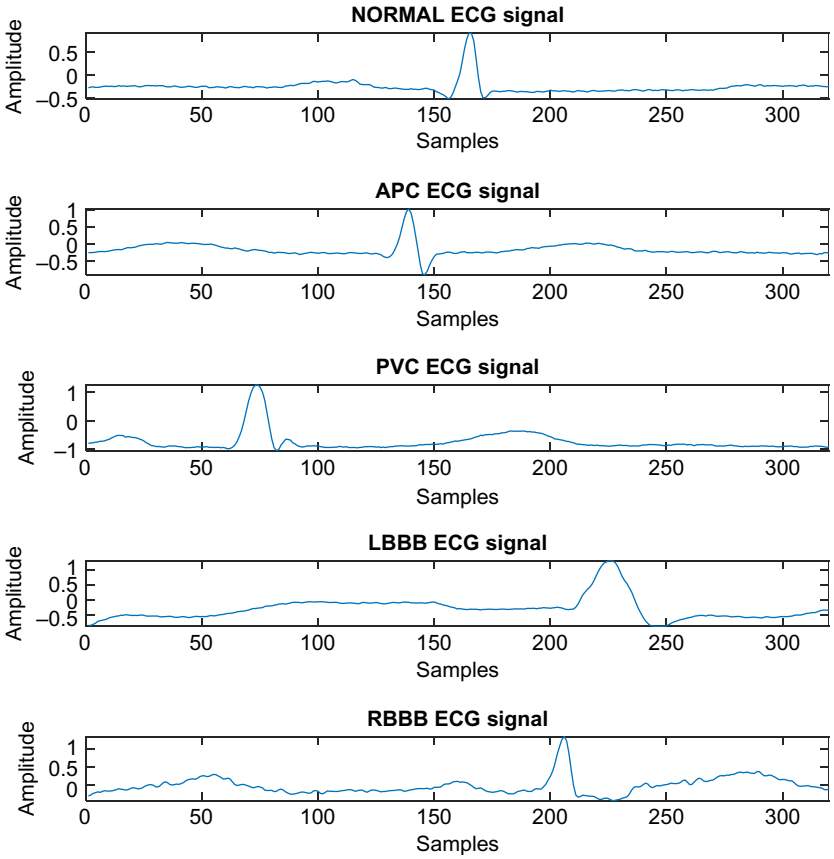

FIG. 2.14 Drawing of different ECG signals (normal, APC, PVC, LBBB, and RBBB).

```
%% Ch2_EX_11.m
clc
clear
%Load Sample ECG Data downloaded from the web site
%https://www.physionet.org/physiobank/database/mitdb/
load MITBIH_ECG.mat

%Plot NORMAL ECG Signal
subplot(5,1,1);
plot(ECGN(:,1));
title('NORMAL ECG Signal')
ylabel('Amplitude')
axis ([0 320 -inf inf])

%Plot APC ECG Signal
subplot(5,1,2);
plot(ECGAPC(:,1))
title('APC ECG Signal')
xlabel('Samples')
ylabel('Amplitude')
axis ([0 320 -inf inf])

%Plot PVC ECG Signal
subplot(5,1,3);
plot(ECGPVC(:,1))
title('PVC ECG Signal')
```

```
xlabel('Samples')
ylabel('Amplitude')
axis ([0 320 -inf inf])

%Plot LBBB ECG Signal
subplot(5,1,4);
plot(ECGLBBB(:,1))
title('LBBB ECG Signal')
xlabel('Samples')
ylabel('Amplitude')
axis ([0 320 -inf inf])

%Plot RBBB ECG Signal
subplot(5,1,5);
plot(ECGRBBB(:,1))
title('RBBB ECG Signal')
xlabel('Samples')
ylabel('Amplitude')
axis ([0 320 -inf inf])
```

EXAMPLE 2.12 The following MATLAB code was used to plot the normal, APC, PCV, and RBBB ECG signals. For this example, St. Petersburg Institute of Cardiological Technics 12-lead Arrhythmia Database data was used. You can download the data from the following website: https://www.physionet.org/pn3/incartdb/

Dataset Information: This database contains of 75 annotated ECG signals taken from 32 Holter records. Every signal is 30 min long and contains 12 standard leads, sampled at 257 Hz, with gains varying from 250 to 1100 analog-to-digital converter units per millivolt. Gains for each signal is specified in its .hea file. The reference annotation files contain more than 175,000 beat annotations in all. The original ECG signals were recorded from patients undergoing tests for coronary artery disease (17 men and 15 women, aged 18–80; mean age: 58). None of the patients had pacemakers; most had ventricular ectopic beats. In choosing the ECG signals to be contained in the database, preference was given to subjects with ECGs composed of arrhythmias, coronary artery disease, ischemia, and conduction abnormalities. The annotations were formed by an automated algorithm and then revised manually, following the standard PhysioBank beat annotation definitions. The algorithm usually places beat annotations in the middle of the QRS complex; the locations have not been manually corrected, and there might be rare misaligned annotations as a result. This database was donated by the St. Petersburg Institute of Cardiological Technics (Incart), St. Petersburg, Russia. Exemplary ECGs are depicted in Fig. 2.15. The following MATLAB code was used to plot each signal:

```
%% Ch2_EX_12.m
clc
clear
%Load Sample ECG Data downloaded from the web site
%https://www.physionet.org/pn3/incartdb/
load PetersburgECG.mat

%Plot NORMAL ECG Signal
subplot(4,1,1);
plot(ECGN(:,1));
title('NORMAL ECG Signal')
ylabel('Amplitude')
axis ([0 1000 -inf inf])

%Plot APC ECG Signal
subplot(4,1,2);
plot(ECGAPC(:,1))
```

```
title('APC ECG Signal')
xlabel('Samples')
ylabel('Amplitude')
axis ([0 1000 -inf inf])

%Plot PVC ECG Signal
subplot(4,1,3);
plot(ECGPVC(:,1))
title('PVC ECG Signal')
xlabel('Samples')
ylabel('Amplitude')
axis ([0 1000 -inf inf])

%Plot RBBB ECG Signal
subplot(4,1,4);
plot(ECGRBBB(:,1))
title('RBBB ECG Signal')
xlabel('Samples')
ylabel('Amplitude')
axis ([0 1000 -inf inf])
```

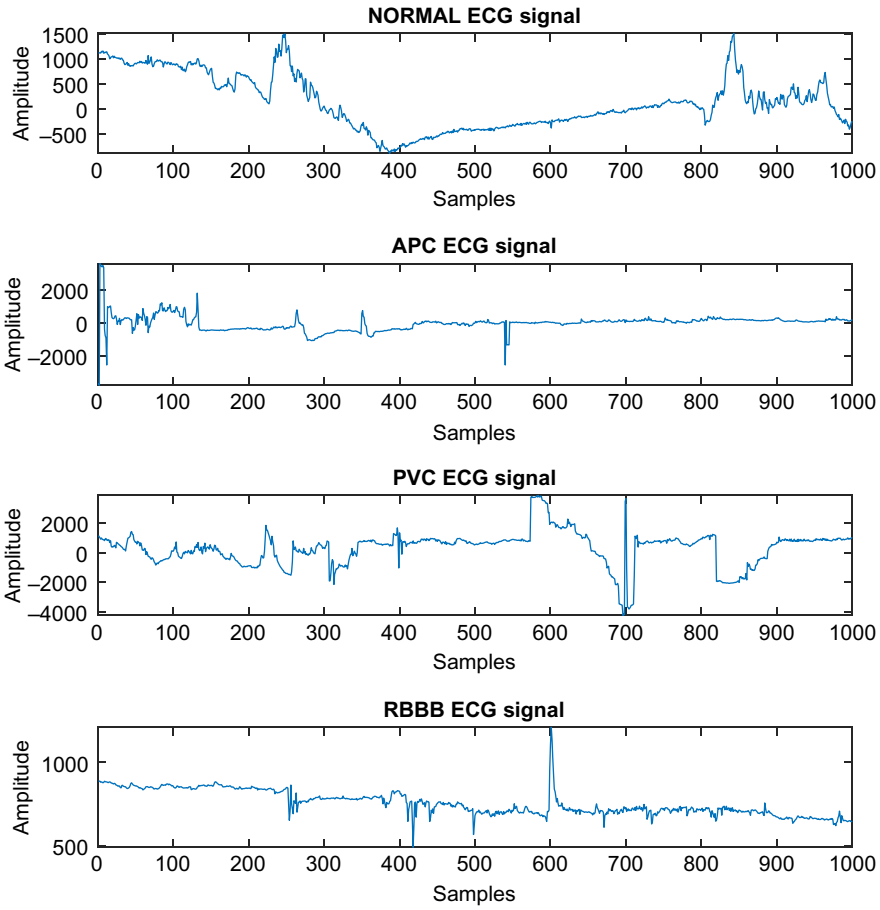

FIG. 2.15 Drawing of different ECG signals (normal, APC, PVC, and RBBB).

2.3.7 Uses of ECG Signals in Congestive Heart Failure Detection

The human heart is the most crucial muscle in human body, which together with blood vessels forms the cardiovascular system. It pumps blood into every cell of the human body. Moreover, heart muscle is the engine of the human body (Horobin, 2008). Heart failure is a common syndrome that progresses gradually but causes cardiac dysfunction due to the failure of the heart to effectively pump blood to all the cells of the human body. The heart deteriorates through heart attacks, long-term high blood pressure, or an anomaly of one of the heart valves. Hence, heart failure is usually not realized until it comes to the more progressive phase, called congestive heart failure (CHF), which causes fluid to flow to the lungs, feet, and abdominal cavity. CHF is a disorder that can result from heart diseases, such as coronary artery disease, damage to the heart after a heart attack, high blood pressure, valvular heart disease, diabetes, and even alcoholism (Masetic & Subasi, 2016; Quinn, 2006).

Considering that there is no exact diagnosis of heart failure, medical diagnosis such as history or physical examinations, ECG, echocardiography, or chest radiography is critical for recognizing CHF. ECG is a noninvasive tool that records electrical activity of the heart and reveals the heartbeat irregularities. It safely studies and records the electrical impulses of the heart, representing possible damage of the heart or irregularities of its heartbeats (Passanisi, 2004). Therefore, ECG is an imperative tool for defining the function and health of the cardiovascular system. Furthermore, it is substantial to describe precise and appropriate diagnosis of physicians to circumvent more damage and to define appropriate approaches and techniques (Son, Kim, Kim, Park, & Kim, 2012). However, a problem arises when there is an inadequate number of physicians to meet the needs of patients. Hence, it is essential to implement an efficient and automated diagnostic system based on ECG signals, together with the application of machine learning techniques for classification of heart diseases. These diagnostic systems support medical experts in distinguishing the anomalies in the cardiovascular system. The diagnostic system first processes the ECG signals taken from several subjects, which are then decomposed into a few applications that perform feature extraction. Extracted ECG signals are employed to distinguish different kinds of heart failure by utilizing several machine learning techniques (Masetic & Subasi, 2016; Subasi, 2013).

According a number of studies implemented, the field of heartbeat classification employing several methods is widespread. Beth Israel Deaconess Medical Center (BIDMC) CHF Database was employed in many researches. Baim et al. (1986)) employed this database to represent the effect of treatment with oral milrinone. Thuraisingham (2009) employed BIDMC CHF Database in distinguishing CHF from normal heartbeats, utilizing *k*-nearest neighbor algorithm and features from the second-order difference plot taken from Holter monitor cardiac RR intervals. The same database was employed by Kuntamalla and Reddy (2010), and they used sequential trend analysis to discriminate CHF patients from subjects with normal heartbeats. Moreover, Kuntamalla and Reddy (2014) employed multiscale entropy (MSE) to heart rate variability (HRV) signals, to distinguish healthy, young, and elderly subjects from CHF patients. They used Reduced Data Dualscale Entropy Analysis to decrease the data size for clear differentiation of subjects. Hossen and Al-Ghunaimi (2008) employed a technique based on recognition of power spectral density patterns of decomposed subbands of RR interval to recognize patients with CHF. They used 12 subjects from the BIDMC CHF Database. The same authors, Hossen and Al-Ghunaimi (2007) employed different wavelet-decomposition filters with soft-decision algorithm to evaluate the power spectral density of RR-interval data for screening patients with CHF. Yu and Lee (2012) focused on choosing the best feature selector to achieve high accuracy in identifying CHF. The authors employed conditional mutual information feature selector with SVM classifier. Isler and Kuntalp (2007) combined classical HRV and wavelet entropy measures to differentiate healthy patients from subjects with CHF. They utilized a genetic algorithm to choose the best ones among all possible combinations of measures. Moreover, they employed *k*-nearest neighbor classifier with several *k* values. Similar study was implemented by Asyali (2003), and the author employed linear discriminant analysis to observe the differentiation power of nine long-term HRV measures, validating the result by employing Bayesian classifier. Pecchia, Melillo, Sansone, and Bracale (2011) studied the differentiation power of HRV in distinguishing normal subjects and subjects with CHF. They employed time and frequency analysis to measure HRV features. The result was assessed by using classification and regression tree (CART) classifier. Also, the authors presented two nonstandard features: average of normal intervals and low/high frequencies recorded over 24 h (Masetic & Subasi, 2016).

EXAMPLE 2.13 The following MATLAB code was used to plot CHF ECG signals. For this example, the BIDMC CHF Database was used. You can download the data from the following website: https://www.physionet.org/physiobank/database/chfdb/

Dataset Information: This database includes long-term ECG signals taken from 15 subjects (11 men, aged 22–71, and 4 women, aged 54–63) with severe CHF (NYHA class 3–4). This group of subjects was part of a larger study group taking conventional medical therapy before taking the oral inotropic agent, milrinone. The different signals are each about 20 h in duration and include two ECG signals each sampled at 250 Hz with 12-bit resolution over a range of ±10 mV. The original analog signals were recorded at

Boston's Beth Israel Hospital (now the Beth Israel Deaconess Medical Center) employing ambulatory ECG recorders with a typical recording bandwidth of approximately 0.1–Hz. Annotation files (with the suffix.ecg) were prepared employing an automated detector and have not been corrected manually. Exemplary ECGs are depicted in Fig. 2.16. The following MATLAB code was used to plot each signal:

```
%% Ch2_EX_13.m
clc
clear
%Load Sample Congestive Heart Failure (CHF) ECG Data downloaded from the web site
%https://www.physionet.org/physiobank/database/chfdb/
load chf01m.mat

%Plot Congestive Heart Failure (CHF) ECG signal
subplot(2,1,1);
plot(val(1,1:2048));
title('Congestive Heart Failure (CHF) ECG signals')
xlabel('Number of Samples')
ylabel('Amplitude')
legend('Channel I')
axis ([0 2048 -inf inf])

%Plot Congestive Heart Failure (CHF) ECG signal
subplot(2,1,2);
plot(val(2,1:2048));
xlabel('Number of Samples')
ylabel('Amplitude')
legend('Channel II')
axis ([0 2048 -inf inf])
```

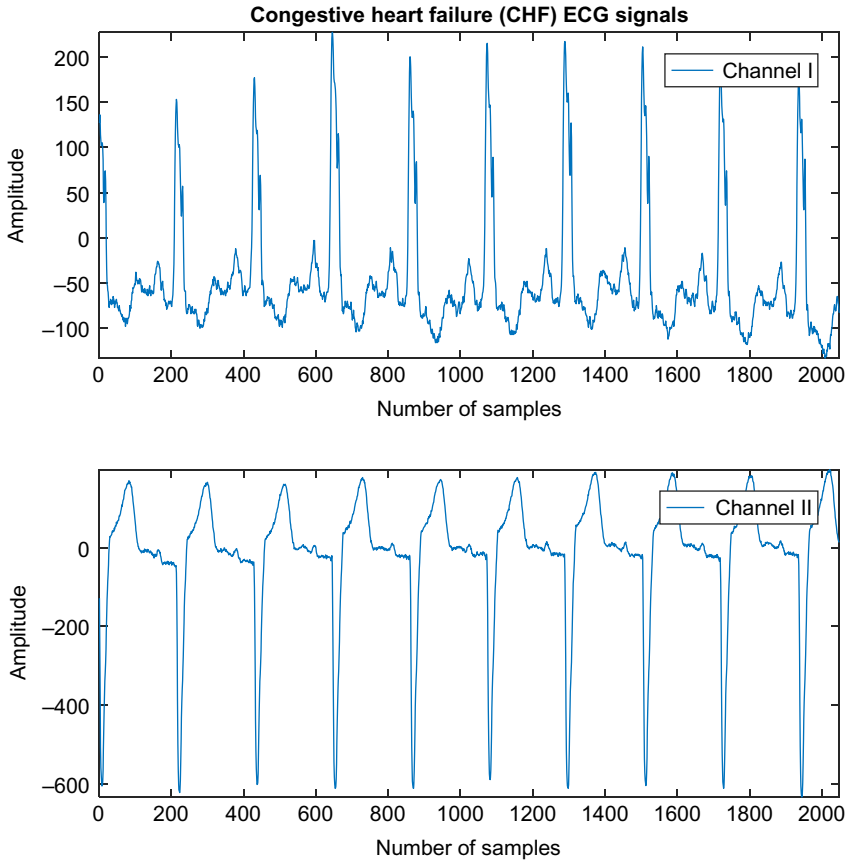

FIG. 2.16 Drawing of CHF ECG signals.

2.3.8 Uses of ECG Signals in Sleep Apnea Detection

Obstructive sleep apnea (OSA) is a type of sleep-disordered breathing represented by repeated cycles of partial (hypopnea) or complete (apnea) failure of the pharyngeal airway (Baguet, Barone-Rochette, Tamisier, Levy, & Pépin, 2012). It disturbs about 10% of middle-aged adults, mainly overweight or obese men. If untreated, OSA can cause cognitive impairment, somnolence, ischemic heart disease, cardiovascular morbidity, and mortality. Nevertheless, almost 80% of people with such conditions persist undiagnosed and consequently untreated because of the various problems related to present diagnostic techniques (Jin & Sánchez-Sinencio, 2015). Conventionally, OSA is diagnosed by expert physicians by manual observation of PSG signals. OSA screening based on visual inspection is challenging. First, PSG is expensive and requires the subject to sleep in a special sleep center. Due to the unfamiliar environment of the sleep center, the subject's quality of sleep is degraded. Second, manual screening of OSA is time-consuming, burdensome, reliant on expensive human resources and physicians' level of expertise and experience, and error-prone due to fatigue. Hence, there is a need for a computer-aided OSA detection scheme. ECG signals are extensively employed for computerized OSA detection (Hassan & Haque, 2016)

EXAMPLE 2.14 The following MATLAB code was used to plot the ECG signals related to the sleep apnea. For this example, data for development and evaluation of ECG-based apnea detectors database was used. The data can be downloaded from the following website:https://www.physionet.org/physiobank/database/apnea-ecg/

Dataset Information: This database is described by Penzel, Moody, Mark, Goldberger, and Peter (2000). The data consist of 70 records, divided into a LEARNING SET of 35 records, and a TEST SET of 35 records. Signals vary in length from slightly less than 7 h to nearly 10 h each. Each signal contains a continuous digitized ECG signal, a set of apnea annotations, and a set of machine-generated QRS annotations. The digitized ECG signals were sampled at 100 Hz with 16 bits per sample. Exemplary ECGs are depicted in Fig. 2.17. The following MATLAB codewas used to plot each signal:

```
%% Ch2_EX_14.m
clc
clear
%Load Sample Sleep Apnea ECG Data downloaded from the web site
%https://www.physionet.org/physiobank/database/apnea-ecg/
load ucddb002_recm.mat

%Plot Sleep Apnea ECG signal
subplot(2,1,1);
plot(val(1,10000:15000));
title('Sleep Apnea ECG signal')
xlabel('Number of Samples')
ylabel('Amplitude')
legend('Channel I')
axis ([0 5000 -inf inf])

%Plot Sleep Apnea ECG signal
subplot(2,1,2);
plot(val(2,10000:15000));
title('Sleep Apnea ECG signal')
xlabel('Number of Samples')
ylabel('Amplitude')
legend('Channel II')
axis ([0 5000 -inf inf])
```

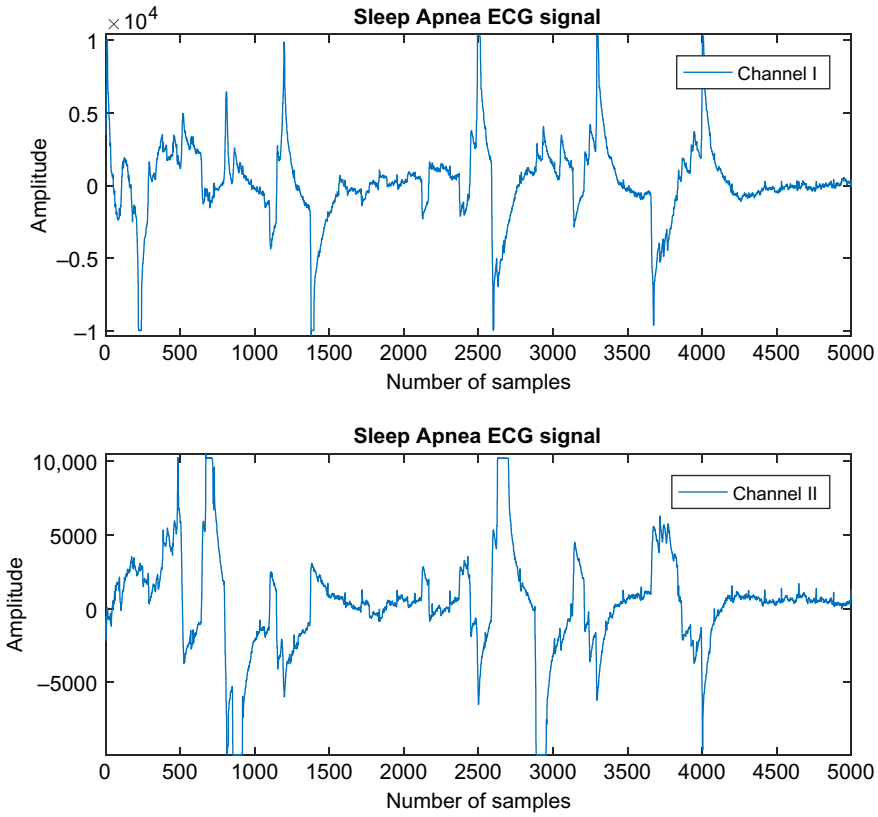

FIG. 2.17 Drawing of sleep apnea ECG signals.

2.3.9 Uses of ECG Signals in Fetal Analysis

Fetal health conditions can be evaluated utilizing ECG signals, which allows discovery of possible distress or congenital heart defects in early stages of pregnancy and during delivery (Kennedy, 1998). Fetal heart rate (HR) monitoring and recognition of the fetal ECG (f-ECG) provides early diagnosis of fetal arrhythmias, making it possible to treat them with drug administration or to preschedule the delivery. In abdominal f-ECG recording, the electrical signal generated by the fetal heart is measured by noninvasive electrodes placed on the mother's abdomen surface. This type of measurement is obviously appropriate for long-term observation as well as for at-home monitoring during all pregnancy (Da Poian, Bernardini, & Rinaldo, 2016).

EXAMPLE 2.15 The following MATLAB code was used to plot the f-ECG signals. For this example, Abdominal and Direct Fetal Electrocardiogram Database was used, and the data can be downloaded from the following website: https://physionet.org/physiobank/database/adfecgdb/

Dataset Information: The Abdominal and Direct Fetal Electrocardiogram Database includes multichannel f-ECG signals taken from five different women in labor, between 38 and 41 weeks of gestation. The signals were recorded in the Department of Obstetrics at the Medical University of Silesia by means of the KOMPOREL system for acquisition and analysis of f-ECG. Every signal contains four differential signals recorded from maternal the abdomen and direct f-ECG registered from the fetal head. The acquisition of direct f-ECG was implemented with a typical spiral electrode, usually employed in a direct f-ECG channel of popular fetal monitors. The signal bandwidth was 1–150 Hz and sampled at 1 kHz with 16-bits resolution (Kotas, Jezewski, Horoba, & Matonia, 2011). Exemplary ECGs are depicted in Fig. 2.18. The following MATLAB code was used to plot each signal:

```
%% Ch2_EX_15.m
clc
clear
%Abdominal and Direct Fetal Electrocardiogram Database
%Load Sample Abdominal and Direct Fetal ECG Database downloaded from the web site
%https://physionet.org/physiobank/database/adfecgdb/
load r01_edfm.mat

%Plot Fetal Electrocardiogram Signal
subplot(2,1,1);
plot(val(1,1:2048));
title('Fetal Electrocardiogram Signals')
xlabel('Samples')
ylabel('Amplitude')
legend('Channel I')
axis ([0 2048 -inf inf])

%Plot Fetal Electrocardiogram Signal
subplot(2,1,2);
plot(val(2,1:2048));
xlabel('Samples')
ylabel('Amplitude')
legend('Channel II')
axis ([0 2048 -inf inf])
```

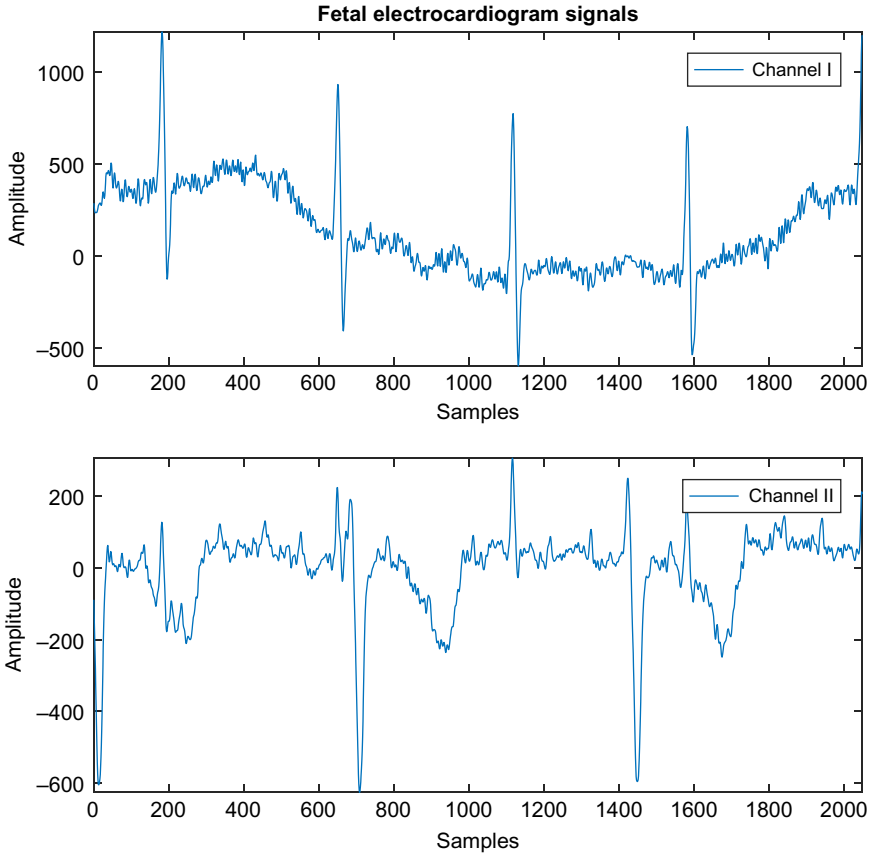

FIG. 2.18 Drawing of fetal ECG signals.

2.4 PHONOCARDIOGRAM

The heart sound signal is a traditional biomedical signal, because the stethoscope is the primary instrument utilized by doctors. Phonocardiogram (PCG) signals produce valuable information related to the heart valves, and consequently several heart diseases can be detected by utilizing this signal (Jia, Song, Tao, & Lu, 2012). Two of the loudest heart sounds are the first (S1) and the second (S2) sounds; the time interval between S2 and S1 is termed diastole and the time interval between S1 and S2 is termed systole. Normal heart sounds produced by the heart valves are low-frequency transient signals, whereas abnormal heart sounds such as heart murmurs are high-frequency, noise-like sounds (Ergen, Tatar, & Gulcur, 2012). Heart murmurs are generated by turbulence in blood flow through narrow cardiac valves or reflow through the atrioventricular valves. Congenital heart faults or detected heart valve diseases are generally the source of abnormal heart murmurs. Aortic stenosis, aortic regurgitation, mitral regurgitation, and mitral stenosis are among the most frequently seen pathological types of murmurs. Research on PCG signals using biomedical signal processing methods is on the rise due to the ability of PCG recordings to characterize significant features of the heart sounds. Many studies have been focused on examining the possibility of the PCG signal classification toward the diagnosis of heart valve disorders (Kao & Wei, 2011). Heart sound is the result of turbulent blood flow and vibrating cardiovascular structures, which propagate to the chest. These vibrations are naturally a consequence of myocardial and valvular events, which are affected by the hemodynamics, function, and electrical activity of the cardiac muscle. These have a direct influence on the spectral, morphological, and timing features of the main heart sounds (S1, S2, and S3) (Carvalho et al., 2011).

In the past, several theories have been posited to describe the source of sounds during the cardiac cycle. Once it was understood that the strength of contraction of the left ventricle had a substantial effect on the strength of the first heart sound, the myocardial theory of the source of the sound was hypothesized. All heart sounds are achieved when a moving column of blood comes to an abrupt stop or slows down significantly. The strength of a heart sound will depend on the level of energy the moving column of blood has accomplished. The abrupt slowing down causes dissipation of energy that produces vibrations affecting the contiguous cardiohemic mass. The factors affecting the acceleration and deceleration of columns of blood included in the creation of the several heart sounds are diverse. These must be taken into consideration for each sound separately, considering the pathophysiology and the physiology of the phase of the cardiac cycle involved (Oweis, Hamad, & Shammout, 2014)

Sound is produced and transmitted by vibrations. These vibrations consist of a series of waves, which are made up of compressions (areas of increased pressure) and subsequent rarefactions (areas of decreased pressure). These waves travel through solid, liquid, or gaseous media. In general, the ease and speed of transmission of sound waves are inversely proportional to the density of the media in which they are traveling. We generally use a stethoscope to transmit the cardiovascular sounds from the chest wall to our ears. Cardiovascular sound can be divided into brief, circumscribed sounds or transients (heart sounds and clicks) and longer combinations of vibrations (heart murmurs) (Ranganathan, Sivaciyan, & Saksena, 2007)

In some situations, a third heart sound (S3) might be heard, related to abrupt termination of the ventricular rapid-filling phase. Because the ventricles are full of blood and their walls are relaxed during this part of diastole, the vibrations of S3 are of very low frequency. In late diastole, a fourth heart sound (S4) may be heard occasionally, produced by atrial contractions transferring blood into the enlarged ventricles. In addition to these sounds, valvular clicks and snaps are rarely heard (Rangayyan, 2015).

2.4.1 Heart Murmurs

The intervals between S1 and S2 (ventricular systole), and S2 and S1 (ventricular diastole) of the next cycle are normally silent. Murmurs, which may happen in these intervals, are produced by certain cardiovascular imperfections and disorders. Murmurs are high-frequency, noise-like sounds that occur when the velocity of blood becomes high as it flows through an irregularity. Typical conditions in the cardiovascular system that produce turbulence in blood flow are valvular stenosis and insufficiency. A valve can be insufficient when it cannot close well and achieves reverse leakage or regurgitation of blood through a narrow opening. Systolic murmurs (SM) are generated by conditions such as ventricular septal defect, aortic stenosis (AS), pulmonary stenosis (PS), mitral insufficiency (MI), and tricuspid insufficiency (TI). Semilunar valvular stenosis (aortic stenosis, pulmonary stenosis) generates an obstruction in the path of blood ejected during systole. AV valvular insufficiency generates regurgitation of blood to the atria during ventricular contraction. Diastolic murmurs (DM) are generated by conditions such as aortic or pulmonary insufficiency, and mitral or tricuspid stenosis. Other conditions generating murmurs are atrial septal defect (ASD), patent ductus arteriosus (PDA), as well as certain physiological or functional conditions that cause increased cardiac output or blood velocity (Rangayyan, 2015).

2.4.2 First Heart Sound (S1)

The first heart sound happens at the beginning of ventricular contraction. To better understand the physiology of the first heart sound, the cardiac events that happen around the time

of the first heart sound need to be distinguished. At the end of diastole, the atrium contracts and achieves an extra stretch and filling of the ventricle. This is instantly followed by the ventricular contraction. Once the ventricular pressure increases and surpasses the atrial pressure, the mitral and tricuspid valve leaflets turn out to be apposed and close. As the ventricular pressures continue to increase and surpass that of the aorta and the pulmonary artery, the semilunar valves open and the ejection phase begins. All these actions happen in quick sequence over a short period of time and subsidize the production of the first heart sound. S1 is comparatively wide and is composed of many components that overlap each other. These components are "atrial," "mitral," "tricuspid," and "aortic." The strength of S1 is apparently associated with the strength or intensity of the distinct components (Ranganathan et al., 2007).

2.4.2.1 Atrial Component

The energy of the column of blood pushed by the atrial contraction dissipates as the column slows down against the ventricular walls. This slowing down is steady in most normal subjects because of the good compliance and distensibility of the ventricles. Hence, the sound produced has a very low frequency and is not audible. Nevertheless, when the PR interval on the ECG is short, this component can happen very close to the beginning of the ventricular contraction and essentially becomes a part of the first heart sound and contributes to its duration. Aside from this, it has no clinical implication (Ranganathan et al., 2007).

2.4.2.2 Mitral Component

This is the most imperative component of S1. It corresponds in timing to the closure of the mitral valve leaflets. But the apposition of the valve leaflets cannot yield the sound itself. Once the ventricle begins contracting, the pressure increases and imparts energy into the mass of blood within its cavity. Once the pressure in the ventricle surpasses that of the atrium, the column of blood is put into motion. Meanwhile the aortic pressure is much higher than the atrial pressure, and the aortic valve remains closed at this time; the blood contained in the ventricle can only rush toward the atrium. Because the anatomical structure of the mitral valve is like a parachute, the leaflets are raised by the moving blood into a closed position. The papillary muscles contracting and pulling on the chordae tendineae stop leaflet eversion into the atrium. The closed leaflets are detained back by the papillary muscles, attaining the limits of their stretch, stopping the column of blood from moving into the atrium. This abrupt slowing down of the column of blood produces the mitral component, or M1. The energy dissipation produces vibrations of the column of blood as well as the surrounding structures such as the mitral valve structures and the ventricular wall. The mechanism of sound creation of this M1 is identical to the sound created by a parachute filling with wind as it stretches and produces the deceleration of the moving mass of air or by the sail of a sailboat that snaps when filled with a gust of wind (Ranganathan et al., 2007).

2.4.2.3 Tricuspid Component

This component is apparently analogous to the M1 for similar cardiac events that happen including the right-sided structures, such as the tricuspid valve leaflets and the right ventricular wall. But these events happen at much lower pressures and are slightly delayed. The effects of the mechanical events of the right ventricle start slightly later than that of the left ventricle. Consequently, the tricuspid component (T1) follows the M1. It must be distinguished that this component arises because the lower pressure is generally low in frequency. The T1 in the normal adult subjects, although it can be recordable, might subsidize to the duration of S1 but not be audible as a distinct component (Ranganathan et al., 2007).

2.4.2.4 Aortic Component

The aortic component (A1) is generally the second component of audibly split S1 in adults. After mitral and tricuspid valve closures, the ventricular pressure continues to increase during the phase of isovolumic contraction. Once the pressure surpasses the aortic and pulmonary diastolic pressures, the ejection phase starts as the semilunar valves open. The column of blood ejected into the aorta as it hits the aortic walls slows down, and once slowed will result in an audible sound (Ranganathan et al., 2007).

2.4.3 Second Heart Sound (S2)

The second heart sound happens at the end of the ejection phase of systole. It is associated with the closure of the semilunar valves. As the blood is ejected into the aorta and the pulmonary artery during systole (stroke volume), the aortic and the pulmonary pressures increase, and these two vessels become swollen. At the end of systole, as the ventricular pressures start to decrease, the elastic components of the great vessels preserving a higher pressure results in a pressure gradient that drives the columns of blood back into the ventricles. Because of the lower resistance with the dropping ventricular pressures compared to the periphery, the columns of blood in the great vessels flow toward the ventricles at this time. The opposite flow of the columns of blood in the aorta and the pulmonary artery parachutes the cusps of the aortic and the pulmonary valves, closing them. The abrupt slowing down of the columns of blood against the closed semilunar valves results in dissipation of energy, causing the A2 and the P2 components of S2 (Ranganathan et al., 2007).

The S2 is typically louder, crisper, and shorter in duration compared to S1, because the semilunar valve closures happen at much higher pressures than the AV valves, and the dissipated energy in the columns of blood is much larger. In normal young subjects, one can repeatedly hear both components of S2 (A2 and P2). Hence, the S2 can be heard as a split sound. A2 is the first of the two components. The pulmonary arterial bed is bigger and produces noticeably less resistance to forward flow. This makes the inclination to reverse flow happen later and slower compared to the left side. Moreover, the lower pressures accomplished by the right ventricle during systole may cause a slower rate of relaxation of the right ventricle compared to the left ventricle. Consequently, the P2 component happens later. The A2 component is usually heard over the true aortic area, but P2 is heard over the second and the third left intercostal spaces near the sternal border. If the loudness of the two components is compared, the A2 is always louder than the P2 because the systemic arterial resistance is normally 10 times higher than the pulmonary arterial resistance (Ranganathan et al., 2007).

2.4.4 Third Heart Sound (S3)

After the opening of the mitral and the tricuspid valves, blood flows into the ventricles from the atria during diastole. Diastolic filling of the ventricle is separable into three phases, an early rapid filling phase, followed by a slow filling phase or diastasis, and at the end by the atrial contraction phase. The peak of this filling period is characterized by a sound known as the third heart sound. S3 happens at the end of the rapid filling phase of diastole. This phase of diastolic expansion is normally quick and dynamic. However, there is an inclination for the moving column of blood entering the ventricle during the rapid-filling phase to slow down toward the end of this period (Ranganathan et al., 2007).

2.4.5 Fourth Heart Sound (S4)

The atrium usually contracts at the end of diastole and achieves an extra stretch to the ventricles. Once the ventricular compliance is decreased because of factors such as ischemia, infiltrates, fibrosis, infarction, or hypertrophy, this arouses a more dynamic contraction from the atrium. The improved force of atrial contraction also increases the atrial's wave pressure peak. This increased pressure head inclines to accelerate the diastolic inflow at the end of diastole. Because the ventricular compliance is decreased, the accelerated inflow at this phase of diastole is quickly slowed down. This sudden slowing down of the column of blood entering the ventricle at end-diastole leads to dissipation of energy that produces a sound. The sound is referred to as atrial gallop and is called S4. The sound, produced at low pressures of diastole, has a low frequency like S3. But the timing is not similar; it is closer to S1 (Ranganathan et al., 2007).

2.4.6 Uses of PCG Signals in Diagnosis of Heart Diseases

CVDs are the main reason of death worldwide. To successfully detect CVD, different personal health systems have been developed to improve detection and collection of data for clinical decision support. Usually, ECG and heart sound (HS) auscultation are employed for CVD diagnosis (Carvalho et al., 2011). But some of the heart diseases are hard to detect using ECG. Because heart sound signals are complex and highly nonstationary in nature, it is difficult to examine them in an automated way. An auscultation method employed to support clinicians with precise and objective interpretation of heart sounds can be utilized to detect four sounds, namely, S1, S2, S3, and S4, during the heart cycle. The crucial components for signal analysis are S1 and S2, as well as systolic and diastolic periods. Localization (segmentation) of heart sounds must be done before any analysis (Oweis et al., 2014). Duration of S1 and S2 may help determine the heart sound type and detect abnormal heart sounds, and the amplitude of S1 reveals valuable information about myocardial contractility ability (Zhong & Scalzo, 2013).

The heart sound signals (heartbeats) taken from normal subjects generally comprise two separate tones, S1 and S2. Moreover, an auscultation method employed to deliver clinicians with precise and objective interpretation of heart sounds can be utilized to distinguish four sounds, namely, S1, S2, S3, and S4, during the heart cycle (Ramović, Bandić, Kevrić, Germović, & Subasi, 2017). Precise and early diagnosis of cardiac disorders is of great importance that can be achieved through heart auscultation. It is the most common and widely used technique to screen for structural abnormalities of the cardiovascular system. Distinguishing related features and creating an analysis based on the sounds heard through a stethoscope is an ability that can take years to be learned and improve. The effectiveness and precision of analysis based on heart sound auscultation can be enhanced significantly by employing biomedical signal-processing techniques to investigate the PCG signals (Chen, Wang, Shen, & Choy, 2012; Cherif, Debbal, & Bereksi-Reguig, 2010; Choi, Shin, & Park, 2011; Safara, Doraisamy, Azman, Jantan, & Ranga, 2012).

PCG signals can deliver significant information relevant to the performance of heart valves, thus it has potential for distinguishing several heart diseases (Jia et al., 2012). Normal heart sounds are low-frequency transient signals generated by the heart valves, whereas pathological heart sounds, such as heart murmurs, are high-frequency, noise-like sounds (Ergen et al., 2012). Heart murmurs are generated as a result of turbulence in blood flow through narrow cardiac valves or reflow through the atrioventricular valves.

Congenital heart defects or acquired heart valve diseases are frequently the source of abnormal heart murmurs. Aortic regurgitation, aortic stenosis, mitral regurgitation, and mitral stenosis are among the most common pathological types of murmurs. Studies on PCG signals employing biomedical signal-processing techniques are on the rise due to the ability of PCG signals to characterize significant features of the heart sounds (Kao & Wei, 2011).

EXAMPLE 2.16 The following MATLAB code was used to plot the PCG signals. For this example, PCG Phonogram Dataset was used. You can download the data from the following website: https://www.prweb.com/releases/2004/09/prweb162074.htm

Exemplary PCG signals are depicted in Fig. 2.19. The following MATLAB code was used to plot each signal:

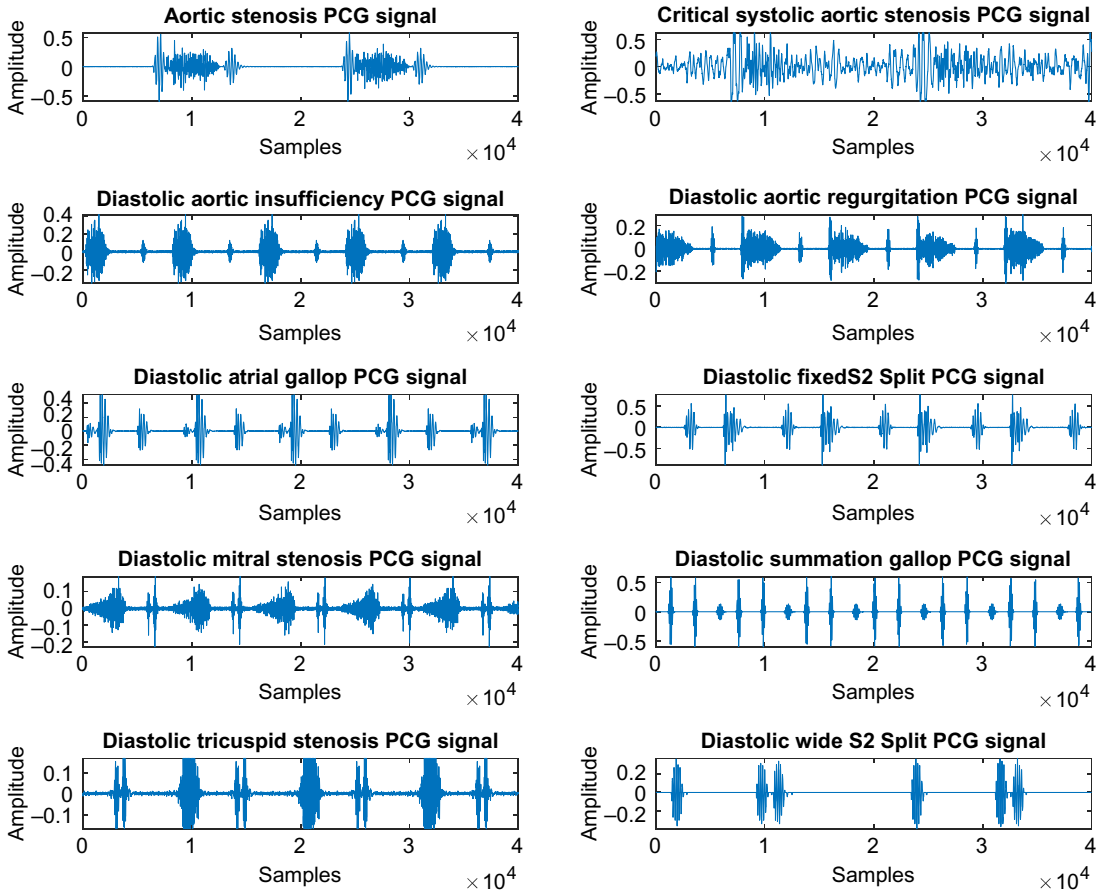

FIG. 2.19 Drawing of different PCG signals.

```
%% Ch2_EX_16.m
clc
clear
%PCG Phonogram Data Set from BioSignetics Corporation
%Load Sample PCG Data downloaded from the web site
%https://www.prweb.com/releases/2004/09/prweb162074.htm
load PCG.mat

%Plot Aortic_Stenosis PCG Signal
subplot(5,2,1);
plot(Aortic_Stenosis_2(1:40000,1));
title('Aortic Stenosis PCG Signal')
ylabel('Amplitude')
axis ([0 40000 -inf inf])
```

```
%Plot Critical_Systolic_Aortic_Stenosis PCG Signal
subplot(5,2,2);
plot(Critical_Systolic_Aortic_Stenosis(1:40000,1))
title('Critical Systolic Aortic Stenosis PCG Signal')
xlabel('Samples')
ylabel('Amplitude')
axis ([0 40000 -inf inf])

%Plot Diastolic_Aortic_Insufficiency PCG Signal
subplot(5,2,3);
plot(Diastolic_Aortic_Insufficiency(1:40000,1))
title('Diastolic Aortic Insufficiency PCG Signal')
xlabel('Samples')
ylabel('Amplitude')
axis ([0 40000 -inf inf])

%Plot Diastolic_Aortic_Regurgitation PCG Signal
subplot(5,2,4);
plot(Diastolic_Aortic_Regurgitation(1:40000,1))
title('Diastolic Aortic Regurgitation PCG Signal')
xlabel('Samples')
ylabel('Amplitude')
axis ([0 40000 -inf inf])

%Plot Diastolic_Atrial_Gallop PCG Signal
subplot(5,2,5);
plot(Diastolic_Atrial_Gallop(1:40000,1))
title('Diastolic Atrial Gallop PCG Signal')
xlabel('Samples')
ylabel('Amplitude')
axis ([0 40000 -inf inf])

%Plot Diastolic_FixedS2_Split PCG Signal
subplot(5,2,6);
plot(Diastolic_FixedS2_Split_II(1:40000,1))
title('Diastolic FixedS2 Split PCG Signal')
xlabel('Samples')
ylabel('Amplitude')
axis ([0 40000 -inf inf])

%Plot Diastolic_Mitral_Stenosis PCG Signal
subplot(5,2,7);
plot(Diastolic_Mitral_Stenosis(1:40000,1))
title('Diastolic Mitral Stenosis PCG Signal')
xlabel('Samples')
ylabel('Amplitude')
axis ([0 40000 -inf inf])

%Plot Diastolic_Summation_Gallop PCG Signal
subplot(5,2,8);
plot(Diastolic_Summation_Gallop(1:40000,1))
title('Diastolic Summation Gallop PCG Signal')
xlabel('Samples')
ylabel('Amplitude')
axis ([0 40000 -inf inf])
```

```
%Plot Diastolic_Tricuspid_Stenosis PCG Signal
subplot(5,2,9);
plot(Diastolic_Tricuspid_Stenosis(1:40000,1))
title('Diastolic Tricuspid Stenosis PCG Signal')
xlabel('Samples')
ylabel('Amplitude')
axis ([0 40000 -inf inf])

%Plot Diastolic_Wide_S2_Split PCG Signal
subplot(5,2,10);
plot(Diastolic_Wide_S2_Split(1:40000,1))
title('Diastolic Wide S2 Split PCG Signal')
xlabel('Samples')
ylabel('Amplitude')
axis ([0 40000 -inf inf])
```

2.5 PHOTOPLETHYSMOGRAPHY

Photoplethysmography (PPG), also known as the pulse oximeter waveform, is a simple and low-cost optical tech nique that can be utilized to detect blood volume changes in the microvascular bed of tissue. It is frequently employed noninvasively to take measurements at the skin surface. PPG signals (Allen, 2007; Kamal, Harness, Irving, & Mearns, 1989) are becoming popular for monitoring heart rate (HR) because of their wearable implementation com pared to conventional ECG technology. These signals are obtained through pulse oximeters embedded in a small wearable device worn on the earlobes, fingertips, or at the wrists. The pulse oximeters cast light on the wearer's skin through light emitting diodes (LED) and acquire the reflected or transmitted light whose intensity depends on the volume of blood existing in the arteries under the skin. As the volume of blood changes with the cardiac cycle, the light intensity also changes with the cardiac rhythm, which can be employed to extract HR information. Originally PPG signals were employed to monitor patients' HRs 24 hours in hospital beds, mostly utilizing the fingertip-type devices (Khan, Al Hossain, Uddin, Alam, & Hasan, 2016).

The PPG waveform contains a pulsatile (AC) physiological waveform for synchronous cardiac changes in the blood volume with each heartbeat and is superimposed on a slowly varying (DC) baseline with several lower frequency components attributed to respiration, sympathetic nervous system activity, and thermoregulation. Even though the source of the components of the PPG signal are not fully understood, it is usually known that they can provide valuable information about the cardiovascular system. Recently, there has been great interest in this method, driven by the demand for simple, portable, and low-cost technology for the primary care and community-based clinical environments, wide accessibility of small and low-cost semiconductor components, and the development of computer-based pulse wave analysis techniques. PPG technology has been utilized in a wide range of medical devices for measuring blood pressure, oxygen saturation, and cardiac output; evaluating autonomic function; and detecting peripheral vascular disease (Allen, 2007).

A PPG signal from any location on the skin can be divided into an oscillating (AC) and steady-state (DC) component, and their amplitudes are reliant on the structure and flow in the vascular bed. A good emitter for use in a PPG of skin blood flow is one in the frequency range 600–700 nm, and the best signal for AC analysis can be taken from the finger pulp. The frequency range of the data acquisition should be from 0.01 to 15 Hz, then all the information in the signal can be extracted about the autonomic nervous system control of the cardiovascular system, particularly between 0.01 and 2 Hz (Kamal et al., 1989).

The waveform, as presented on the modern pulse oximeter, is an amplified and highly filtered measurement of light absorption by the local tissue over time. It is adjusted by medical device manufacturers to emphasize its pulsatile components. All modern pulse oximeters extract and present the heart rate and oxygen saturation taken from the PPG measurements at multiple wavelengths. Hence, the PPG is an exceptional monitor for cardiac arrhythmia, mostly when employed in conjunction with ECG. The PPG can be employed to measure the ventilator-induced modulations with slight modifications in the display of the PPG. Exploration of PPG is underway to analyze its use in advanced digital signal-processing techniques to achieve a new physiologic parameter (Alian & Shelley, 2014)

Apart from clinical scenarios, many sportsman, exercisers, and elderly people need real-time mobile observation of their HR, to confine them from extreme physical action

and thereby to prevent any chances of heart attack. When PPG signals are employed during physical exercise, frequently three-axis accelerometry data are acquired (Lee et al., 2010). Although PPG signals can monitor HR rather suitably in hospital environments, trying to include them during fitness programs yields a great challenge, because the signals are heavily corrupted by motion artifacts (MA) (Khan et al., 2016).

PPG is a well-known, noninvasive, heart monitoring technique. Unlike ECG, PPG monitoring can be realized at peripheral sites on the body and does not require a conductive gel to have good body contact. Hence, PPG sensors are finding considerable new applications in wearable devices and smartwatches (Jarchi & Casson, 2016)

EXAMPLE 2.17 The following MATLAB code was used to plot the PPG and related ECG signal. For this example, Wrist PPG During Exercise Dataset was used. You can download the data from the following website: https://physionet.org/physiobank/database/wrist/

Dataset Information: This database includes wrist PPGs collected throughout running, walking, and bike riding. Synchronized motion evaluations are collected utilizing gyroscopes and accelerometers to produce multiple options for the removal of motion interference from the PPG traces. Measurements were collected employing an ECG unit placed on the chest together with a PPG and Inertial Measurement Unit placed on the left wrist while participants employed an indoor treadmill and exercise bike. Single-channel, two -electrode, ECG signals were acquired utilizing an Actiwave (CamNtech, Cambridge, UK) recorder and pregelled, self-adhesive, Silver-Silver Chloride (Ag/AgCl) electrodes, which are standard for ECG monitoring. PPG and motion data were collected employing a Shimmer 3 GSR+ unit (Shimmer Sensing, Dublin, Ireland). This includes a gyroscope, a low-noise accelerometer, a wide-range accelerometer, and a magnetometer combined into a single package. The PPG sensor was glued to the main Shimmer unit to achieve a rigid connection and permit the movement sensors inside the main Shimmer unit to precisely acquire the movement of the PPG sensor. The combined unit was then located on the left wrist in almost the position of a standard watch. All signals were sampled at 256 Hz. Records from eight participants are present (three male, five female), aged 22–32 (mean 26.5). For the walking and running records, the database contains the raw PPG and motion signals existing after segmentation into the suitable activity. The cycling PPG signals were low-pass filtered employing a second-order IIR Butterworth digital filter with ∼15 Hz cutoff frequency. Further details and illustrative example signals can be found in the reference paper (Jarchi & Casson, 2016). Exemplary PPGs are depicted in Fig. 2.20. The following MATLAB code was used to plot each signal:

```
%% Ch2_EX_17.m
clc
clear
%Wrist PPG During Exercise
%Load Sample PPG Data downloaded from the web site
%https://physionet.org/physiobank/database/wrist/
load s1_high_resistance_bikem.mat

%Plot ECG Signal
subplot(2,1,1);
plot(val(1,4097:8192));
title('ECG Signal')
xlabel('Samples')
ylabel('Amplitude')
axis ([0 4096 -inf inf])

%Plot PPG Signal
subplot(2,1,2);
plot(val(2,4097:8192))
title('PPG Signal')
xlabel('Samples')
ylabel('Amplitude')
axis ([0 4096 -inf inf])
```

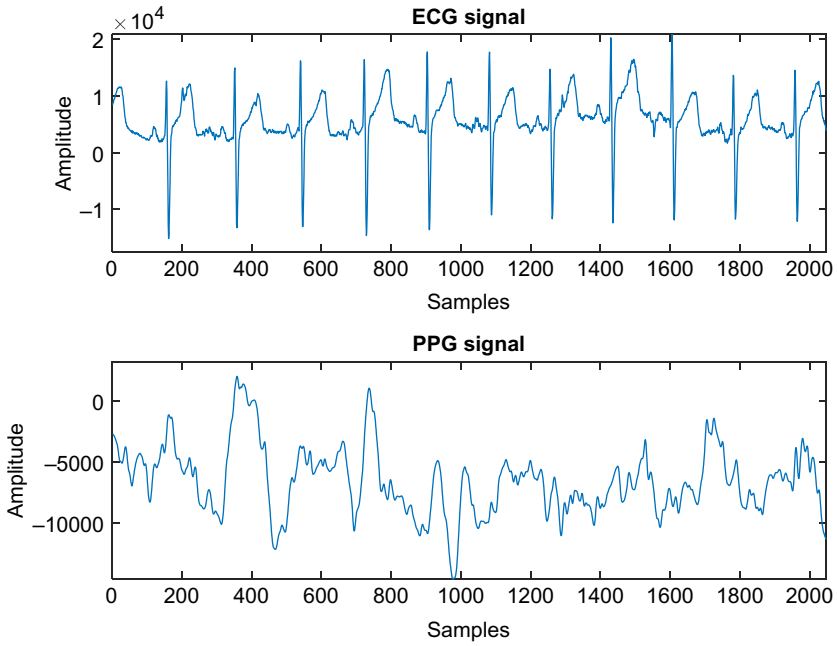

FIG. 2.20 Drawing of ECG and PPG signals.

2.6 OTHER BIOMEDICAL SIGNALS

2.6.1 Electroneurogram

The electroneurogram (ENG) measures consequences of the stimulation of a peripheral nerve with an electric shock so the response along the nerve can be measured. The ENG, generally collected with needle electrodes, is employed to measure conduction velocity of the nerve to help with nerve injury diagnosis. The conduction velocity can be estimated from the distance the resulting two signal waveforms are separated (Sörnmo & Laguna, 2005).

2.6.2 Electroretinogram

An electroretinogram (ERG) is utilized for studying the electrical potentials produced by the retina of the eye during light stimulation. The ERG is acquired by inserting the exploring electrode, encapsulated in a contact lens, on the cornea. The ERG is beneficial for evaluating the electrical response of the rods and cones. A normal ERG presents suitable responses with increased light intensity, whereas an abnormal ERG is attained in conditions such as arteriosclerosis of the retina or detachment of the retina (Sörnmo & Laguna, 2005).

2.6.3 Electrooculogram

The EOG is the recording of the steady corneal-retinal potential that is related to vertical and horizontal movements of the eye to quantify the direction of the gaze. The EOG is of particular interest in people with sleep disorders in which the occurrence of REM is crucial to determine the certain sleep stages. The EOG is acquired when studying a rapid, involuntary oscillation of the eyeballs of patients suffering from vertigo and dizziness. The EOG is also beneficial in virtual reality applications in which a device for eye-tracking may be required (Sörnmo & Laguna, 2005).

2.6.4 Electrogastrogram

The electrogastrogram (EGG) is a recording of the impulses that propagate through the muscles of the stomach to evaluate their contractions. The EGG is studied when the muscles of the stomach or the nerves directing the muscles are not working properly. The EGG is acquired by putting a number of electrodes over the stomach during fasting and after the eating. In normal subjects, a steady "rhythmic" signal is produced by the muscles of the stomach, having an amplitude that increases after eating; the normal frequency of the gastric rhythm is roughly 3 cycles/minute. But in symptomatic patients, the rhythm is usually irregular and occasionally without an increase in the amplitude after the eating (Sörnmo & Laguna, 2005).

The surface EGG represents the overall electrical activity of the stomach, including the electrical control activity and the electrical response activity. Gastric dysrhythmia or arrhythmia can be detected via analysis of the EGG. Precise and consistent measurement of the electrical activity of the stomach necessitates implantation of electrodes within the stomach that limits practical usage (Rangayyan, 2015).

2.6.5 Carotid Pulse

The carotid pulse (CP) is a pressure signal acquired over the carotid artery as it passes near the surface of the body at the neck. It delivers a pulse signal signifying the variations in arterial blood pressure and volume with each heartbeat. Because of the proximity of the recording site to the heart, the CP signal closely looks like the morphology of the pressure signal at the root of the aorta. The CP is a beneficial assistant to the PCG and can help in the recognition of S2 and its components. The CP increases sharply with the ejection of blood from the left ventricle to the aorta, reaching a peak called the percussion (P) wave. This is followed by a plateau or a secondary wave known as the tidal (T) wave, resulting from a reflected pulse returning from the upper body. Next, closure of the aortic valve results in a notch known as the dicrotic (D) notch. The dicrotic notch may be followed by the dicrotic wave (DW) because of the reflected pulse from the lower body. The carotid pulse trace is affected by valvular imperfections such as mitral insufficiency and aortic stenosis; however, it is not commonly employed in clinical diagnosis. The CP signals have a nominal bandwidth of 0–100 Hz and usually recorded with the PCG and ECG signals. Location of the CP transducer needs careful choice of a location on the neck as close to the carotid artery as possible, in which the pulse is felt the strongest, usually by a trained technician (Rangayyan, 2015).

2.6.6 Vibromyogram

The vibromyogram (VMG) is the direct mechanical manifestation of contraction of a skeletal muscle and is a vibration signal that escorts the EMG. The signal has also been called the sound-, acoustic-, or phonomyogram. Muscle sounds or vibrations are associated with the change in contraction of the fundamental muscle fibers, and can be acquired utilizing a contact microphone or accelerometer located on the muscle surface. The intensity and frequency of the VMG can change directly proportional to the contraction level. The VMG, along with the EMG, can be beneficial in studies associated with neuromuscular control, athletic training, muscle contraction, and biofeedback. Nevertheless, VMG signal analysis is not as well established or as popular as EMG analysis (Rangayyan, 2015).

2.6.7 Vibroarthrogram

The knee joint is formed between the femur, the patella, and the tibia. The knee joint is the main articulation in the human body which can efficiently change from 0 degrees extension to 135 degrees flexion, together with 20–30 degrees rotation of the flexed leg on the femoral condyles. The knee joint is known as a synovial joint, as it encompasses a lubricating substance known as the synovial fluid. The patella (knee cap), a sesamoid bone, protects the joint, and is exactly associated with the slide in the groove (trochlea) of the femur during leg movement. The knee derives its physiological movement and typical rolling-gliding mechanism of flexion and extension from its six degrees of freedom. Considerable noise is frequently related to degeneration of knee-joint surfaces. The vibroarthrogram (VAG) is the vibration signal taken from a joint during movement. Normal joint surfaces are smooth and yield little or no sound, whereas joints affected by osteoarthritis and other degenerative disorders suffer from tendon loss and yield grinding sounds. Detection of knee-joint disorders via the analysis of VAG signals may support physicians to circumvent needless exploratory surgery, and also aid better selection of patients who would benefit from surgery. The VAG signal is not yet well understood and is a difficult signal to investigate due to its complex nonstationary characteristics (Rangayyan, 2015).

REFERENCES

Abdullah, A. A., Subasi, A., & Qaisar, S. M. (2017). Surface EMG signal classification by using WPD and ensemble tree classifiers. In: *Presented at the CMBEBIH 2017: Proceedings of the international conference on medical and biological engineering 2017*, Vol. 62. (p. 475). Springer.

Akben, S. B., Subasi, A., & Tuncel, D. (2010). *Analysis of repetitive flash stimulation frequencies and record periods to detect migraine using artificial neural network: Vol. 36*. (pp. 925–931). Springer.

Akben, S. B., Subasi, A., & Tuncel, D. (2011). Analysis of EEG signals under flash stimulation for migraine and epileptic patients. *Journal of Medical Systems*, *35*(3), 437–443.

Alian, A. A., & Shelley, K. H. (2014). Photoplethysmography. *Hemodynamic Monitoring Devices*, *28*(4), 395–406. https://doi.org/10.1016/j.bpa.2014.08.006.

Alickovic, E., & Subasi, A. (2018). Ensemble SVM method for automatic sleep stage classification. *IEEE Transactions on Instrumentation and Measurement*.

Allen, J. (2007). Photoplethysmography and its application in clinical physiological measurement. *Physiological Measurement*, *28*(3), R1.

Andrzejak, R. G., Schindler, K., & Rummel, C. (2012). Nonrandomness, nonlinear dependence, and nonstationarity of electroencephalographic recordings from epilepsy patients. *Physical Review E*, *86*(4), 046206.

Andrzejak, R. G., Chicharro, D., Lehnertz, K., & Mormann, F. (2011). Using bivariate signal analysis to characterize the epileptic focus: the benefit of surrogates. *Physical Review E*, (046203), 83.

Andrzejak, R. G., Widman, G., Lehnertz, K., David, P., & Elger, C. E. (2006). Improved spatial characterization of the epileptic brain by focusing on nonlinearity. *Epilepsy Research*, *69*, 30.

Aschenbrenner-Scheibe, R., Maiwald, T., Winterhalder, M., Voss, H., Timmer, J., & Schulze-Bonhage, A. (2003). How well can epileptic seizures be predicted? An evaluation of a nonlinear method. *Brain*, 2616–2626.

Asyali, M. H. (2003). Discrimination power of long - term heart rate variability measures. In: *Engineering in medicine and biology society:*

Proceeding of the 25th annual international conference of the IEEE EMBS, Cancum, pp. 200–203.

Baguet, J.-P., Barone-Rochette, G., Tamisier, R., Levy, P., & Pépin, J.-L. (2012). Mechanisms of cardiac dysfunction in obstructive sleep apnea. *Nature Reviews Cardiology*, *9*(12), 679.

Bailey, J. J., Berson, A. S., & Garson, A. (1990). Recommendations for standardization and specifications in automated electrocardiography: bandwidth and digital signal processing: a report for health professionals by an ad hoc writing group of the Committee on Electrocardiography and Cardiac electrophysiology of the Council on Clinical Cardiology, American Heart Association. *Circulation*, *81*, 730.

Baim, D. S., Colucci, W. S., Monrad, E. S., Smith, H. S., Wright, R. F., Lanoue, A., … Braunwald, E. (1986). Survival of patients with severe congestive heart failure treated with oral milrinone. *Journal of American College of Cardiology*, *7*(3), 661–670.

Barlow, J. S. (1993). *The electroencephalogram. Its patterns and origins*. Cambridge, MA: The MIT Press.

Bear, M. F., Connors, B. W., & Paradiso, M. A. (1996). *Neuroscience. Exploring the brain*. Baltimore: Williams & Wilkins.

Begg, R., Lai, D. T., & Palaniswami, M. (2007). *Computational intelligence in biomedical engineering*. CRC Press.

Berbari, E. (2000). Principles of electrocardiography. In J. D. Bronzino (Ed.), *The biomedical engineering handbook*. 2nd ed.: CRC Press LLC.

Berbari, E. J., Lazzara, R., Samet, P., & Scherlag, B. J. (1973). Noninvasive technique for detection of electrical activity during the PR segment. *Circulation*, *48*, 1006.

Brazier, M. (1968). *Electrical activity of the nervous system*. Baltimore: Williams & Wilkins.

Bronzino, J. D. (1999). *Biomedical engineering handbook*. Vol. 2. CRC Press.

Carvalho, P., Paiva, R. P., Kumar, D., Ramos, J., Santos, S., & Henriques, J. (2011). *A framework for acoustic cardiac signal analysis*: (pp. 151–160). Presented at the BIOSIGNALS.

Chen, Y., Wang, S., Shen, C.-H., & Choy, F. K. (2012). Intelligent identification of childhood musical murmurs. *Journal of Healthcare Engineering*, *3*(1), 125–139.

Chazal, P., O'Dwyer, M., & Reilly, R. B. (2004). Automatic classification of heartbeats using ECG morphology and heartbeat interval features. *IEEE Transactions on Biomedical Engineering*, *51*(7), 1196–1206.

Cherif, L. H., Debbal, S. M., & Bereksi-Reguig, F. (2010). Choice of the wavelet analyzing in the phonocardiogram signal analysis using the discrete and the packet wavelet transform. *Expert Systems With Applications*, *37*(2), 913–918. https://doi.org/10.1016/j.eswa.2009.09.036.

Chi, Y. M., Wang, Y.-T., Wang, Y., Maier, C., Jung, T.-P., & Cauwenberghs, G. (2012). Dry and noncontact EEG sensors for mobile brain–computer interfaces. *IEEE Transactions on Neural Systems and Rehabilitation Engineering*, *20*(2), 228–235.

Choi, S., Shin, Y., & Park, H.-K. (2011). Selection of wavelet packet measures for insufficiency murmur identification. *Expert Systems With Applications*, *38*(4), 4264–4271.

Corsini, J., Shoker, L., Sanei, S., & Alarcon, G. (2006). Epileptic seizure predictability from scalp EEG incorporating constrained blind source separation. *IEEE Transactions on Biomedical Engineering*, *56*, 790–799.

Da Poian, G., Bernardini, R., & Rinaldo, R. (2016). Separation and analysis of fetal-ECG signals from compressed sensed abdominal ECG recordings. *IEEE Transactions on Biomedical Engineering*, *63*(6), 1269–1279.

Dale, A. M., & Sereno, M. J. (1993). Improved localization of cortical activity by combining EEG and MEG with MRI cortical surface reconstruction. *Journal of Cognitive Neuroscience*, 162–176.

D'Alessandro, M., Esteller, R., Vachtsevanos, G., Hinson, A., Echauz, J., & Litt, B. (2003). Epileptic seizure prediction using hybrid feature selection over multiple intracranial EEG electrode contacts: a report of four patients. *IEEE Transactions on Biomedical Engineering*, *50* (5), 603–615.

da Silva-Sauer, L., Valero-Aguayo, L., de la Torre-Luque, A., Ron-Angevin, R., & Varona-Moya, S. (2016). Concentration on performance with P300-based BCI systems: a matter of interface features. *Applied Ergonomics*, *52*, 325–332. https://doi.org/10.1016/j.apergo.2015.08.002.

Deutsch, S., & Deutsch, A. (1993). *Understanding the nervous system: An engineering perspective*. New York: IEEE Press.

Dornhege, G., Blankertz, B., Curio, G., & Muller, K.-R. (2004). Boosting bit rates in noninvasive EEG single-trial classifications by feature combination and multiclass paradigms. *IEEE Transactions on Biomedical Engineering*, *51*(6), 993–1002.

EC11a, A. (1984). *Voluntary standard for diagnostic electrocardiographic devices*. Arlington: Association for the Advancement of Medical Instrumentation.

Einthoven, W. (1903). Die galvanometrische Registrirung des menschlichen Elektrokardiogramms, zugleich eine Beurtheilung der Anwendung des Capillar-Elecktrometers in der Physiologie. *Pflugers Arch Ges Physiol*, *99*, 472.

Elger, C. E. (2001). Future trends in epileptology. *Current Opinion in Neurology*, *14*, 185–186.

Emly, M., Gilmore, L. D., & Roy, S. H. (1992). Electromyography. *IEEE Potentials*, *11*(2), 25–28.

Ergen, B., Tatar, Y., & Gulcur, H. O. (2012). Time-frequency analysis of phonocardiogram signals using wavelet transform: a comparative study. *Computer Methods in Biomechanics and Biomedical Engineering*, *15*(4), 371–381.

Esteller, R., Echauz, J., D'Alessandro, M., Worell, G., Cranstoun, S., Vachtsevanos, G., & Litt, B. (2005). Continuous energy variation during the seizure cycle: towards an online accumulated energy. *Clin Neurophy*, 517–526.

Feldt, S., Osterhage, H., Mormann, F., Lehnertz, K., & Zochowski, M. (2007). Internetwork and intra-network communications during bursting dynamics: applications to seizure prediction. *Phys Rev E*, *76*.

Farwell, L. A., & Donchin, E. (1986). The brain detector-P300 in the detection of deception. In: *Presented at the psychophysiology, Vol. 23, Soc Psychophysiol Res 1010 Vermont Ave NW Suite 1100, Washington, DC2005*, (p. 434). 434.

Gao, W., Guan, J., Gao, J., & Zhou, D. (2015). Multi-ganglion ANN based feature learning with application to P300-BCI signal classification. *Biomedical Signal Processing and Control*, *18*, 127–137.

Geselowitz, D. B. (1989). On the theory of the electrocardiogram. *Proceedings of IEEE*, *77*, 857–876.

Gevins, A. S., & Bressler, S. L. (1988). Functional topography of the human brain. In G. Pfurtscheller, & F. L. Silva (Eds.), *Functional brain mapping* (pp. 99–116). Toronto: Hans Huber Publishers.

Goldberger, E. (1942). A simple, indifferent, electrocardiographic electrode of zero potential and a technique of obtaining augmented, unipolar, extremity leads. *American Heart Journal*, *23*, 483.

Gopura, R. A. R. C., Kiguchi, K., & Li, Y. (2009). SUEFUL-7: A 7DOF upper-limb exoskeleton robot with muscle-model-oriented EMG-

based control. In: *Presented at the intelligent robots and systems, 2009. IROS 2009. IEEE/RSJ international conference on IEEE*, pp. 1126–1131.

Graimann, B., Allison, B., & Pfurtscheller, G. (2009). Brain-computer interfaces: a gentle introduction. In *Brain-computer interfaces* (pp. 1–27). Springer.

Grozea, C., Voinescu, C. D., & Fazli, S. (2011). Bristle-sensors—low-cost flexible passive dry EEG electrodes for neurofeedback and BCI applications. *Journal of Neural Engineering*, *8*(2).

Guger, C., Daban, S., Sellers, E., Holzner, C., Krausz, G., Carabalona, R., … Edlinger, G. (2009). How many people are able to control a P300-based brain-computer interface (BCI)? *Neuroscience Letters*, *462*(1), 94–98.

Guger, C., Schlogl, A., Neuper, C., Walterspacher, D., Strein, T., & Pfurtscheller, G. (2001). Rapid prototyping of an EEG-based brain-computer interface (BCI). *IEEE Transactions on Neural Systems and Rehabilitation Engineering*, *9*(1), 49–58.

Hassan, A. R., & Haque, M. A. (2016). Computer-aided obstructive sleep apnea screening from single-lead electrocardiogram using statistical and spectral features and bootstrap aggregating. *Biocybernetics and Biomedical Engineering*, *36*(1), 256–266.

Harrison, M., Frei, M. G., & Osorio, I. (2005). Accumulated energy revisited. *Clinical Neurophysiology*, 527–531.

Himanena, S.-L., & Hasan, J. (2004). Limitations of Rechtschaffen and Kales. *Sleep Medicine Reviews*, *4*(2), 149–167.

Hirshkowitz, M. (2000). Standing on the shoulders of giants: the Standardized Sleep Manual after 30 years. *Sleep Medicine Reviews*, *4*(2), 169–170.

Horobin, W. (Ed.). (2008). *Diseases and disorders*. Marshall Cavendish Corporation.

Hossen, A., & Al-Ghunaimi, B. (2007). A wavelet-based soft decision technique for screening of patients with congestive heart failure. *Biomedical Signal Processing and Control*, *2*, 135–143.

Hossen, A., & Al-Ghunaimi, B. (2008). *Identification of patients with congestive heart failure by recognition of sub-bands spectral patterns*: (pp. 21–24). World Academy of Science, Engineering and Technology.

Huang, Y.-J., Wu, C.-Y., Wong, A. M.-K., & Lin, B.-S. (2015). Novel active comb-shaped dry electrode for EEG measurement in hairy site. *IEEE Transactions on Biomedical Engineering*, *62*(1), 256–263.

Iber, C., Ancoli-Israel, S., Chesson, A. L., & Quan, S. F. (2007). *The AASM manual for scoring of sleep and associated events-rules: Terminology and technical specification*. Darien, IL, USA: American Academy of Sleep Medicine.

Isler, Y., & Kuntalp, M. (2007). Combining classical HRV indices with wavelet entropy measures improves to performance in diagnosing congestive heart failure. *Computers in Biology and Medicine*, *37*, 1502–1510.

Jasper, H. (1958). The ten twenty electrode system of the international federation. *Electroencephalography and Clinical Neurophysiology*, 371–375.

Jarchi, D., & Casson, A. J. (2016). Description of a database containing wrist PPG signals recorded during physical exercise with both accelerometer and gyroscope measures of motion. *Data*, *2*(1), 1.

Jenkins, J. M. (1981). Computerized electrocardiography. *CRC Critical Reviews in Bioengineering*, *6*.

Jerger, K., Weinstein, S., Sauer, T., & Schiff, S. (2005). Multivariate linear discrimination of seizures. *Clinical Neurophysiology*, 545–551.

Jia, L., Song, D., Tao, L., & Lu, Y. (2012). Heart sounds classification with a fuzzy neural network method with structure learning. In *Presented at the international symposium on neural networks* (pp. 130–140). Springer.

Jin, J., & Sánchez-Sinencio, E. (2015). A home sleep apnea screening device with time-domain signal processing and autonomous scoring capability. *IEEE Transactions on Biomedical Circuits and Systems*, *9*(1), 96–104.

Jones, S. A. (2008). *ECG success exercises in ECG interpretation*. Philadelphia: F.A. Davis Company.

Jouny, C., Franaszczuk, P., & Bergey, G. (2005). Signal complexity and synchrony of epileptic seizures: is there an identifiable preictal period. *Clinical Neurophysiology*, 552–558.

Julian, D. G., Campbell-Cowan, J., & McLenachan, M. J. (2005). *Cardiology* 8th ed.Edinburgh, NY: Saunders.

Kamal, A., Harness, J., Irving, G., & Mearns, A. (1989). Skin photoplethysmography—a review. *Computer Methods and Programs in Biomedicine*, *28*(4), 257–269.

Kao, W.-C., & Wei, C.-C. (2011). Automatic phonocardiograph signal analysis for detecting heart valve disorders. *Expert Systems With Applications*, *38*(6), 6458–6468.

Kennedy, R. G. (1998). Electronic fetal heart rate monitoring: retrospective reflections on a twentieth-century technology. *Journal of the Royal Society of Medicine*, *91*(5), 244–250.

Khan, E., Al Hossain, F., Uddin, S. Z., Alam, S. K., & Hasan, M. K. (2016). A robust heart rate monitoring scheme using photoplethysmographic signals corrupted by intense motion artifacts. *IEEE Transactions on Biomedical Engineering*, *63*(3), 550–562.

Khan, Y. U., & Gotman, J. (2003). Wavelet based automatic seizure detection in intra-cerebral electroencephalogram. *Clinical Neurophysiology*, 898–908.

Kim, K. S., Choi, H. H., Moon, C. S., & Mun, C. W. (2011). Comparison of *k*-nearest neighbor, quadratic discriminant and linear discriminant analysis in classification of electromyogram signals based on the wrist-motion directions. *Current Applied Physics*, *11*(3), 740–745.

Kimura, J. (1989). *Electrodiagnosis in diseases of nerve and muscle: Principles and practice* (2nd ed.). Quest-Meridien Ltd. F.A. Davis.

Koelstra, S., Muhl, C., Soleymani, M., Lee, J.-S., Yazdani, A., Ebrahimi, T., … Patras, I. (2012). Deap: a database for emotion analysis; using physiological signals. *IEEE Transactions on Affective Computing*, *3*(1), 18–31.

Kohler, B., Hennig, C., & Orglmeister, R. (2002). The principles of software QRS detection. *IEEE Engineering in Medicine and Biology Magazine*, *21*(1), 42–57.

Kotas, M., Jezewski, J., Horoba, K., & Matonia, A. (2011). Application of spatio-temporal filtering to fetal electrocardiogram enhancement. *Computer Methods and Programs in Biomedicine*, *104*(1), 1–9.

Kondraske, G. V. (1986). Neurophysiological measurements. In J. D. Bronzino (Ed.), *Biomedical engineering and instrumentation* (pp. 138–179). Boston: PWS Publishing.

Kuntamalla, S., & Reddy, L. R. (2010). Detecting congestive heart failure using heart rate sequential trend analysis plot. *International Journal of Engineering Science and Technology*, *2*(12), 7329–7334.

Kuntamalla, S., & Reddy, L. R. (2014). Reduced data dualscale entropy analysis of HRV signals for improved congestive heart failure detection. *Measurement Science Review*, *14*(5), 294–301.

Kurzynski, M., Krysmann, M., Trajdos, P., & Wolczowski, A. (2016). Multiclassifier system with hybrid learning applied to the control of

bioprosthetic hand. *Computers in Biology and Medicine*, *69*, 286–297. https://doi.org/10.1016/j.compbiomed.2015.04.023.

Lafuente, V., Gorriz, J. M., Ramirez, J., & Gonzalez, E. (2017). P300 brainwave extraction from EEG signals: an unsupervised approach. *Expert Systems With Applications*, *74*, 1–10.

Lee, B., Han, J., Baek, H. J., Shin, J. H., Park, K. S., & Yi, W. J. (2010). Improved elimination of motion artifacts from a photoplethysmographic signal using a Kalman smoother with simultaneous accelerometry. *Physiological Measurement*, *31*(12), 1585.

Lee, Y.-R., & Kim, H.-N. (2018). A data partitioning method for increasing ensemble diversity of an eSVM-based P300 speller. *Biomedical Signal Processing and Control*, *39*, 53–63.

Lehnertz, K. (2008). Epilepsy and nonlinear dynamics. *Journal of Biological Physics*, (253), 34.

Lenzi, T., De Rossi, S., Vitiello, N., Chiri, A., Roccella, S., Giovacchini, F., … Carrozza, M. C. (2009). The neuro-robotics paradigm: NEURARM, NEUROExos, HANDEXOS. In: *Presented at the Engineering in Medicine and Biology Society, 2009. EMBC 2009. Annual International Conference of the IEEE*, IEEE, pp. 2430–2433.

Liu, N.-H., Chiang, C.-Y., & Hsu, H.-M. (2013). Improving driver alertness through music selection using a mobile EEG to detect brainwaves. *Sensors*, *13*(7), 8199–8221.

Lo, H. S., & Xie, S. Q. (2012). Exoskeleton robots for upper-limb rehabilitation: state of the art and future prospects. *Medical Engineering and Physics*, *34*(3), 261–268.

Lum, P. S., Burgar, C. G., Shor, P. C., Majmundar, M., & Van der Loos, M. (2002). Robot-assisted movement training compared with conventional therapy techniques for the rehabilitation of upper-limb motor function after stroke. *Archives of Physical Medicine and Rehabilitation*, *83*(7), 952–959.

Maiwald, T., Winterhalder, M., Aschenbrenner-Scheibe, R., Voss, H. U., Schulze-Bonhage, A., & Timmer, J. (2004). Comparison of three nonlinear seizure prediction methods by means of the seizure prediction characteristic. *Physica D*, *194*, 357–368.

Malmivuo, J., Suikho, V., & Eskola, H. (1997). Sensitivity distributions of EEG and MEG measurements. *IEEE Transactions on Biomedical Engineerin*, 196–208.

Masetic, Z., & Subasi, A. (2016). Congestive heart failure detection using random forest classifier. *Computer Methods and Programs in Biomedicine*, *130*, 54–64.

McFarland, D. J., & Wolpaw, J. R. (2017). EEG-based brain-computer interfaces. *Synthetic Biology and Biomedical Engineering/Neural Engineering*, *4*, 194–200. https://doi.org/10.1016/j.cobme.2017.11.004.

Meier, R., Dittrich, H., Schulze-Bonhage, A., & Aertsen, A. (2008). Detecting epileptic seizures in long-term human EEG: a new approach to automatic online and real-time detection and classification of polymorphic seizure patterns. *Journal of Clinical Neurophysiology*, 119–131.

Mormann, F., Andrzejak, R. G., Elger, C. E., & Lehnertz, K. (2007). Seizure prediction: the long and winding road. *Brain*, *130*, 314–333.

Mormann, F., Kreuz, T., Rieke, C., Andrzejak, R., & Kraskov, A. (2005). On the predictability of epileptic seizures. *Clinical Neurophysiology*, 569–587.

Muthuswamy, J. (2004). Biomedical signal analysis. *Standard handbook of biomedical engineering and design*Vol. 14, 18–1.

Nikolic, M. (2001). *Findings and firing pattern analysis in controls and patients with myopathy and amytrophic lateral sclerosis*. Copenhagen: Faculty of Health Science, University of Copenhagen.

Niedermayer, E. (1999a). Abnormal EEG patterns: epileptic and paroxysmal. In E. Niedermayer, & F. L. Silva (Eds.), *Electroencephalography. Basic principles, clinical applications and related fields* (pp. 235–260). Baltimore: Williams & Wilkins.

Niedermayer, E. (1999b). Epileptic seizure disorders. In E. Niedermayer, & F. L. Silva (Eds.), *Electroencephalography. Basic principles, clinical applications and related fields* (pp. 476–585). Baltimore: Williams & Wilkins.

Niedermayer, E. (1999c). The normal EEG of the waking adult. In E. Niedermayer, & F. L. Silva (Eds.), *Electroencephalography. Basic principles, clinical applications and related fields* (pp. 149–173). Baltimore: Williams & Wilkins.

Oweis, R. J., Hamad, H., & Shammout, M. (2014). Heart sounds segmentation utilizing Teager Energy Operator. *Journal of Medical Imaging and Health Informatics*, *4*(4), 488–499.

Pan, J., & Tompkins, W. J. (1985, May). A real-time QRS detection algorithm. *IEEE Transactions on Biomedical Engineering*, *BME-32*(3), 230–236.

Passanisi, C. (2004). *Electrocardiography*. New York: Delmar Learning.

Pecchia, L., Melillo, P., Sansone, M., & Bracale, M. (2011). Discrimination power of short-term heart rate variability measures for CHF assessment. *IEEE Transactions on Information Technology in Biomedicine*, *15*(1), 40–46.

Pedro, C.-C. E., Joyce, W. Y., Leo, C. L., Kirk, S., Sandy, D., & Marc, N. R. (2012). Quantification and localization of EEG interictal spike activity in patients with surgically removed epileptogenic foci. *Clinical Neurophysiology*, *123*, 471–485.

Penzel, T., Moody, G. B., Mark, R. G., Goldberger, A. L., & Peter, J. H. (2000). The apnea-ECG database. In: *Presented at the Computers in cardiology 2000*, IEEE, pp. 255–258.

Pereda, E., Quian Quiroga, R., & Bhattacharya, J. (2005). Nonlinear multivariate analysis of neurophysiological signals. *Progress in Neurobiology*, *77*, 1), 1–37.

Pfurtscheller, G., Leeb, R., Keinrath, C., Friedman, D., Neuper, C., Guger, C., & Slater, M. (2006). Walking from thought. *Brain Research*, *1071*(1), 145–152.

Plonsey, R. (1972). Capabilities and limitations of electrocardiography and magnetocardiography. *IEEE Transactions on Information Technology in Biomedicine*, 239–244.

Preedy, V., & Peters, T. (2002). *Skeletal muscle: Pathology, diagnosis and management of disease*. Cambridge: Cambridge University Press.

Preston, D. C., & Shapiro, B. E. (2012). *Electromyography and neuromuscular disorders: Clinical-electrophysiologic correlations*. London: Elsevier Health Sciences.

Pryor, T. A., Drazen, E., & Laks, M. (1980). *Computer systems for the processing of diagnostic electrocardiograms*. Los Alamitos, CA: IEEE Computer Society Press.

Quinn, C. E. (2006). *100 questions and answers about congestive heart failure*. Jones and Bartlett Publishers, Inc.

Ralph, A. G., Kaspar, S., & Rummel, C. (2012). Nonrandomness, nonlinear dependence, and nonstationarity of electroencephalographic. *Physical Review E*, *86*.

Rechtschaffen, A., & Kales, A. (1968). *A manual of standardized terminology, techniques, and scoring system for sleep stages of human subjects*. Los Angeles, CA: UCLA, Brain Research Institute/Brain Information Service.

Ramović, A., Bandić, L., Kevrić, J., Germović, E., & Subasi, A. (2017). Wavelet and Teager Energy Operator (TEO) for heart sound processing and identification. In *CMBEBIH 2017* (pp. 495–502). Springer.

Ranganathan, N., Sivaciyan, V., & Saksena, F. B. (2007). *The art and science of cardiac physical examination: With heart sounds and pulse wave forms on CD*. Springer Science & Business Media.

Rangayyan, R. M. (2015). *Biomedical signal analysis*. (Vol. 33). John Wiley & Sons.

Riener, R., Nef, T., & Colombo, G. (2005). Robot-aided neurorehabilitation of the upper extremities. *Medical and Biological Engineering and Computing*, *43*(1), 2–10.

Robyn, B. R., Mingui, S., Mark, S. L., & Robert, S. J. (2000). Detection of seizure foci by recurrent neural networks. In: *22nd annual EMBS international conference, Chicago, IL*.

Rutkowski, T. M., Zdunek, R., & Cichocki, A. (2006). Multichanned EEG brain activity patterns analysis in time frequency domain with nonnegative matric factorization support. In: *Third international conference on brain-inspired information technology. Hibikino, Kitakyushu, Japan*.

Safara, F., Doraisamy, S., Azman, A., Jantan, A., & Ranga, S. (2012). Wavelet packet entropy for heart murmurs classification. *Advances in Bioinformatics*, *2012*.

Sammler, D., Grigutsch, M., Fritz, T., & Koelsch, S. (2007). Music and emotion: electrophysiological correlates of the processing of pleasant and unpleasant music. *Psychophysiology*, *44*(2), 293–304.

Sanei, S. (2013). *Adaptive processing of brain signals*. John Wiley & Sons.

Sanei, S., & Chambers, J. A. (2013). *EEG signal processing*. John Wiley & Sons.

Sapsanis, C., Georgoulas, G., & Tzes, A. (2013). EMG based classification of basic hand movements based on time-frequency features. In: *Presented at the Control & Automation (MED), 2013 21st Mediterranean Conference on IEEE*, pp. 716–722.

Sasaki, D., Noritsugu, T., & Takaiwa, M. (2005). Development of active support splint driven by pneumatic soft actuator (ASSIST). Presented at the Robotics and Automation, 2005. ICRA 2005. Proceedings of the 2005 IEEE International Conference on IEEE, pp. 520–525.

Schelter, B., Winterhalder, M., Maiwald, T., Brandt, A., Schad, A., Timmer, J., & Schulze-Bonhage, A. (2006). Do false predictions of seizures depend on the state of vigilance? A report from two seizure-prediction methods and proposed remedies. *Epilepsia*, *47*(12), 2058–2070.

Schlkopf, B., & Smola, A. (2002). Learning with kernels: support vector machines, regularization, optimization and beyond. In *Adaptive computation and machine learning*. Cambridge, MA: MIT Press.

Sellers, E. W., Krusienski, D. J., McFarland, D. J., Vaughan, T. M., & Wolpaw, J. R. (2006). A P300 event-related potential brain-computer interface (BCI): the effects of matrix size and inter stimulus interval on performance. *Biological Psychology*, *73*(3), 242–252.

Shahriari, Y., & Erfanian, A. (2013). Improving the performance of P300-based brain-computer interface through subspace-based filtering. *Neurocomputing*, *121*, 434–441.

Simson, M. B. (1981). Use of signals in the terminal QRS complex to identify patients with ventricular tachycardia after myocardial infarction. *Circulation*, *64*, 235–242.

Siuly, S., Li, Y., & Zhang, Y. (2016). *EEG signal analysis and classification*. Springer.

Son, C.-S., Kim, Y.-N., Kim, H.-S., Park, H.-S., & Kim, M.-S. (2012). Decision-making model for early diagnosis of congestive heart failure using rough set and decision tree approaches. *Journal of Biomedical Informatics*, 999–1008.

Sörnmo, L., & Laguna, P. (2005). *Bioelectrical signal processing in cardiac and neurological applications*. (Vol. 8). Academic Press.

Stam, C. J. (2005). Nonlinear dynamical analysis of EEG and MEG: review of an emerging field. *Clinical Neurophysiology*, *16*(2266).

Subasi, A. (2013). Classification of EMG signals using PSO optimized SVM for diagnosis of neuromuscular disorders. *Computers in Biology and Medicine*, *43*, 576–586.

Swiderski, B., Osowski, S., Cichocki, A., & Rysz, A. (2007). Epileptic seizure characterization by Lyapunov exponent of EEG signal. *Compel*, *26*, 1276–1287.

Swiderski, B., Osowski, S., Cichocki, A., & Rysz, A. (2008). Single-Class SVM Classifier for localization of epileptic focus on the basis of EEG. In: *International joint conference on neural networks*.

Thaler, M. S. (1999). *The only EKG book you'll ever need*. (Vol. 3). Philadelphia, PA: Lippincott Williams & Wilkins.

Thuraisingham, R. A. (2009). A classification system to detect congestive heart failure using second-order difference plot of RR intervals. *Cardiology Research and Practice*.

Togawa, T., Tamura, T., & Oberg, P. A. (1997). *Biomedical transducers and instruments*. Boca Raton, FL: CRC Press.

Trust, T. M. (2014). *Facts and figures*. Retrieved April 7, 2016 from: (2014). https://www.migrainetrust.org/about-migraine/migraine-what-is-it/facts-figures/.

Uni-Freiburg (2011). *Seizure prediction project Freiburg*. Retrieved October 2, 2011 from:(2011). https://epilepsy.uni-freiburg.de/freiburg-seizure-prediction-project/eeg-database.

Varotto, G., Tassi, L., Franceschetti, S., Spreafico, R., & Panzica, F. (2012). Epileptogenic networks of type II focal cortical dysplasia: a stereo-EEG study. *Neuroimage*, *61*, 591.

Waller, A. D. (1889). One of the electromotive changes connected with the beat of the mammalian heart, and the human heart in particular. *Philosophical Transactions of the Royal Society B*, *180*, 169.

van Erp, J., Lotte, F., & Tangermann, M. (2012). Brain-computer interfaces: beyond medical applications. *Computer*, *45*(4), 26–34.

Waterhouse, E. (2003). New horizons in ambulatory electroencephalography. *IEEE Engineering in Medicine and Biology Magazine*, 74–80.

WIlson, F. N., Johnson, F. S., & Hill, I. G. (1934). The interpretation of the falvanometric curves obtained when one electrode is distant from the heart and the other near or in contact with the ventricular surface. *American Heart Journal*, *10*, 176.

Winterhalder, M., Maiwald, T., Voss, H. U., & Aschenbrenner-Scheibe, R. (2003). The seizure prediction characteristic: a general framework to assess and compare seizure prediction methods. *Epilepsy and Behavior*, 318–325.

Wojtczak, P., Amaral, T. G., Dias, O. P., Wolczowski, A., & Kurzynski, M. (2009). Hand movement recognition based on biosignal analysis. *Engineering Applications of Artificial Intelligence*, *22*(4), 608–615.

Wołczowski, A., & Zdunek, R. (2017). Electromyography and mechanomyography signal recognition: experimental analysis using multi-way array decomposition methods. *Biocybernetics and Biomedical Engineering*, *37*(1), 103–113. https://doi.org/10.1016/j.bbe.2016.09.004.

Wolpaw, J. R., Birbaumer, N., McFarland, D. J., Pfurtscheller, G., & Vaughan, T. M. (2002). Brain-computer interfaces for communication and control. *Clinical Neurophysiology*, *113*(6), 767–791.

Xiaoying, T., Li, X., Weifeng, L., Yuhua, P., Duanduan, C., Tianxin, G., & Yanjun, Z. (2012). Analysis of frequency domain of EEG signals in clinical location of epileptic focus. *Clinical EEG Neuroscience*.

Yu, S.-N., & Lee, M.-Y. (2012). Conditional mutual information-based feature selection for congestive heart failure recognition using heart rate variability. *Computer Methods and Programs in Biomedicine*, *I*(08), 299–309.

Zarei, R., He, J., Siuly, S., & Zhang, Y. (2017). A PCA aided cross-covariance scheme for discriminative feature extraction from EEG signals. *Computer Methods and Programs in Biomedicine*, *146*, 47–57.

Zhang, H., Guan, C., & Wang, C. (2008). Asynchronous P300-based brain-computer interfaces: a computational approach with statistical models. *IEEE Transactions on Biomedical Engineering*, *55*(6), 1754–1763.

Zheng, W.-L., & Lu, B.-L. (2015). Investigating critical frequency bands and channels for EEG-based emotion recognition with deep neural networks. *IEEE Transactions on Autonomous Mental Development*, *7*(3), 162–175.

Zhong, J., & Scalzo, F. (2013). Automatic heart sound signal analysis with reused multi-scale wavelet transform. *International Journal of Engineering and Science*, *2*(50), 50–57.

FURTHER READING

Schelter, B., Winterhalder, M., Drentrup, H. F., Wohlmuth, J., Nawrath, J., Brandt, A., … Timmer, J. (2007). Seizure Prediction: the impact of long prediction horizons. *Epilepsy Research*, 213–217.

Townsend, N., Luengo-Fernandez, R., Leal, J., Gray, A., & Nichols, M. (2012). *European cardiovascular disease statistics 2012*. European Heart Health Strategy II Project, European Heart Network (Brussels), European Society of Cardiology (Sophia Antipolis).